NTNU
Norwegian University of
Science and Technology

Investigations of a harmonic oscillatory flow

Isak Bergset

MASTER THESIS

for

Student Isak Bergset

Spring 2017

Investigations of a harmonic oscillatory flow

Undersøkelse av en harmonisk oscillerende strømning

Background and objective

Flow transients are more the rule than the exception in hydropower conduits and tunnels. The reason for the transients is the ever-present governing of the hydropower machines, where governors change the opening of wicket gates and induce dynamics in the system. One of these dynamics oscillations is known as the U-tube oscillation, which is mass flow oscillating between free water surfaces in the hydraulic system. The friction losses in this dynamic oscillation is not very well described, but represent loss in energy production that the power companies are not able to include in their operational strategies. The intended operational changes might for this reason appear to give an unrealistic high benefit, since the losses in the induced dynamics are not taken into account.

A test rig for investigation of such harmonic flow oscillations have been initiated at the Waterpower laboratory, and a model for computing these losses involved in such flow have been proposed. The objective of this Master work will be to complete the installation and instrumentation of the rig, and to complete measurements of the oscillatory losses and compare with simulations.

The following tasks are to be considered:

1. Literature study on the dynamics of closed conduit flow and the losses involved in harmonic oscillatory flow
2. Complete the installation, instrumentation and calibration of the test rig
3. Perform measurements in the rig measuring the losses
4. Perform simulations of the flow using the proposed loss model and compare with the experimental results
5. The previous project work and the future work in this thesis shall be described in a paper which will be presented at 7th International symposium on Current Research in Hydraulic Turbines (CRHT-VII) at Kathmandu University in April 2017

-- ” --

Within 14 days of receiving the written text on the master thesis, the candidate shall submit a research plan for his project to the department.

When the thesis is evaluated, emphasis is put on processing of the results, and that they are presented in tabular and/or graphic form in a clear manner, and that they are analyzed carefully.

The thesis should be formulated as a research report with summary both in English and Norwegian, conclusion, literature references, table of contents etc. During the preparation of the text, the candidate should make an effort to produce a well-structured and easily readable report. In order to ease the evaluation of the thesis, it is important that the cross-references are correct. In the making of the report, strong emphasis should be placed on both a thorough discussion of the results and an orderly presentation.

The candidate is requested to initiate and keep close contact with his/her academic supervisor(s) throughout the working period. The candidate must follow the rules and regulations of NTNU as well as passive directions given by the Department of Energy and Process Engineering.
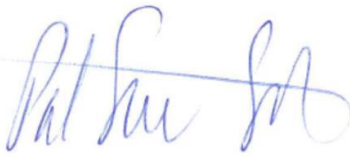
Risk assessment of the candidate's work shall be carried out according to the department's procedures. The risk assessment must be documented and included as part of the final report. Events related to the candidate's work adversely affecting the health, safety or security, must be documented and included as part of the final report. If the documentation on risk assessment represents a large number of pages, the full version is to be submitted electronically to the supervisor and an excerpt is included in the report.

Pursuant to "Regulations concerning the supplementary provisions to the technology study program/Master of Science" at NTNU §20, the Department reserves the permission to utilize all the results and data for teaching and research purposes as well as in future publications.

The final report is to be submitted digitally in DAIM. An executive summary of the thesis including title, student's name, supervisor's name, year, department name, and NTNU's logo and name, shall be submitted to the department as a separate pdf file. Based on an agreement with the supervisor, the final report and other material and documents may be given to the supervisor in digital format.

☒ Work to be done in lab (Water power lab, Fluids engineering lab, Thermal engineering lab)

☐ Field work

Department of Energy and Process Engineering, 15. January 2017

_____

Pål-Tore Storli

Academic Supervisor

Research Advisor: Bjørnar Svingen

PREFACE

The work of this master thesis is completed through the autumn of 2017 at the Waterpower Laboratory at the Norwegian University of Science and Technology (NTNU). My supervisor, Pål-Tore Selbo Storli in cooperation with Torbjørn Nielsen, had an interesting idea creating this thesis case problem. The idea they had in mind was a new simplified one-term friction model valid for unsteady flow conditions. The assignment handed to me was thus to test the new one-term friction model, and see how it would perform for unsteady flow. The work was divided into two stages. First, a practical part, establishing a dynamic test rig inside the laboratory, providing with real data to evaluate simulation results. Secondly, performing simulations of selected friction models and comparing the results against laboratory measurements.

It has been an excellent and enjoyable learning process, providing me with great experiences on simulation tools, associated laboratory work, and knowledge in fluid theory. I am thankful for the opportunity to accomplish such an interesting and varying assignment in an indescribable good job environment.

I will accentuate a great thank to my supervisor Pål-Tore Selbo Storli for providing me with excellent guidance, discussions and help at any time through the project. I would also like to give a big thank to Trygve Opland for an incredibly good work on the dynamic test rig, and Bård Aslak Brandåstrø for guidance on the management of the machinery in the laboratory. Finally, thanks to the Ph.D. students Bjørn Solemslie and Carl Bergan for their help and general tips and tricks.

<div align="center">

Trondheim, 10 June, 2017

Isak Bergset

</div>

ABSTRACT

Power companies are on a daily basis making operational strategies to operate power plants in an efficient and good way. To do this must all impacts and challenges with influence be comprised in the analytical work. In a hydropower plant, one of these challenges is related to the estimation of friction impact from dynamics generated after regulating the water flow in the conduit. Usually are power plants constructed to operate at specific flow conditions, such operation condition may nowadays be difficult to maintain or not desirable as price and demand in the power network are always changing. To operate with economic advantage, is it thus important to find the optimal production that corresponds to the optimal combination of price and demand. Hence, the plants has to be regulated. Similar experience occur at some large hydropower plants as they have the responsibility for maintaining the stability of the network frequency by balancing the power production against consumption. Regulation introduce as mention the system to harmonic oscillatory flow, which further presents the challenge of friction modeling. The frictional effect may be difficult to foresee, as the knowledge on the frictional response is undesirably low. Economic losses and expected production are thus hard to estimate. It is thus of interest to purpose a model that can estimate the losses in a manageable way, not requiring too much computational power.

In hydropower plants are one of the generated dynamics called mass oscillations, where the water mass is oscillating between two free surfaces, the surface of the upper reservoir and the surge shaft. There are today few simple models suited to predicting these oscillations. The existing models require a lot of computational power, making them unfit for power companies to use in their daily work. This challenge is one of the main motivation for this thesis, and will thus be the subject of interest to investigate closer.

In the early phase of this thesis was a paper written on the work presented in a project work made by the author in the autumn of 2016 [1], and additionally the planed work of this thesis. The paper was presented at the 7th International symposium on Current Research in Hydraulic Turbines (CRHT-VII) at Kathmandu University in April 2017 and is attached in Appendix H.

The thesis starts with presenting fundamental theory and existing literature on the subject of conduit flow, friction modeling and flow dynamics in hydropower plants. Further, is the experimental test described with laboratory facilities and supported preliminary work. The thesis provides with knowledge and experience on frictional losses through five test cases,

which is tested in the established dynamic test rig. The test results are compared against simulations. Four transient friction models are tested, the Quasi-steady model, the model by Ogawa et al., the model by Vitkovsky and the idea of the one-term friction model. The simulation approach for all models is described in detail before results are presented and further discussed.

In the preliminary work was a dynamic test rig for measurements on harmonic oscillatory flow designed, where necessary instruments, sensors and components are installed. Four static pressure transducers and one electromagnetic flowmeter respectively measure pressure and flow rate. One of the pressure probes was located in the surge shaft to measure the water fluctuation. Five meters downstream the upper tank is the EMF located, giving the flow rate and mean velocity. All sensors installed are located at preferred locations, satisfying fully developed flow. Additionally, a test section is established, facilitated for water flow visualization with particle image velocimetry. The dynamic test rig performed well, running with both the traditional surge shaft and the siphon system. Test results from laboratory measurement showed good correspondence on dynamic transient theory and how the dynamics are expected to propagate.

Unsteady flow conditions introduced the fluid to additional friction, where acceleration, deceleration and zero average velocity was present. Simulation results from different models showed large variety in performance. The change in velocity seems to be the main parameter affecting the performance of the diverse modeling results. Performance showed strong relation to how each model was implementing the velocity. Flow acceleration and zero average velocity in the turnings of the oscillations seems to be the main challenges of friction modeling. The new "one-term" model shows a positive trend by providing extra friction in relation to the original Darcy-Weisbach equation under acceleration and deceleration, which correspond to measurement results.

The thesis will describe the challenges closer and evaluate the models in more detail, and thus positively contribute to increasing the knowledge on the subject.

SAMMENDRAG

Hver dag lager kraftprodusenter en strategis plan for å drive kraftverk effektiv og tilfredsstillende. I en slik strategi er det nødvendig å inkludere alle elementer som er med på å påvirker sluttresultatet både med tanke på sikkerhet, økonomi og krav. I et vannkraftverk er ett av disse elementene relatert til ustabil strømning ved volumstrømsregulering, et element som kan være utfordrende å estimere.

Vannkraftverk er normalt konstruert for å driftes i et gitt best-punkt. I dagens samfunn kan dette punktet være vanskelig å opprettholde eller til tider ugunstig ettersom pris og etterspørsel på kraft varierer. Derfor er det ønskelig å legge en strategisk driftsplan for å kunne drifte kraftverk best mulig økonomisk. Et varierende best-punkt gir et ønske om å regulere driften, for å oppnå et optimalt sluttresultat. Reguleringen er med på å generere uønskede dynamikker som gir ugunstige harmonisk oscillerende strømninger. Utfordringen ved regulering oppstår også for de største kraftverkene når de driftes for å opprettholde en balansert nettfrekvens, ettersom frekvensen er avhengig av balansen mellom produksjon og etterspørsel.

Ustabile strømninger viser seg å påtrykke en ekstra friksjon på vannet, en friksjon som kan være utfordrende å identifisere eller bergene i den daglige driftsplanleggingen. Økonomiske tap og forventet produksjon er dermed vanskelig å forutse for kraftprodusentene, noe som gir grunnlag for et ønske om å kunne utvikle en modell som kan estimer friksjonen i ustabil strømning på en effektiv og enkel måte.

En av dynamikkene som genereres ved regulering er masseoscillasjoner, der vannet strømmer frem og tilbake mellom vannreservoaret og svingekammeret. I dag eksisterer det få enkle modeller for å beregne slike masseoscillasjoner, og de modellene som er tilgjengelige er ofte komplekse og krever generelt mye bergeningskraft, noe som gjør dem ugunstige i det daglige planleggingsarbeidet. Det er derfor et ønske om å oppnå mer kunnskap på slike strømningssituasjoner og modelleringen av selve friksjonen, noe som er en stor motivasjon for oppgavens studie.

I en tidlig fase av arbeidet ble det skrevet en fagartikkel, som baserer seg på forarbeidet og deler av masteroppgavens startfase med mål og beskrivelse. Forarbeidet ble gjennomført av forfatteren i en prosjektoppgave høsten 2016 [1]. Fagartikkelen ble presentert på et seminar i Katmandu den 4.mars 2017 (7th International symposium on Current Research in Hydraulic Turbines (CRHT-VII) at Kathmandu University in April 2017) med interessante og spennende

tilbakemeldinger som gav godt grunnlag for videre studie. Fagartikkelen, slik som den ble presentert i Katmandu ligger vedlagt i Appendix H.

Masteroppgaven starter med å presentere grunnleggende teori innenfor rørstrømning, dynamiske strømningsforhold, friksjon og metoder for å beskrive vannets oppførsel matematisk. Videre tar oppgaven for seg etableringen av en dynamisk test rig med tilhørende sensorer og komponenter. Rigen er designet for å gjennomføre tester på harmoniske strømningsforhold, med fire trykksensorer og en volumstrømsmåler. En av trykksensorene er installert lengst nede i svingekammeret for å kunne gjøre gode målinger på de nevnte masseoscillasjonene. Alle målesensorer er installert på tilfredsstillende lokasjoner, der strømningen er antatt å være fult utviklet. Det er i tillegg blitt etablert en testseksjon av pleksiglass, tilpasset optisk fotografering av vannprofilen.

Studiet tar for seg en testkampanje gjennomført på den dynamiske testrigen. Kampansjen tar for seg fem ulike strømningssituasjoner, og ble gjennomført uten problem og med gode måleresultater. Målingene har så blitt satt opp mot simuleringsresultater, der fire friksjonsmodeller er simulert for de fem ulike strømningssituasjonene. Modellene som er testet er den Quasi-stasjonere modellen, modellen av Ogawa et al, Vitkovskys modell og en ny «one-term» modell. Modellene og simuleringsmetode er beskrevet i detalj før resultatene er presentert og diskutert nærmere.

Resultatene viser stor variasjon i nøyaktighet fra modell til modell, og fra case til case. Det kommer tydelig fram at de modellene som er spesifikke designet for ustabil strømning gir best estimering av vannets oppførsel. Beregning av friksjonen i akselerasjonsfasen og i toppunktet til oscillasjonene, der gjennomsnittshastigheten er null, viser seg å være de største utfordringene. Oppgaven tar for seg disse utfordringen nærmere ved å evaluer målinger opp mot simuleringsresultater, modellstruktur og bidrag fra ulike strømningsparametere som er bygd inn i modellene. Den nye og enkle en-dimensjonale «one-term» modellen viser positive tendenser ved å gi ekstra friksjon i forhold til den originale Darcy-Weisbach ligningen under ustabile strømninger, noe som samsvarer med måleresultatene.

TABLE OF CONTENTS

LIST OF TABLES

Appendix

LIST OF FIGURES

Appendix

LIST OF SYMBOLS

Latin	Unit	Description
A	m^2	Cross-section
a	m/s	Speed of sound
a	m/s^2	Acceleration
B	-	The one-term model constant
C	-	Vardy shear decay coefficient
C0	-	Calibration constants
C1	-	Calibration constants
D	m	Diameter
D$_H$	m	Hydraulic diameter
E	Pa	Young modulus
e	m	Thickness of the pipe
e	-	Error
g	m/s^2	Gravity
H	mWC	Piezometric Head
h	mWC	Head loss
k$_i$	-	Loss coefficient, minor losses
K	-	Compressibility factor or bulk modulus
K$_V$	Pa	Ogawa et al. velocity constant
L	m	Length
Q	m^3/s	Flow rate
R	mWC	Loss term
R	m	Radius
Re	-	Reynold number
S	-	Standard deviation
t	s	Time
T	s	Time period
V	m/s	Velocity
v	m^2/s	Kinematic viscosity

X	-	Measurement
x	m	Distance
Z	m	Water level in the surge shaft
ϵ	mm	Roughness
ρ	Kg/m^3	Density
ω	1/s, Hz	Frequency
f	-	Friction factor
f	%	Uncertainty
θ	°, degree	Angle
$\emptyset$	mm	Diameter
Δ	-	Fluctuation, Change
μ	Ns/m^2	Dynamic viscosity
∞	-	Infinity

ABBREVIATION

CFD	Computational fluid dynamics
DAQ	Data acquisition
EMF	Electromagnetic flowmeter
NTNU	The Norwegian University of Science and technology
PIV	Particle image velocimetry
PT	Pressure transducer
RSS	Root-sum-squared
VS	Versus

1 INTRODUCTION

1.1 BACKGROUND

The society is relying on a stable and predictable electrical network. Demand and price alternating by yearly and daily variations make it necessities to regulate the power production. "Norges vassdrag- og energidirektorat" formed in 2004 a regulation on supply quality in the Norwegian power network to prevent damage on electrical devices and avoid undesired downtime [2]. The regulation considers several demands on distribution in the power network, where limits on frequency and maximum voltage fluctuations are of great importance. The frequency is set to be stable at 50 Hz and the maximum voltage fluctuation on $\pm$ 10% nominal voltage [2]. Power balance achieves a stable frequency, and it is thus important to regulate the power production to satisfy power demands. Power plants of a certain size are mainly utilizing the balance work, having the available capacity to influence the power fluctuations. Such regulations can cause operational disadvantages, since operating outside their optimal operation point will affect their efficiency.

1.2 INTRODUCTION TO WATER FLOW IN HYDROPOWER

Hydropower plants produce power by utilizing the head difference between the water surface in the upper reservoir and down to the turbine inlet. The pressure difference works as the driven force of the system. The most common way to transport the water from the upper reservoir to the turbine is by a closed conduit. The water can either flow in steady or unsteady condition depending on the system operation. To obtain good and satisfying results on system analyses, are system conditions and flow regimes essential to identify. Rate and change in pressure and velocity are key parameters to predict and understand to be able to foresee the behavior of the water. The study of water flow in a closed conduit is an interesting and relevant topic for both power companies, to establish a good operational strategy, and for research, obtaining increased knowledge about conduit flow. Undesired flow conditions happen regularly in the daily operation, resulting in complex calculations to predict the impact of the dynamics, which further may lead to an unrealistic high-expected output benefit. The subject is a discussed issue and of

Introduction

great interest to both industry and research. Over the last 60 years, several models have been presented to estimate and describe the dynamic behaviors. These models show good approximations for steady state conditions, but provides variating results for the transitional flow. The knowledge on the frictional losses in such conditions are limited, and existing models usable in such flow require massive computational power to be solved. The specific dynamic investigated in combination with how many directional dimensions to consider decides the complexity of the calculation. The most common source of transient flow conditions in hydropower plants are [3]

- Load regulation in the turbine
- Sudden load change
- Valve and pump operations

In closed conduit, transient behavior is common to divide into two phenomena. One called the water hammer, and the other called mass oscillation. Both dynamics cause substantial negative consequences on safety, and contribute to additional energy losses. It is therefore important for power companies to foresee the behavior to handle or minimize the applied dynamics and predict the additional losses. A hydropower plant in steady state flow is depicted in **Figure 1-1**, assuming normal operation conditions. The difference between the water level in the upper reservoir, H_R, and the water level in the surge shaft, H_S, is the head loss generated in the horizontal pipe. This total head loss is divided into two, one representing the frictional losses and the second one the additional disturbances, also called minor losses.
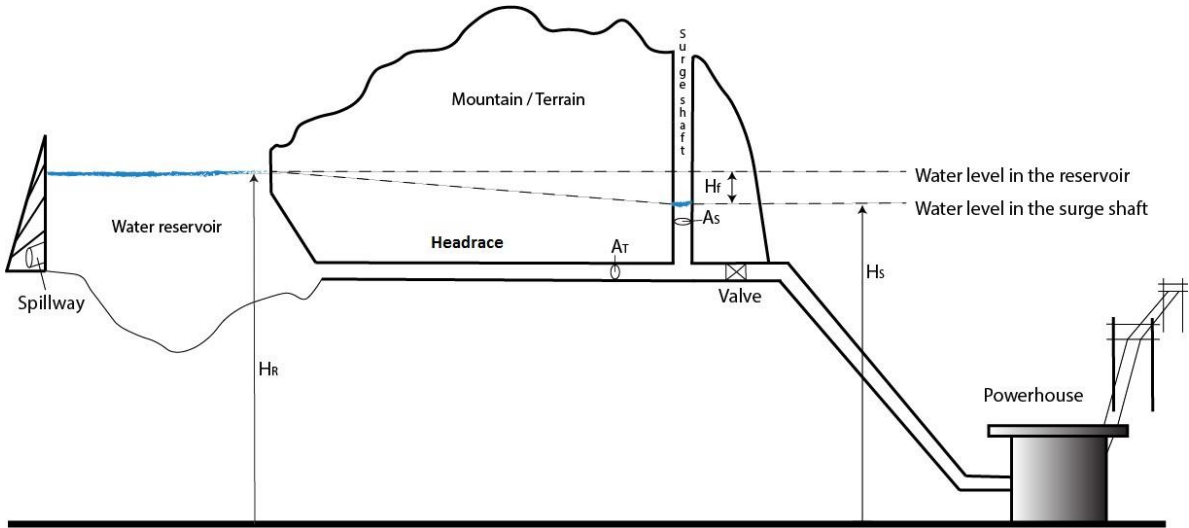
Figure 1-1: *Schematic drawing of a hydropower plant*

The total head from the upper reservoir to the powerhouse, subtracting the head losses, provides the total output power available for electrical conversion. It is thus important to identify each source of power loss and be able to predict their rate of impact. The size and influence of the frictional losses depend on the present flow condition. In closed conduit flow, the frictional loss of interest is generated between the fluid particles and the friction between the fluid and the surface of the pipe, while minor losses take care of the additional disturbances.

Disturbances and flow regulations are as mention one of the main sources of generating hydraulic transients. These dynamics propagates in uncountable ways, considering size and frequency, experienced as oscillating waves. The behavior is mainly determined by the system specification if it is not disturbed by other external systems. Chapter (2.1) describes these dynamics closer.

1.3 OBJECTIVE

The purpose of this thesis is to investigate the slow transient behavior of mass oscillation. The aim is to achieve a greater understanding of the frictional losses concerning the generated dynamic. A dynamic test rig provides the opportunity to investigate the subject further, by performing a test campaign on different flow scenarios. The test rig generates the mass oscillations by sudden valve closure or a water column separation.

Dynamic transients in water is a broad and complex topic, and may, therefore, be needless and unnecessary to study all aspects if the impact has insignificant small influence on the particular issue. A selection of three existing friction models and one new friction model are simulated and compared up against real data collected from the dynamic test rig in the laboratory.

Pål-Tore Selbo Storli and Torbjørn Nielsen at the waterpower laboratory at NTNU discussed a curious idea on a simplified one-term friction model valid for both steady and unsteady flow conditions. A test of this new one-term model is one of the primary motivations for this thesis. The results will show if this is an idea to work further with or if the idea is useless. The idea bases on developing a model that just involve one friction term, modified to be valid at unsteady flow conditions, and having a low demand of computational power. Hopefully, will the idea contribute to a simpler and less demanding equation to calculate the frictional losses in unsteady flow.

1.4 FRAMEWORK

This thesis` is a continuance of a preliminary work by the author in the autumn of 2016, *Establishing a test rig for investigations of flow transient* [1]. The preliminary work was to design a dynamic test rig for the purpose of investigating flow transients and prepare for the work presented in this master thesis. The rig was almost finally established, having just small efforts remaining before the tests could start. The work was initially started by Lise Rikstad in her master thesis from autumn of 2015 to the spring of 2016 investigating the expected behaviors and limitation of the system [4]. This thesis has finalized the remaining work from the preliminary assignment. The remaining was divided into two stages. First, mount the horizontal pipe system to the test section, and connect the upper reservoir to both the supply water and the spillway. Secondly, all measuring devices needed to be installed and calibrated. All pipe sections were assembled, and are now ready for the establishment. Required instruments are available in stock. The Water Power Laboratory located at NTNU Gløshaugen hosts the dynamic rig, providing the necessary space, equipment and flow requirements. The test rig was designed with three different test lengths and two different shaft designs. The shaft may run as a traditional surge shaft or as a siphon system. Both systems are generating the desired transitional flow but in two different ways. The siphon shaft provides the opportunity to investigate energy behavior in more precise condition since the energy needed to accelerate the water may be neglected, as the water in the siphon shaft will be in motion when the dynamics are generated.

1.5 THESIS STRUCTURE

The final report presents the thesis work in seven main chapters including appurtenant subchapters to create a systematic and natural reading. The first part of the thesis introduces the reader to the phenomena of mass oscillation and water hammer. An introduction on how to use mathematical methods to describe fluid motion and how to modeling the experienced friction through friction models are further presented, before considering the established dynamic test rig and experimental test campaign. The results and discussion are merged to present the findings in a reader-friendly approach, where measurements and modeling results are evaluated. The work is at the end summarized in a short conclusion, followed by a proposal for further work. Some accompanying calculations, instrument specifications, and two written materials, covering a paper on the thesis and a risk assessment for the laboratory work are found as Appendix.

2 THEORY

The theory chapter addresses a closer review of the phenomena of mass oscillations and an introduction to the water hammer. Subsequently, the approach on how to model fluid motion with a numerical method using friction models and related parameters are described.

2.1 GENERATED DYNAMICS IN HYDROPOWER

There are as mention two main dynamics generated in the operation of a hydropower plant. In separated subchapters below are these dynamics described closer, providing with knowledge to help understand the results of the modeling and observations in the dynamic test rig.

2.1.1 Slow transients – Mass oscillations

Mass oscillations are propagating with a relatively low frequency. In such conditions, may elasticity be neglected and all changes in flow parameters may be assumed to happen at the same time throughout the whole water string as the wave propagates towards infinity and thereby no velocity change in the space variable. U-tube oscillation is a common name of these mass oscillations, as the flow is oscillating between the surge shaft and the upper reservoir. The surge shaft is installed to reduce the applied force from the dynamics of the pipe system making the oscillations be slowly damped until it eventually goes to rest.

Figure 2-1 illustrates the basic U-tube oscillation in a hydropower plant, where the water level in the upper reservoir is assumed stationary throughout the whole sequence. The water level in the surge shaft will, on the other hand, oscillate between maximum and minimum swing boundary with a constant time period. The system friction will gradually damp the oscillations back to stationary level.

Theory
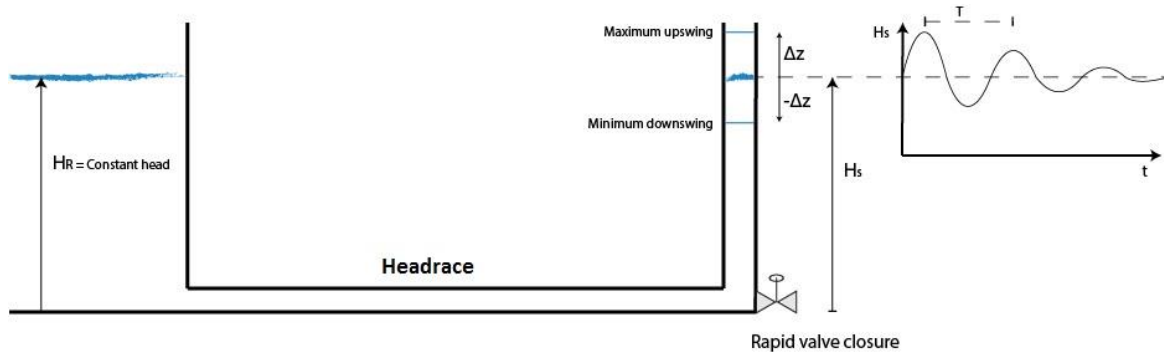
Figure 2-1: *Schematic illustration of mass oscillation in a traditional surge shaft*

Eq.(1) and Eq.(2) estimate the maximum and minimum water fluctuation, ΔZ, counting the system friction. Where the sign in front of the volume flow states if the level rises or decreases [3].

$$\Delta Z_{max} = \Delta Q \sqrt{\frac{\Sigma \frac{L}{A_T}}{gA_s}} + \frac{1}{3}h_f \qquad (1)$$

$$\Delta Z_{min} = -\Delta Q \sqrt{\frac{\Sigma \frac{L}{A_T}}{gA_s}} - \frac{1}{9}h_f \qquad (2)$$

Where, A_T and A_S are the cross-section of the headrace and surge shaft respectively. L is the length of the pipe, g is the gravitational acceleration, Q is the flow rate and h_f the experienced head loss.

The natural frequency, ω, of the oscillation is given by Eq.(3), and the time period, T, in Eq.(4).

$$\omega = \sqrt{\frac{g}{A_s * \left(\frac{L}{A_T}\right)}}$$ (3)

$$T = \frac{2\pi}{\omega}$$ (4)

2.1.2 Fast transients – Water hammer

The water hammer is the high pressure arising in front of the closing valve immediately after closure. The pressure will further propagate in a fast oscillating behavior, back and forth in the pipe, until it is eventually is damped out by the system friction. Even if the main focus of this thesis is the slow transient of mass oscillations, may it be important to have knowledge of the water hammer, as the fast dynamics are visible in the raw data from the pressure measurements.

Below is a short step-by-step illustration of the water hammer phenomena. A rapid closure of a valve downstream a reservoir in a though hydropower plant generates the water hammer.
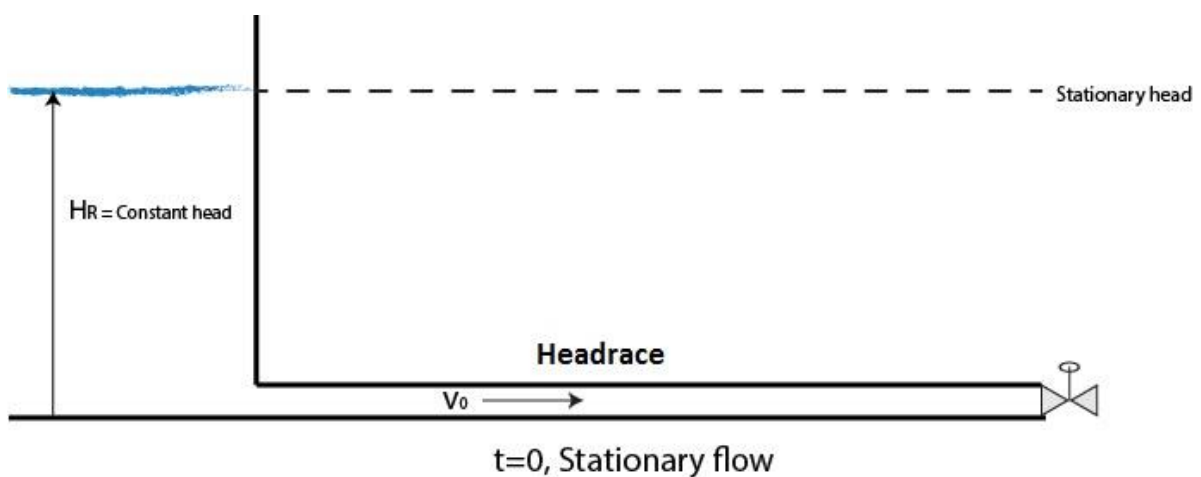
Figure 2-2: *Expected pipe flow at stationary flow*

Theory

$$0 < t < L/a, \text{Valve closed}$$
$$\partial v/\partial t < 0 \text{ and } \partial v/\partial x < 0$$
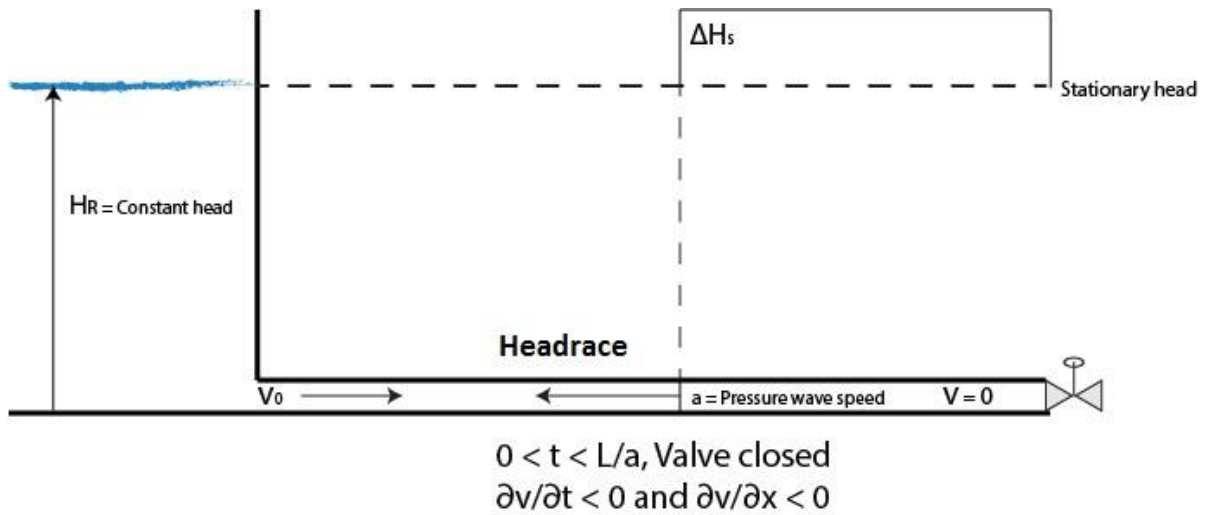
Figure 2-3: Expected pipe behavior at deceleration in first time period

Figure 2-2 depict the system at stationary flow, while **Figure 2-3** illustrates the behavior after the valve closure at the end section. At this point will the water velocity be brought to zero, generating a pressure increase in front of the valve. The pressure will further propagate as a wave towards the reservoir, stretching the pipe wall and finally bring the fluid to rest, as depicted in **Figure 2-4**. When the pressure reaches the reservoir, all kinetic energy has converted to elastic energy [5].

$$t = L/a, \text{Valve closed}$$
$$\partial v/\partial t < 0 \text{ and } \partial v/\partial x > 0$$
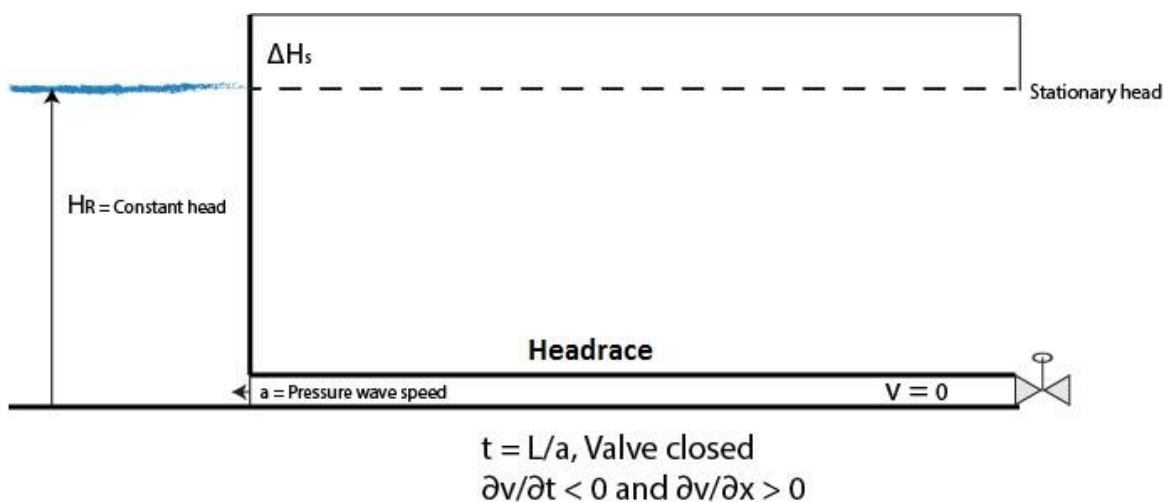
Figure 2-4: Expected water hammer behavior at the time equivalent to (L/a)

The pressure in the pipe inlet is, however, unchanged and the fluid starts to flow backwards into the reservoir, as depict in **Figure 2-5**. This neutralizes the pressure in the pipe converting it

back to the original pressure before the closure of the valve. This information reaches the valve and the velocity is negative throughout the pipe.

$$L/a < t < 2L/a, \text{Valve closed}$$
$$\partial v/\partial t < 0 \text{ and } \partial v/\partial x > 0$$
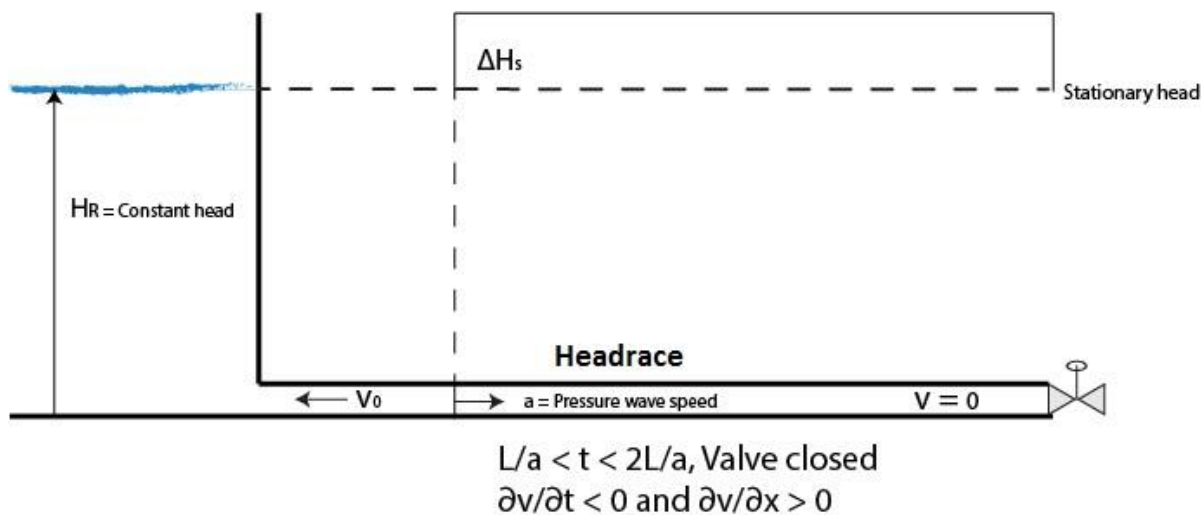
Figure 2-5: Expected water hammer behavior at time equivalent to (L/a) to (2L/a)

The fluid at the valve is brought to rest and a negative pressure develops, since the valve is closed, as depict in **Figure 2-6**.

$$2L/a < t < 3L/a, \text{Valve closed}$$
$$\partial v/\partial t > 0 \text{ and } \partial v/\partial x > 0$$
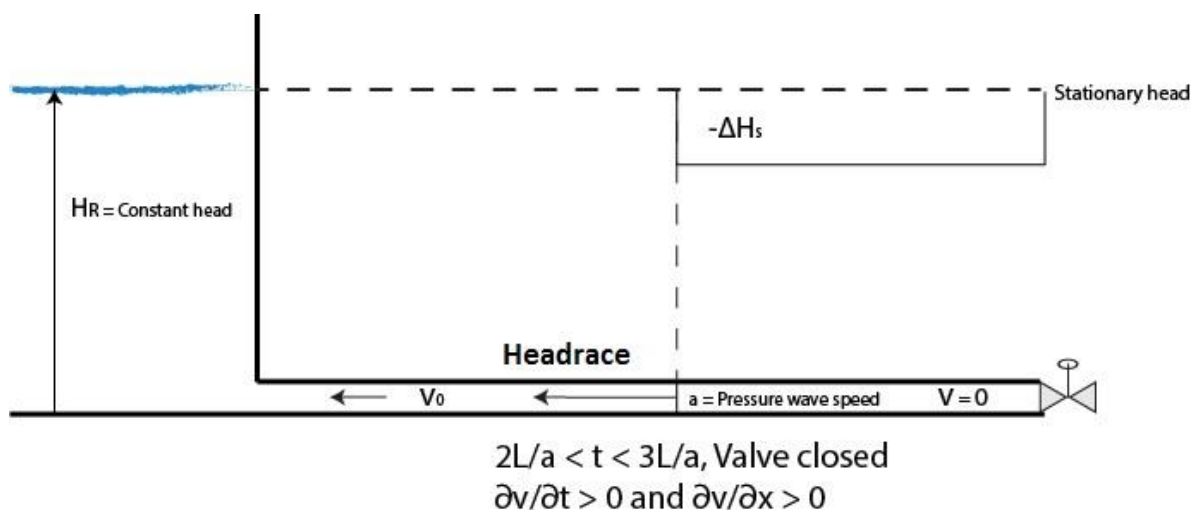
Figure 2-6: Expected water hammer behavior at time equivalent to (2L/a) to (3L/a)

This pressure wave contracts the pipe walls as it travels back to the reservoir, where it is neutralized and starts to flow back into the pipe, as depict in **Figure 2-7**

Theory
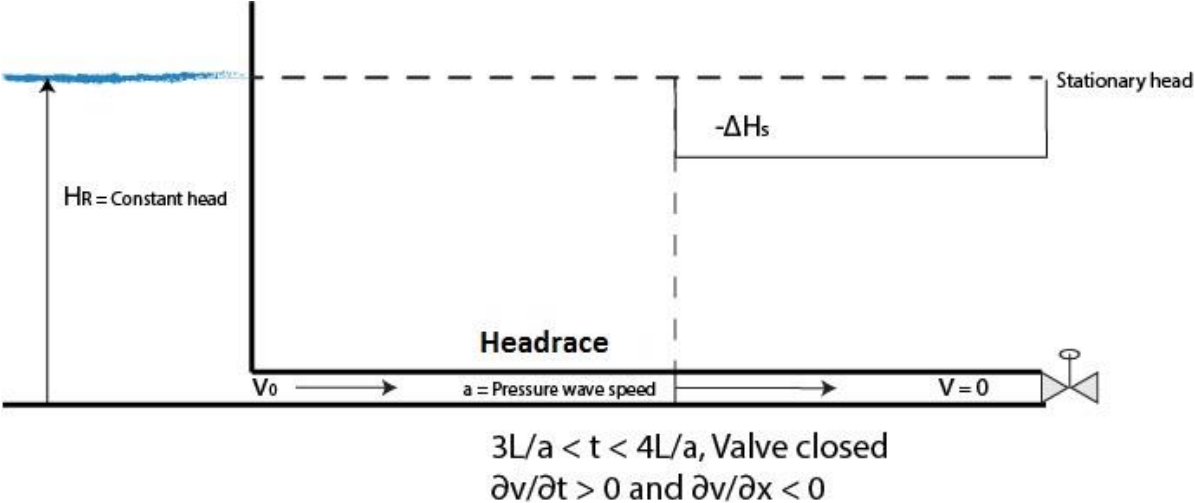
Figure 2-7: Expected water hammer behavior at time equivalent to (3L/a) to (4L/a)

This process repeats itself until it is dampened out by the friction and the imperfect elasticity in the pipe. Eventually the fluid is brought to rest.

The time period, T_p, of the oscillating pressure in a non-friction system is depending on the water way length and speed of sound.

The time period is found by Eq.(5).

$$T_p = \frac{4L}{a} \tag{5}$$

The next subchapter address the topic of how to describe the fluid motion mathematical by use of the fundamental Navier-Stoke equation.

2.2 NAVIER-STOKES

Fluid may consist of gas, water or plasma. These conditions are depending on several properties, which for a real case will always change in time and position. The fluid can be compressible or incompressible, static or dynamic, steady or unsteady, and likewise [6]. All these conditions are important to determine or be able to assume when describing fluid behavior and it abilities.

The basic equations of Navier-Stoke describe the motion of viscous fluid and gasses. The solution of the equations presents the flow velocity, which may further be used to describe other flow parameters like pressure and temperature. Considering Newton second low on the fluid of interest, may these equations be formed. It is common to look at fluid as real or ideal, where the main difference between them is that for ideal flow is the fluid assumed incompressible and with no viscosity. In hydraulic engineering is the flow typically considered ideal, since water shows significantly small deformation under shear force [6].

The incompressible Navier-Stoke equation, given in Eq.(6), acts as the fundamental equation for water flow, which describes the behavior of water in conduit flow [6].

$$\frac{\partial V}{\partial t} + V\nabla * V - v\nabla^2 V = -\nabla H \tag{6}$$

Where, V is the velocity, t is the time variable, v is the kinematic viscosity, H is the piezometric head and ∇ is the Nabla-operator counting for the change in three-dimension. The Nabla operator is defined as Eq.(7) considering a cartesian coordinate system.

$$\nabla = u\frac{\partial}{\partial x} + v\frac{\partial}{\partial y} + w\frac{\partial}{\partial z} \tag{7}$$

Where the component u, v, w are functions of the variables x, y, z, describing the change in space. The three terms are called the convective terms and describe the movement of a flow variable from one point in the space to another [6].

Theory

In unsteady flow conditions, the flow may changes in x, y and z directions. Hence, all convective terms should be incorporated. In steady conditions may y and z be neglected. This condition is valid to assume where fluctuations of properties in some directions are negligibly small. Two-dimensional change at the inlet may be assumed when considering flowing water in a closed conduit. When reaching the fully developed flow, one-dimension representation is justified to assume. In the case of a circular pipe, the one-dimension variation will be in the radial direction. The simplifications on reducing the dimensions require boundary conditions. It is common to predict the wall as non-slip and to have knowledge of velocity and pressure at inlet and outlet [6].

In this thesis will the calculations be simplified with assumptions valid for slow transients, as the subject of interest is narrowed down on the slow mass oscillations generated.

2.3 GOVERNING EQUATIONS – PIPE FLOW

Navier-Stokes forms the governing equation describing the transient conditions in pipes, considering the law of momentum and continuity. The literature derive simplified equations valid for ideal fluids reduced to a one-dimensional representation [7]. The equation of momentum and continuity in one-dimension is derived respectively as Eq.(8) and Eq.(9).

$$\frac{\partial H}{\partial x} + \frac{1}{g}\left(\frac{\partial V}{\partial t}\right) + h_{f,\ Total} = 0 \tag{8}$$

$$\frac{\partial H}{\partial t} + \frac{a^2}{g}\left(\frac{\partial V}{\partial x}\right) = 0 \tag{9}$$

Where, D is the pipe diameter, $h_{f,Total}$ is the total head loss term and a is the wave propagation speed.

These two equations are the basic equations describing water in motion and thus used as a ground equations for transient modeling. In the equation of momentum are the Newton second law describing that all forces acting on a mass of fluid in a given direction is equal to the product

of mass and acceleration. In the equation of continuity is the principle built on that the total applied mass into a system must equal the time rate of change of mass inside the system [5].

The propagation speed of the wave depends on the dynamic of interest to model. The wave speed considering a stiff and thick pipe is found by Eq.(10).

$$a = \frac{\sqrt{\frac{K}{\rho}}}{\sqrt{1 + \left(\frac{K}{E}\right)\left(\frac{D}{e}\right)}}$$

(10)

Where K is the compressibility factor or bulk modulus. E is the Young modulus corresponds to the stiffness of the material and e is the thickness of the pipe [3]. The system and water at slow transients are as mention typical to assume incompressible. Hence, the wave speed goes towards infinity, making the acceleration in space equal to zero. In water the speed of sound is assumed to be approximately, $a \approx 1450 \left[\frac{m}{s}\right]$ [3].

Frictional forces, on the other hand, affects the fluid motion significantly more. It is thus important to enable suitable equations to estimate the frictional force experienced by the water. The next subchapter introduces the friction term.

2.4 HEAD LOSS

The head loss in conduit flow is as mention dependent on both frictional forces, h_f, and minor losses, $h_{f\,minor}$, applied by objects, components or encroachment in the flow path. Following equation expresses the total head loss.

$$h_{f\,Total} = h_f + h_{f\,minor}$$

(11)

Theory

2.4.1 Frictional losses h_f

In unsteady flow, the frictional losses are commonly divide into a quasi-steady term and an unsteady term, as depict in Eq.(12). The quasi-steady term counts for the losses at steady state, while the unsteady term counts for the additional losses caused by the unsteady flow. Separating the steady state friction from the unsteady friction term introduces the advantage of just considering the steady state friction term at steady state. If just considering the steady state friction at unsteady flow, the model approach is called Quasi-steady friction model.

$$h_f = h_{f,q} + h_{f,u} \tag{12}$$

Where the indices u and q are referred as quasi-steady and unsteady term, respectively.

The experienced friction on the fluid depends on the flow condition, usually divided into three regimes, laminar, turbulent and transitional flow. The structure of the flow is separating the regimes, which depends on the fluid velocity. The non-dimensional Reynolds number (Re number) defines the regime. The Re number indicates the viscous effect compared to the inertia effect [6]. Eq.(13) determines the Re number.

$$Re = \frac{\rho V D_H}{\mu} = \frac{Q * D_H}{v * A} \tag{13}$$

Where, ρ is the density of the fluid, D_H is the hydraulic diameter, μ is the dynamic viscosity, A is the pipe cross-section.

Following is a the boundaries between the different regimes described by the Re number

Laminar, at low velocity and Re < 2300

Transitional, at moderate velocity and $2300 <$ Re < 4000

Turbulent, at high velocity and $4000 <$ Re

Flow in transitional condition behaves with fluctuating streamlines, where both the laminar and turbulent regime is present. The unsteady conditions divide the flow into uniform and non-

uniform flow, depending on the velocity of the specific dynamic in the fluid. Uniform flow assumes an equal average velocity over the whole cross-section of the conduit and is common to assume in existing friction modeling on slow transients. Non-uniform flow regards fast transients, where the change in a specific cross-section of the pipe occurs before reaching another cross-section. The pressure in the conduit after a sudden valve closure in a hydropower plant will propagate as the non-uniform behavior.

The next subchapter describes the estimation of the quasi-steady friction term at laminar and turbulent flow regimes before the next subchapter considers the unsteady friction term.

2.4.1.1   The quasi-steady friction term $h_{f,q}$

Julius Weisbach presented in 1845 a further developed equation from Henry Darcy, which made it possible to estimate the frictional head loss in steady state pipe flow [6]. The equation is called the Darcy-Weisbach equation, and is depicted as follows

$$h_{f,q} = f \frac{L}{D} * \frac{V * |V|}{2g} = f \frac{L}{D} * \frac{Q * |Q|}{2 * g * A^2} \ [mWC] \tag{14}$$

Where f is the friction factor.

Eq.(14) uses the average velocity expressed by $V = \frac{Q}{A}$ to express the head loss to take care of the change in velocity. The absolute sign handle the direction of the flow, making the head loss always act against the flow. The size of the frictional impact depends on the flow conditions and the value of the friction factor.

The flow regimes separate the approach on how to calculate the friction factor. At steady state, the friction factor is assumed constant, while in the unsteady flow where the flow varies must the friction factor be estimated for each time step. The two next subchapters describe how to estimate the friction factor in laminar and turbulent flow.

Theory

2.4.1.1.1 Laminar friction factor

Laminar flow assumes the flow to just act in the x-direction, and is as mention present if the Re number is lower than 2300. In a circular pipe at laminar flow is the friction factor, also called the Darcy-Weisbach friction factor found directly from Eq.(15).

$$f_{laminar} = \frac{64\mu}{\rho D V_{avg}} = \frac{64}{Re} \tag{15}$$

2.4.1.1.2 Turbulent friction factor

At turbulent flow is the friction factor more complex to estimate. Now, will the velocity have radial components, and in addition to the laminar friction factor will the roughness of the pipe wall have an influence on the friction. The non-dimensional Moody chart and the implicit formula from Colebrook is two common methods of estimating the turbulent friction factor. Lewis Ferry Moody presented in 1944 a chart that plots the relationship between the friction factor and the Re number at different values of the relative roughness of the specific material. The friction factor, found from the chart, may be directly added into the Darcy-Weisbach equation to estimate the pressure loss.
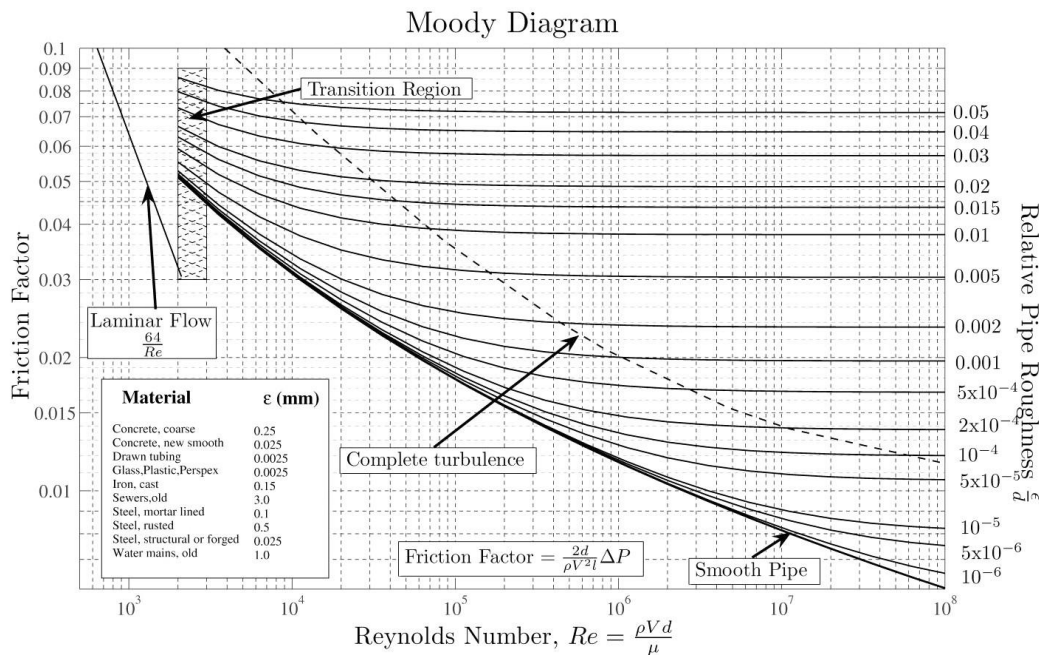
Figure 2-8: *Moody chart [6]*

The Moody charts, shown in **Figure 2-8**, depict the parameters of interest in the x- and y-direction, suitable for steady state flow for both laminar and turbulent condition. At the transitional area, illustrated with a shaded zone, the friction factor will always fluctuate. Hence, the chart is not applicable in this zone.

The second approach is the implicit Colebrook-White equation presented by Colebrook and White in 1939, where they expressed the friction factor at turbulent flow in a logarithmic equation, taking the friction factor and the relative roughness of the pipe material into consideration.

Colebrook-White equation is depict by Eq.(16), where the friction factor is found for each time step by an iterative approach [6].

$$\frac{1}{\sqrt{f}} = -2\log\left(\frac{2.51}{Re * \sqrt{f}} + \frac{\epsilon}{3.7D}\right) \tag{16}$$

Where $\epsilon \in [mm]$ is the roughness of the pipe surface.

Eq.(16) was further developed by Haaland in 1983, presenting an explicit approximation with 1.5 % accuracy [8]. Further in this thesis is the Haaland approximation used to calculate the friction facot at turbulten condition.

Haaland approximation is given by Eq.(17).

$$\frac{1}{\sqrt{f}} = -1.8\log\left[\left(\frac{\frac{\varepsilon}{D}}{3.7}\right)^{1.11} + \frac{6.9}{Re}\right] \tag{17}$$

2.4.1.2 The unsteady friction term $h_{f,u}$

The presence of unsteady flow complicate the calculations on the frictional losses, due to complex and unpredictable flow. The assumption is as mention commonly assumed to make the calculation easier, as far as it is valid. However, assumptions may be difficult to set, or worse, contributing to a decrease in performance if not handled correctly.

Theory

If the dynamics are large enough may the flow oscillate between laminar and turbulent regime. Hence, the water will not be able to flow in steady state, but rather be a combination of both regimes. In oscillatory behaviors the velocity will always change, making the methods described in the steady state condition insufficient. The study of unsteady flow modeling has been of interest since the middle of the nineteenth century giving several alternative methods to predict the transient losses. They are usually more complex and demands large computational power to be solved, but performs with better accuracy than the common steady state model [7].

The velocity component in the Darcy-Weisbach head loss equation is as mention decided by the average velocity. This average velocity is not giving a proper relation to the friction in unsteady flow, estimating an erroneous result. Hence, an additional unsteady term compensating for the deviation is necessary to implement. The literature presents studies on the velocity profile, if no-slip condition is assumed, the center velocity will be two times larger than the average velocity in steady state [9]. When unsteady flow is generated will the velocity experience large changes with different impact over the cross-section [10]. This fact supports the deviation in performance by just using the average velocity to predict the friction. Use of the average velocity introduces additionally the challenge of zero velocity in the area of turning. Since the flow rate at this point will be zero throughout the whole pipe, is the quasi-steady head losses term estimated equal to zero, $h_{f,q} = 0$. This zero estimation deviates from the real behavior, as the local velocity in the pipe differs from zero. Hamid Zidouh presented in 2009 a laboratory test, looking at the velocity profile at dead end conditions. He investigated the velocity profiles and wall shear stress in turbulent transient pipe flow with Re = 140000. The real velocity profile showed a negative velocity close to the wall and positive velocity in the center [11]. Hence, the local velocity is not zero. **Figure 2-9** illustrates Zidoun's findings.
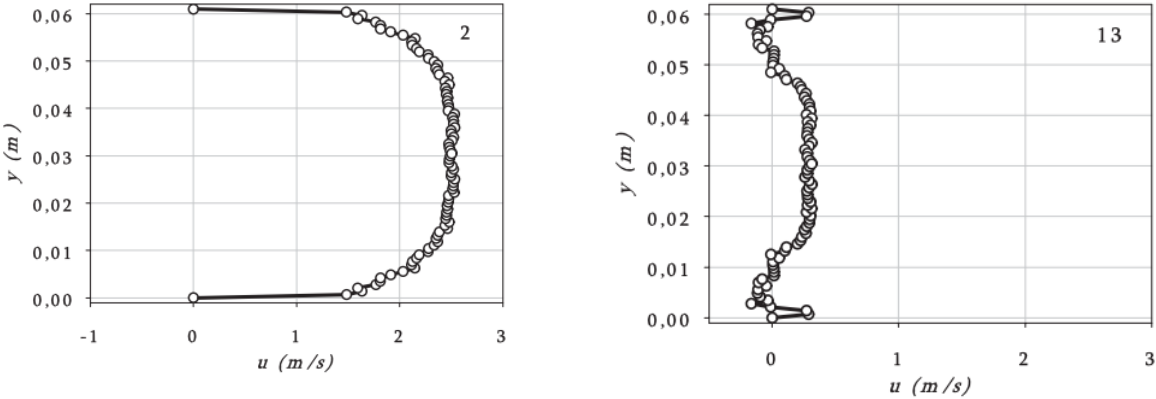
Figure 2-9: *Zidoun's velocity test in unsteady flow. Shows how the velocity profile develops over time*

Another researcher, Pingju Li, presented in 2004 a Ph.D investigating the velocity profile in an oscillating water string in a closed conduit [9]. The results from Li was quite similar to the transient velocity profile presented by Zidouh. The difference was that the center velocity at transient flow had a smoother front, akin to the front of the steady state turbulent velocity profile, being flat in approximately 80 % of the cross-section.

It is tested two existing unsteady friction models in this thesis. These models are the model by Ogawa et al. and the model by Vitkovsky. Chapter (2.6) presents the models closer.

2.4.2 Minor losses $h_{f,minor\ losess}$

Objects, components or encroachment in the flow contribute to additional losses by disturbing the flow. Each type of minor loss has a loss coefficient, defined as k_i, which indicates how large the additional losses are. Eq.(18) determines the pressure loss from minor losses [3].

$$h_{f\ minor\ losses} = k_i * \frac{|V| * V}{2g} = k_i * \left(\frac{Q|Q|}{2 * g * A^2} \right) \tag{18}$$

Now, after deriving the pipe flow equation and the head loss equation, the next step would be to look at the method of simulating the time dependent motion.

2.5 EULER METHOD

A valid and suitable method to solve the governing equations for slow transients is the well-known Euler method. The Euler method is a first-order numerical method solving ordinary differential equations with known initial values. Through Eq.(19) describes the Euler method the water fluctuation in the surge shaft by determining the equation for each time step. The size of the time step decides the accuracy of the calculation [6].

$$Z_{new} = Z_n + dt * \frac{Q_{new}}{A} \tag{19}$$

Where Z_{new} and Z_n are respectively the new and present water level in the surge shaft. The new flow rate, Q_{new}, is found by the continuity equation depending on the flow specification and selected friction model. The next subchapter provides with an introduction on the selected unsteady friction models used in the modeling of the slow mass oscillations generated in the dynamic test rig.

2.6 EXISTING UNSTEADY FRICTION MODELS

In the closer study on friction modeling is the model by Ogawa et al. and the model by Vitkovsky selected. The curiosity is to observe the performances from two models that uses differently approaches. Chapter (2.6.1) presents the model by Ogawa et al., before Chapter (2.6.3) describes the modified model by Vitkovsky, with an introduction to fast transient models in Chapter (2.6.2).

2.6.1 Ogawa et al. friction model

Slow transients seem from the literature to be less studied than the fast transients. Even if there are limited research directly aimed against slow transients, are there some good friction models specified directly on U-tube oscillations. Akira Ogawa et al. presented in 2007 a model. with good performance [12]. The model counts for the mention flat velocity profile described by Li in his Ph.D. in 2004 [9]. The approach by Ogawa et al. describes the U-tube oscillations without the steady state term given by the Darcy-Weisbach head loss equation. Eq.(35) depicts how it uses the equation of motion to describe the fluid motion

$$\rho * A * L * \frac{dV}{dt} = -2 * \rho * g * A * Z - \pi * D * L * v * \frac{dV}{dy} \tag{20}$$

Where the velocity gradient, $\frac{dV}{dy}$, giving y as the distance from the pipe wall to the center of the pipe. Ogawa et al. introduced a velocity constant, K_v, to take care of the change in velocity. The representation is described as follows

$$\frac{dV}{dy} = K_v * \frac{V}{R} \tag{21}$$

Where, R is the pipe radius.

The velocity constant, K_v, is determined by the imaginer Re number, Re_i, taking the imaginary maximum velocity, V_{max}, of the liquid column in the vertical U-tube into consideration. Below is the associated equations presented.

$$V_{max} = Z_0 * \sqrt{\frac{2 * g}{L}} \tag{22}$$

$$Re_i = \frac{V_{max} * D}{v} = Z_0 * \sqrt{\frac{2 * g}{L}} * \frac{D * Z_0}{v} \tag{23}$$

The relationship between the imaginer Re_i and the K_v is empirically estimated as,

$$K_v = 25 * D * \left(1 + \frac{4.5 * 10^{-9}}{D^4}\right) * K_v{'} \tag{24}$$

$$K_v' = \frac{Re_i}{8.75 + 0.00233 * Re_i} \tag{25}$$

Considering the equation of motion and the statements presented by Ogawa et al., the oscillating behavior in a surge shaft can be written as Eq.(26) [12].

$$\frac{d^2Z}{dt^2} + \frac{2 * v * K_v}{R^2} * \frac{dZ}{dt} + \frac{2 * g}{L} * Z = 0 \tag{26}$$

In the paper of Ogawa et al. was the model tested for different liquids with a maximum Re number of 6600. The test showed good results at low Re numbers considering oscillations between two vertical pipes connected by a horizontal pipe [12]. To evaluate the model, is it thus of interest to see if the model fits behaviors on hydropower similar cases, as in the dynamic test rig. The rig will generate relatively higher Re numbers with a system boundary more analogous to a hydropower plant.

2.6.2 Fast transient friction models

How may fast transient models perform at slow transient estimation? This thesis looks closer on the model by Vitkovsky to try proven this question. After a short review on fast transient modeling is the model by Vitkovsky described closer.

Bergant et al. has divided the selection of unsteady friction models into six groups [14]. These groups are further organized into two main categories. One based on the model by Zielke (1968) and the other one from the model by Brunone (1991) [6]. Both models have the similar approach on implementing an additional friction term to the original Darcy-Weisbach head loss equation, counting for the extra friction at unsteady flow.

These two categories are as follows

1) **Empirically based models**:

    Empirical models are made by observation and experiments. Henry Daily presented the first model in 1956 and improved by Brunone in 1991. Brunone implemented a correction coefficient to take care of the reversal in the velocity profile. Several other researchers have then further developed the model by Brunone. Vitkovsky (2001) presented a model

providing the correct sign for the friction loss at different periods of the oscillating behavior [13]. Today this model is widely used.

2) **Physically based models:**

In physically models are the relation described mathematically, and there is no need for calibration constants. The majority of these models are developed from the model presented by Zielke (1968), group five in Bergant et al. Zielke presented a model for laminar flow with frequency-dependent friction. The model used the mean flow velocity and weighted past velocity change to estimate the friction [14]. This model showed great result compared to experimental data but is just considered for low Re number at transient laminar flow. The model has later on been developed further by several other researchers to establish a more accurate model (Trikha 1975, kagawa et al 1983, Suzuki et al 1991) [15], also including turbulent flow (Bratland (1986), Zarzycki (2004), Vardy and Brown (1995,2004)) [14] and specified u-tube dampening model (Svingen (1996)) [16].

Furthermore is a detailed description of the model by Vitkovsky addressed.

Theory

2.6.3 Vitkovsky friction model

The basis for the empirical models are the use of the local acceleration of the mean flow and the convective acceleration to calculate the unsteady term. The model by Brunone showed variating results, performing well for the values of the wave amplitude, but difficulties to predict the shape of the wave satisfyingly. Vitkovsky modified the model to fit better on transients applied by valve operations. The improved model introduced as mention a sign for the convective acceleration term that could predict the direction of the wave at deceleration and acceleration [13].

The equation presented by Vitkovsky is as follow

$$f = f_q + \frac{kD}{V|V|}\left(\frac{\partial V}{\partial t} + asign(V)\left|\frac{\partial V}{\partial x}\right|\right) \tag{27}$$

Where $sign(V)$ is the term correcting the sign in front of the convective term. If $V \geq 0$ the term is +1 and if $V \leq 0$ the term is -1. The k coefficient can be found by utilizing trial and error analyses, or direct use of the Vardy`s shear decay coefficient C. Vardy and Brawn presented the decay coefficient, making it possible to predict the k coefficient at both laminar and turbulent flow. The approach from Vary and Brown are given by the three equations below[13].

$$k = \frac{\sqrt{C}}{2} \tag{28}$$

At laminar flow,

$$C = 0.00476 \tag{29}$$

At turbulent flow,

$$C = \frac{7.41}{Re^{\log\left(\frac{14.3}{Re^{0.05}}\right)}} \tag{30}$$

The most common method to perform simulations on the fast transients is use of the Method of characteristics. The derivation of this method and the approach on how to implanted the method to solve the water hammer may be found well described by J. Paul Tullis in Hydraulics of pipeline [5]. This thesis will not address this topic further.

When considering slow transients and related assumptions, the model by Vitkovsky may be simplified. Chapter (3) derive the simplification and a description on how to implement the model into the head loss estimation.

2.7 THE ONE-TERM FRICTION MODEL

The curiosity on how a one-term friction model, built on the original Darcy-Weisbach head loss equation, modified with a correction term will perform in unsteady flow is desired to test. Eq.(31) describes the idea of the one term model.

$$h_f = B^{\frac{1}{g}*\left(\left(\frac{\partial V}{\partial t}\right)+V_1\left(\frac{\partial V}{\partial x}\right)\right)} * f_1 * \left(\frac{L}{D_1}\right) * \left(\frac{|V_1| * V_1}{2 * g}\right) \tag{31}$$

Where B is the correction coefficient with the acceleration term in the exponent, and the number in the subscript describing the pipe section to consider.

The reason for implementing the unsteady velocity term in the exponent is to enable simulation both for steady and unsteady flow, making the constant, B, equal to one if the flow is steady. To make the one-term model to estimate similar friction as the steady state friction model at a cross-section increase in steady state, must B be calibrated for the specific increase.

As mention earlier has research shown increased friction from velocity change due to acceleration and deceleration [10]. It is therefore natural to design the time-dependent acceleration term, $\left(\frac{\partial V}{\partial t}\right)$, to give an increased friction at transient flow. Since B is found larger

than one after calibration, should the acceleration term always be positive to increase the estimated friction. Hence, the time dependent acceleration term should have an absolute value.

Additionally, to have a reasonably sized correction constant should the original acceleration term be multiplied with a value equal the gravitational acceleration. This will not affect the already non-dimensional expression or the rate of impact from the acceleration term in the exponent. Even the total size of the entire additional term at stationer flow will be unaffected since the value of the correction constant implement the changes. On the other hand, this multiplication increases the time-dependent acceleration at unsteady flow. However, as the friction impact from the acceleration in Eq.(31) is not sized correctly from the beginning, may the change as well improve the model rather worsen it. It may additionally be an advantage with an increased impact from the time-dependent acceleration, making it easier to observe the natural direction of the frictional impact from the acceleration term in the simulation analyzes.

Eq.(32) depicts the purposed equation with the adjustments given above.

$$h_f = B^{\left|\frac{\partial V}{\partial t}\right| + V_1\left(\frac{\partial V}{\partial x}\right)} * f_1 * \left(\frac{L}{D_1}\right) * \left(\frac{|V_1| * V_1}{2 * g}\right) \tag{32}$$

Where the size of the correction constant depends on the change of velocity in time and position. How this modification of the Darcy-Weisbach head loss equation affects the performance at unsteady flow is tested and discussed.

2.7.1 Calibrating of the one-term friction model

The size of the correction constant, B, is dependent on several parameters both in pipe section one and two if cross-section change is considered. Velocity, diameter and flow rate in pipe section one is given. For the second pipe section only the flow rate is known, as the velocity is depending on the length of x and the extension angle, θ, on the conical diffuser. The ratio between the length of the diffuser and the diameter of pipe section one sets the limitation on the extension angle due to preventing backflow. If consider a diffuser length of 1 m and an inlet dimeter on 0.15 m, the maximal extension angle is found to be approximately 5 degrees [6].

This corresponds to a dimeter of 0.3250 m in pipe section two, which equals to a velocity of 0.1929 m/s.

Eq.(34) depicts the estimated correction coefficient by setting the one-term friction model equal to the losses in the second section of the pipe. **Figure 2-10** depicts the calibration case and **Table 2-1** lists the parameters of interest. Appendix C depicts the complete calculation.

$$h_f = B^{|\frac{\partial V}{\partial t}|+V_1\left(\frac{\partial V}{\partial x}\right)} * f_1 * \left(\frac{L}{D_1}\right) * \left(\frac{|V_1| * V_1}{2 * g}\right) = f_2 * \left(\frac{L}{D_2}\right) * \left(\frac{|V_2| * V_2}{2 * g}\right) \qquad (33)$$

$$B = {}^{V_1*\left(\frac{V_2-V_1}{\Delta x}\right)}\sqrt{\frac{f_2}{f_1} * \frac{D_1}{D_2} * \frac{|V_2| * V_2}{|V_1| * V_1}} = 308.67 \qquad (34)$$
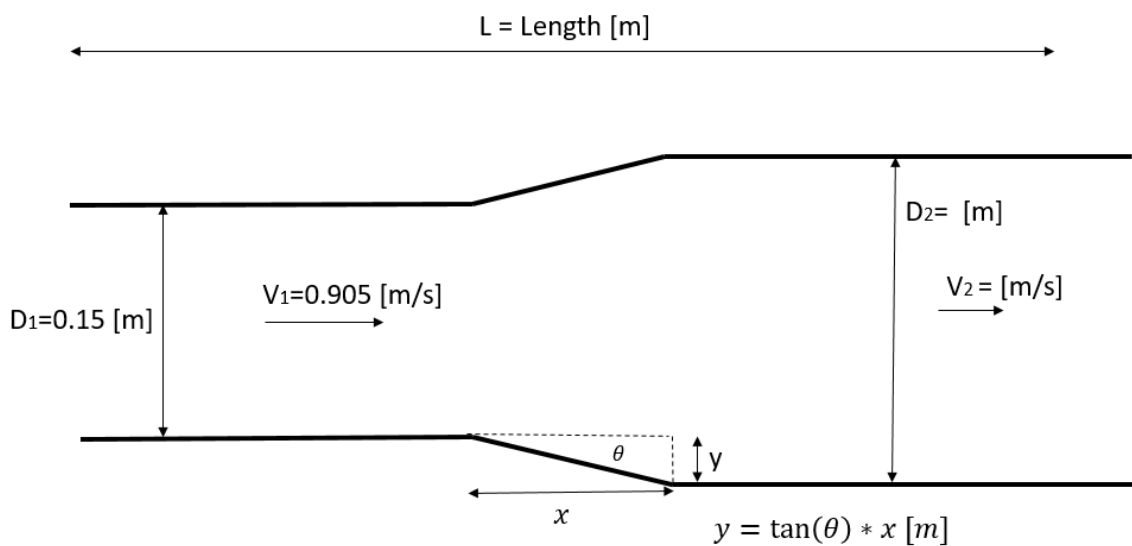
Figure 2-10: Illustration of the cross-section increase calculation, used for the calibration of the B constant

Parameter	Value	Unit
V_1	0.905	m/s
V_2	0.1929	m/s
Q_1	0.016	m^3/s
Q_2	0.016	m^3/s
D_1	0.15	m
D_2	0.3250	m
L	20	m
θ	5	Degree
x	1	m
f_1	0.0177	-
f_2	0.0209	-
g	9.81	m/s^2
y	0.0875	m

Table 2-1: *Parameter specification for the calibration of the one-term correction constant B*

With a B value found in Eq.(34) are both models estimate a stationary head loss due to frictional loss to be 0.0026 mWC considering a 21 m long headrace for the calibration case.

Now, after introducing the theory and equations of the selected friction models of interest, will the next step be to derive how the models are implemented in the water behavior simulation. The next chapter addresses this topic further.

3 CALCULATION APPROACH

This chapter addresses how to implement the friction models into the time-dependent simulation. First is the assumptions at U-tube oscillations listed and applied to the water modeling equation. Secondly, the chapter describe how to implement the different friction models.

3.1 ASSUMPTIONS AT SLOW TRANSIENTS

The knowledge on which assumptions valid to assume or not, is an important part of the initial work. Assumptions at slow transients provide the advantages of a simpler and less demanding calculation.

Following assumption considering U-tube oscillations and system conditions are made and used throughout all calculations and simulation in this thesis, if not otherwise is specified [3, 17].

i)   The upper reservoir has the natural approach on a steady water level throughout the test. This is made possible by the spillway design, draining the excess water.

ii)   With traditional surge shaft is the inertia of the water in the surge shaft neglected. This implies that the kinetic energy in the surge shaft water is negligible small relative to the head pressure from the water level and frictional losses throughout the pipe system.

iii)   The time period of the harmonic oscillations are much greater than the valve closing time, hence the flowrate change rapidly.

iv)   The pipe system is rigid and has tick walls, meaning that the system is assumed incompressible

v)   Elasticity is neglected. All change in water parameters happens at the same time throughout the whole water string. This assumes that propagation speed $a \to \infty$, thereby $\frac{\partial V}{\partial x} = 0$

vi)   Axisymmetric flow of a Newtonian fluid. Hence, the flow is symmetrical around one axis and thus independent of the angular variable. Newtonian fluid means that we may assume to have a constant viscosity, which is not depending on the velocity or stress in the flow.

vii)   Pressure is equally distributed over the cross-section

Calculation approach

> viii) Effects from thermal parameters are neglected. Water temperature is assumed constant at 10°C, which decides the water viscosity

> ix) For calculation and analyzes water density and kinematic viscosity are set to the common value as 999.7 kg/m^3 and 0.000131 m^2/s respectively [6].

Considering the assumptions above and the continuity equation is the change in flow rate described in a simplified approach.

By expressing the wave speed as,

$$a = \frac{dx}{dt} \tag{35}$$

And the pipe system as one large section,

$$dx = L \tag{36}$$

This provides the simplified continuity equation,

$$\frac{L}{gA}\frac{dQ}{dt} = dH - h_{f,Total} \tag{37}$$

$$dQ = dt * \frac{gA}{L}(dH - R * Q_n|Q_n|) \tag{38}$$

$$Q_{new} = Q_n + dQ \tag{39}$$

$$R = \frac{f * L}{2gDA^2} + \left(\frac{k_i}{2 * g * A^2}\right) \tag{40}$$

Where R represent the head loss considering friction losses determined by the specific friction model, and the minor losses through the loss coefficient k_i. Implementing Eq.(39) into the Eq.(19), the water fluctuation in the surge shaft is found.

If considering frictionless simulation, the water level fluctuation from its stationary point is simply found as follows

$$\Delta Z_T = \Delta Z * \sin \frac{2\pi}{T} t \qquad (41)$$

The frictional forces must be included in the calculation to take care of the natural damped motion. The friction is implemented in the computation of the new flow rate as shown above and is dependent on the specific friction model used. The next subchapter address the implementation of selected friction models into the modeling of the flow rate.

3.2 SLOW TRANSIENT MODELING – IMPLEMENTING FRICTION MODELS

This subchapter presents the approach on how to implement the friction from the Quasi-steady model, the model by Ogawa et al., the model by Vitkovsky and the one-term model into the head loss estimation.

3.2.1 Quasi-steady friction model

The Quasi-steady friction model uses the basic Darcy-Weisbach head loss equation. The friction at each time step is found from the steady state friction factor, as depicted in Eq.(42), where the Re number is updated at each time step is updated. The loss term R, in the flow calculation implements the estimated friction factor.

$$f = \begin{cases} Laminar\ (Re < 2300): \quad f = \dfrac{64}{Re} \\[4mm] Turbulent\ (Re > 4000): \quad \dfrac{1}{\sqrt{f}} = -1.8\log\left[\left(\dfrac{\frac{\varepsilon}{D}}{3.7}\right)^{1.11} + \dfrac{6.9}{Re}\right] \end{cases} \qquad (42)$$

Calculation approach

3.2.2 Model of Ogawa et al.

Ogawa et al. use as mention a different approach to estimating change in flow rate at U-tube oscillations. Eq.(47), derived below, is presenting the model by Ogawa et al. and is directly implemented in the flow rate term in the Euler method described in Eq.(19).

$$\frac{d^2Z}{dt^2} + \frac{2*v*K_v}{R^2} * \frac{dZ}{dt} + \frac{2*g}{L} * Z = 0 \tag{43}$$

$$\frac{dZ}{dt} + \frac{2*v*K_v*dZ}{L} + \frac{2*g*Z*dt}{L} = 0 \tag{44}$$

Where,

$$\frac{dZ}{dt} = \frac{Q}{A} \tag{45}$$

$$\frac{Q}{A} + \frac{2*v*K_v*Q*dt}{L*A} + \frac{2*g*Z*dt}{L} = 0 \tag{46}$$

The change in flow rate may then be found as,

$$dQ = dt\left(\frac{2*g*Z*A}{L} - \frac{2*v*K_v*Q_{new}}{R^2}\right) \tag{47}$$

3.2.3 Model by Vitkovsky

The modified model by Vitkovsky has the advantage of carrying an acceleration term in combination with the quasi-steady term. In mass oscillations are the convective term neglected, and the propagation speed assumed infinitely high. Hence, $a \rightarrow \infty$ and $\Delta x = \Delta L$, the Vitkovsky model can thus be expressed as Eq.(48), implementing the correction of direction to the change in time. Updating the velocity at each time step estimates the expected friction in each step. Similar as for the Quasi-steady model is the friction counted for by implementing the head loss into the change in flow rate .

$$h_f = h_{f,q} + \frac{kD}{V|V|}\left(\frac{\partial V}{\partial t}\right) sign(V) \tag{48}$$

3.2.4 The one-term friction model

The one-term model works and execute the calculation in the same approach as the Quasi-steady model but replaces the original Darcy-Weisbach head loss equation with the one-term model given in Eq.(32).

Calculation approach

4 THE DYNAMIC TEST RIG AND EXPERIMENTAL TEST CAMPAIGN

Inside the waterpower laboratory at NTNU is a dynamic test rig designed and established. The rig is designed to investigate flow transients, by collecting specified measurements related to applied dynamics generated by a sudden closure of a downstream valve and water column separation, respectively with a traditional surge shaft and a siphon system. The construction process was completed without major modifications to the original plan. There were still some changes. The dynamic rig was initially designed to run with a headrace tunnel of 11 m, 18 m and 29 m, but due to new changes in the laboratory after the design process, was 11 m and 21 m headrace length established for the test campaign. The final length of 29 m is still available to pursue. Due to lack of time was the 29 m length not established. The original plan with particle image velocimetry (PIV) measurements and associated pressure measurements in the test section was nor performed. The reason was mainly due to the availability of the PIV instrument. A description of the already established test section are described later on in Chapter (4.5.6).

The purpose of the experimental test is to collect reference data to validate model simulations and to perform a closer investigation on how the water acts in different flow conditions. This chapter will present the design of the test rig in additional subchapters for components and sensors installed. Then a closer description of the flow management, the pressure transducers (PT) and the electromagnetic flowmeter (EMF), before a description of the accomplished experimental test campaign ends the chapter. More information and details on the test rig design process may be found in the design work presented in the project work by the author [1].

The dynamic test rig and experimental test campaign

4.1 COMPONENTS AND SENSORS

To operate the rig and to collect necessary measurements are valves and sensors mounted. **Table 4-1** list the components and sensor installed.

Component/Sensor	Type	Field of application
PT 1	UNIK 5000	Static pressure
PT 2*	UNIK 5000	Static pressure
PT 3	UNIK 5000	Static pressure
PT 4	UNIK 5000	Static pressure
EMF	OPTIFLUX 2000F	Flow rate
PIV*	FlowSense 2M	Velocity profile
Valve 1	VAG EKOplus gate valve	Water control and management
Valve 2	EBRO butterfly valve	Water control and management
Valve 3	EBRO butterfly valve	Water control and management
Valve 4	VAG EKOplus gate valve	Water control and management

***Table 4-1:** List of components and sensors. *Temporary not installed*

4.2 SETUP – TEST RIG

A simplified drawing of the established dynamic test rig with valves and sensors are depict in **Figure 4-1**.
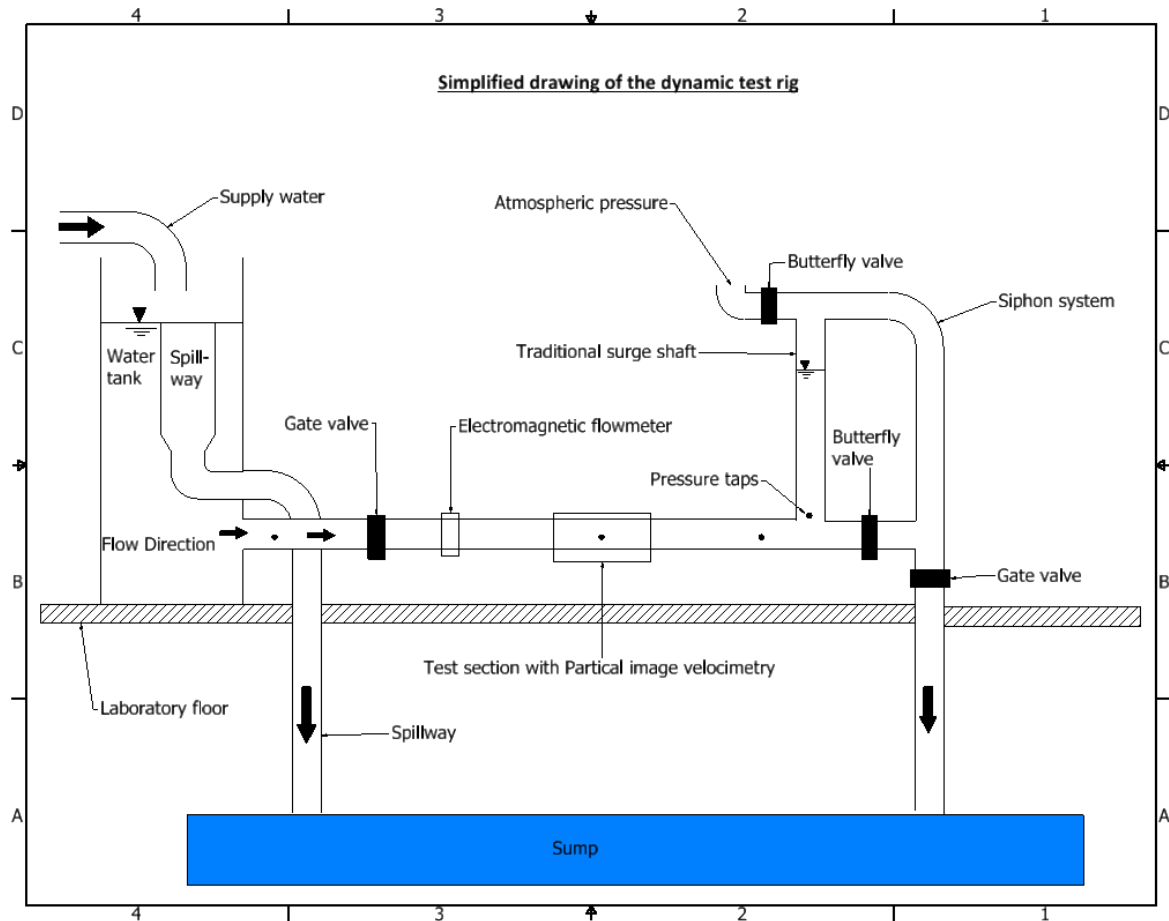
Figure 4-1: *Simplified drawing of the established dynamic test rig*

The rig consists of an upper reservoir that provides a constant pressure head at 1 mWC or 2 mWC, depending on the spillway setup. The headrace is a horizontal steel pipe reaching from the upper reservoir to the closing valve downstream the surge shaft. It has a 150 mm inner diameter and flanged together by several pipe sections. The boundary of maximum upswing and downswing in the surge shaft limits the flow in the conduit, preventing water to increase over the surge shaft or decrease down in the headrace. The highest flow rate is found to be 0.007 m³/s at 1 mWC for 29 m length, due to upswing, and minimum flow rate at 0.016 m³/s at 2 mWC for 11 m length, due to downswing [1].

4.3 FLOW MANAGEMENT

Four valves are installed, respectively two butterfly and two gate valves. The valves obtain the desired flow operations for the different cases of interest in the test campaign. Levers with a gear system, making the necessary accuracy, control all valves manually. **Table 4-2** depicts type, location, and function of each valve.

Name	Type	Location	Function
Valve 1	VAG EKOplus gate valve	3 m downstream the upper reservoir	Shut down / dry the pipe system
Valve 2	EBRO butterfly valve	At the top of the traditional surge shaft	Traditional: Air control into the top of the surge shaft Siphon: initiate the column separation
Valve 3	EBRO butterfly valve	Right downstream from the inlet to the traditional surge shaft	Traditional: Initiate the water hammer Siphon: Guide the water in to the siphon shaft
Valve 4	VAG EKOplus gate valve	At the end, upstream the outlet.	Flow control

Table 4-2: *Valves used for the management of the dynamic test rig*

4.4 WORKING PROCEDURE AND MANAGEMENT

It is of interest to generate mass oscillations with a traditional surge shaft and a siphon system. Below, is a step-by-step list describing the working procedure on how to generate the dynamics.

Traditional surge shaft

1) Initial condition:
   a. Water is flowing at steady state
   b. Valve 1, 2 and 3 is fully open
   c. Valve 4 adjusted to control the flow rate.
2) Generating the dynamics:
   a. A rapid closure of Valve 3
3) Measurements:
   a. Static PT recording the pressure changes in the headrace and the water level in the surge shaft
   b. EMF measures the mean velocity and flow rate
   c. PIV generates a visualization of the water flow and depicts the local velocity in the test section

Water column separation:

1) Water flow is generated by:
   a. Closing Valve 1, 3 and 4. Valve 2 is open.
   b. The pipe system is filled up from the top of the surge shaft, trough Valve 2
   c. The flow is generated by closing Valve 2 before opening Valve 1 and 4
   d. Valve 4 adjusted to control the flow rate.
2) Initial condition:
   a. Water is flowing at steady state
3) Generating the water separation:
   a. Opening Valve 2, letting air in to the system
4) Measurements:
   a. Static PT recording the pressure changes in the headrace and the water level in the surge shaft
   b. EMF measures the mean velocity and flow rate
   c. PIV generates a visualization of the water flow and depicts the local velocity in the test section

4.5 MEASUREMENTS

The setup and calibration of instruments and processing collected data is a central part of the laboratory work. This subchapter presents theory on required flow condition, uncertainty in measurements, signal processing and description on each sensor. The subchapter ends with a description of the five different test cases tested in the dynamic test rig and simulated by the friction models.

4.5.1 Hydrodynamic entry length and time to steady state flow

The development of the flow is an important aspect to consider when performing measurements, both time to steady state and distance to fully developed flow. These conditions are necessary to fulfill to collect good and satisfying measurements.

Time from start-up (flow at rest) to reach steady state flow is found by Eq.(49). This equation consider frictional losses at steady state flow [4].

$$t = \frac{L}{V_0 * f\left(\frac{L}{D}\right)} \ln[\frac{V_0 + 0{,}99V_0}{V_0 - 0{,}99V_0}] \tag{49}$$

Fully developed flow is assumed reached at the length called the hydrodynamic entry length [18]. The length depends on the pipe diameter and flow regimes. Eq.(50) and Eq.(51) determine the hydrodynamic entry length at respectively laminar and turbulent flow. **Figure 4-2** illustrates the length.

Laminar flow,

$$L_{h,laminar} = 0.005 ReD \tag{50}$$

Turbulence flow,

$$L_{h,turbulent} = 1.359 D Re_D^{\frac{1}{4}} \tag{51}$$
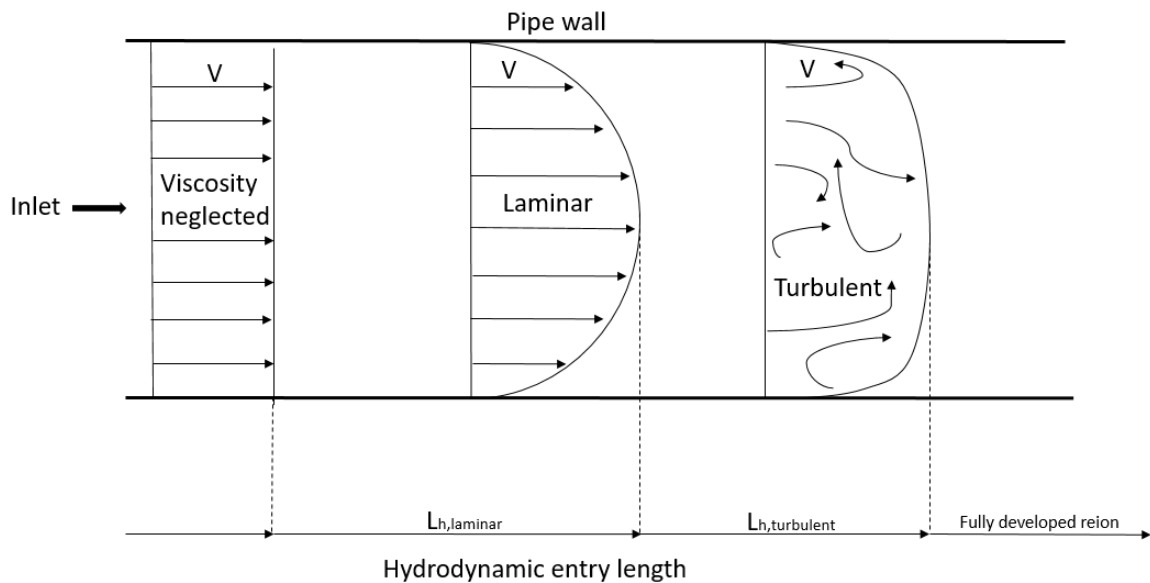
Figure 4-2: *Illustration of the Hydrodynamic entry length*

4.5.2 Uncertainty in instruments and measurements

When working with measurements, such as tests and calibrations, an important thing to implement is the uncertainty of the generated results. The uncertainty states the quality of the measurements, which is essential for the validation and understanding of the outcome. All measurements has a degree of uncertainty. It is normal to express the uncertainty by an interval or confidence level. The international standard IEC 41, recommend test measurements and industry to have a confidence level with a probability of 95 % [19].

Guidance from Bjørn Winther Solemslie and his written compendium on instrument uncertainty has provided with great help on the uncertainty calculation and theoretical background presented in this subchapter [20].

The error of a measurement is the difference between the actual value and the measured value. The error in a measurement is not found as an exact value but predicted using statistical methods. The sources of errors are typically divided into three types, as follows

➢ **Spurious errors**, often caused by human faults or instrument failure, usually recognized after analyzing the measurement results. If the entire test is affected by the fault, could the result be useless and not vailed for further use. However, spurious errors may also occur in single points, called outliers. If neglecting these outliers from the test, the result may be useable for further analyses.

➢ **Systematic errors,** mainly caused by uncertainties from calibration or instrument bias. These errors are found before collecting the measurements, by analyzing the calibration results and include the deviation of linearity in the instrument. The systematic error based on the upper measuring limit of the instrument is often specified by the fabricant.

➢ **Random errors** are uncertainties from small unknown and incidental disturbances that has no common pattern. The random errors makes the instrument to produce different results of the same measured property. Random errors may be sourced from change in environmental conditions, additional work in the laboratory or small internal changes in the instrument. These errors are not easily to detect and remove, and will unfortunately affect the final result. It is however possible to decrease the rate of uncertainty in a single point by its mean of several measurements. Normal distribution for an infinitely high number of measurements describes the measurements around a mean. If the number of measurements cannot be expected to be infinitely high, the uncertainty will follow the student-t distribution. The student-t has the same shape as the normal distribution, but the outer limits are further apart as the number of measurements decreases. The random error are usually given as a confidence interval around the mean, as shown in Eq.(52).

$$\bar{X} \pm \frac{t_{\frac{\alpha}{2}} * S}{\sqrt{N}} \tag{52}$$

Where $\bar{X}$ is the mean value and S the standard deviation, these are calculated by Eq.(53) and Eq.(54) respectively. N is the amount of measurements used to determine the mean value, and t is the value of the student-t distribution found in **Table A-1** in Appendix A considering a confidence level of 1-α.

$$\bar{X} = \frac{1}{N} \sum_{i=1}^{N} X_i \tag{53}$$

$$S = \sqrt{\frac{\sum_{i=N}^{N}(X_i - \bar{X})^2}{N-1}} \qquad (54)$$

Where X is a specific measurement number specified by the nominator i. The total uncertainty is the sum of all three types of errors, including instrument specific errors and errors generated in the measurements. It defines the spread where the true value of the measurements are most likely to be located. The total uncertainty, f_T, calculated by the Root-Sum-Square (RSS) method is shown in Eq.(55).

$$f_T \pm \sqrt{f_{SP}^2 + f_S^2 + f_R^2} \qquad (55)$$

Where, f_{SP}, f_S and f_R are the spurious, systematic and random errors respectively.

As mention is the total error depending on several uncertainties, sourced from calibration, instrument and measurements. **Table 4-3** depicts an overview of general errors related to measurements in the laboratory. X is the value of the measured property from the sensors.

Error	Description
$e_a \pm fX_a$	Systematic error of the primary calibration method
$e_b \pm fX_b$	Random error of the primary calibration method
$e_c \pm fX_c$	Systematic error of the secondary instrument
$e_d \pm fX_d$	Random error of the secondary instrument
$e_e \pm fX_e$	Physical phenomena and external influences
$e_f \pm fX_f$	Error in physical properties
$e_{cal} \pm fX_{cal}$	Systematic errors in calibration
$e_h \pm fX_h$	Additional systematic error in the instrument
$e_j \pm fX_j$	Error in physical properties
$e_{ks} \pm fX_{ks}$	Systematic errors due to physical phenomena and external influences
$e_{kr} \pm fX_{kR}$	Random errors due to physical phenomena and external influence
$e_l \pm fX_l$	Random error in repeatability of secondary instrument

Table 4-3: *Common types of errors in calibration and instruments [20]*

The dynamic test rig and experimental test campaign

To display the estimated uncertainty correctly, are the uncertainty limits plotted together with the measured result. Eq.(56) calculates the error at each measured point.

$$f_T \pm \sqrt{\left(\frac{e_{calibration}}{X}\right)^2 + \left(\frac{e_{instrument}}{X}\right)^2 + (f_{measurement})^2} \tag{56}$$

Where, $e_{calibration}$ is the total systematic error in the calibration, $e_{instrument}$ is the total systematic error in the instrument and $f_{measurement}$ is the random uncertainty from the measurements.

4.5.3 Signal processing and Nyquist sampling theorem

A data acquisition (DAQ) system converts the analog data from the continuous time process into a digital numerical discrete time space. The DAQ device reads the electrical signal measured by the sensors connected to the pipe before it converts and sends a digital signal to the computer application called LabVIEW. The LabVIEW workspace used in this thesis was designed in great help from Carl Bergan to fit the specific measurements. The LabVIEW application, process the signal into a graphical representation and collects all information into an organized and readable txt-file, making the post process analyses easier. The organized LabVIEW data is converted from the original TDMS file to readable MATLAB format by using the MATLAB-function *carlsConvertTDMS,* made by Carl Bergan.

When conducting measurements from continues time and converts them into the numerical discrete time space, the sampling frequency on the measuring instrument is of great importance. In an oscillating system, high enough sampling frequency is an essential requirement not to miss necessary data. Too low sampling frequency introduces the phenomena of aliased signal, as illustrated in **Figure 4-3**.
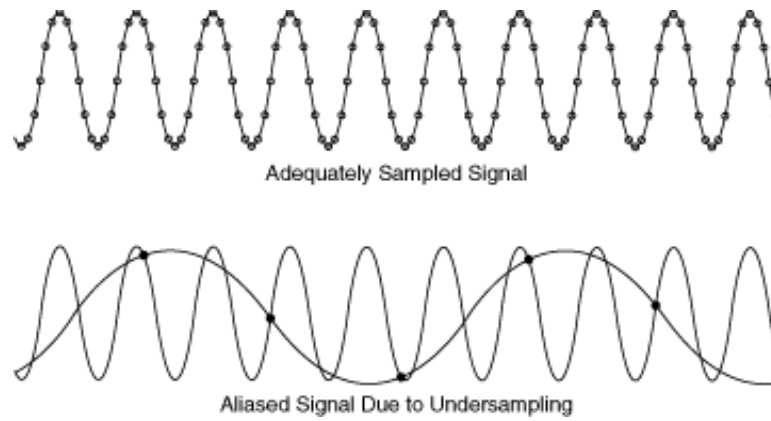
Figure 4-3: An example of aliasing, where the sampling frequency is too low [21]

The real continues analog data containing an infinitely amount of data at every given time step. For the digital discrete time is the amount of data in the specific time step decided by the sampling frequency. The required sampling frequency to get valid and satisfying results is found by the Nyquist frequency, depict in Eq.(57). It specifies that the sampling frequency needs to be twice as high as the system frequency not to miss necessary data [22]. In our case, the sampling frequency needs to be larger or equal to the twice of the mass oscillation wave frequency.

$$\omega_{sampling} > 2 * \omega_{system} \tag{57}$$

4.5.4 Static pressure transducers (PT)

Three UNIK 5000 static pressure transducers installed at three different locations measures the pressure variation in the pipe system. A fourth pressure device is calibrated and made ready for pressure measurements in the test section. This pressure sensor titled PT 2 is associated with the PIV measurements. The PT 2 was never installed, as the PIV measurements were not carried out. Location of each sensor is depict in **Figure 4-1** as black dots in the pipe. Additional information is given in **Table 4-4**. All sensors are proven to have an accuracy of 0.04 % from the fabricant. The operation range is between 0-5 bar gauge and an output signal from 4-20 mA. The three sensors located in the horizontal headrace conducts the information on transient pressure oscillations, while the sensor in the surge shaft indicates the water level in the shaft.

The dynamic test rig and experimental test campaign

All sensors are located in areas where a fully developed flow is satisfied. For the analytical work, comparing results from the friction models up against measured data is it mainly the pressure sensor in the surge shaft, called PT4, which is used.

All pressure sensors uses gage as reference pressure, meaning that the measured pressure is the difference between absolute pressure and atmospheric pressure, as depict in Eq.(58).

$$P_{absolute} = P_{gage} + P_{atmospheric} \tag{58}$$

When using atmospheric pressure is it important to be aware of the ambient temperature, altitude and local weather to perform best possible results. Atmospheric pressure of 1 atm is assumed constant for all cases in this thesis.

Name	Type	Location	Function/Measuring
PT 1	UNIK 5000	1.5 m downstream the upper reservoir	Static pressure in the headrace
PT 2*	UNIK 5000	In the test section (8m downstream the upper reservoir)	Static pressure in the headrace
PT 3	UNIK 5000	In the headrace right upstream the inlet to the surge shaft	Static pressure in the headrace
PT 4	UNIK 5000	Right above the headrace, in the lower part of the surge shaft	Water level in the surge shaft

*Table 4-4: List of the static pressure transducers with location and functionality *Temporary not installed*

4.5.4.1 Calibration

To obtain accurate measurements, are the UNIK 5000 static PT calibrated with a digital pressure indicator DPI 603. The DPI has an accuracy of ± 0.075 % given by the fabricant. The aim of the calibration is to find the calibration constants between pressure and voltage for each sensor. The procedure is to apply a known air pressure on the UNIK 5000 from the digital indicator and compare the applied pressure from the digital indicator with the measured output signal from the UNIK 5000 sensor. The output signal from the UNIK 5000 is in mA. Hence, the signal is converted to voltage by an NI-USB 6211 converter, using a 500 Ohm drop

resistance. The converter provides good and desired result with a 16 bit`s resolution. The output signal from the converter is giving the mean of 10000 measurements per second.

The measuring range of the PT is as mention between 0-5 bar. The compared output signal to the computer from the converter is from 2-10 V. This corresponds to 0 bar when the readable output signal from the converter is approximately 2 V, and 10 V when the value is 5 bar. Since the measuring range for this experiment will be from about 0.1-0.3 bar, the calibration is made between 0-1 bar with six numbers of measurements and a step length of 0.2 bar. Two constants provide the linear relation between measured voltage and pressure, here called CO and C1. Microsoft Excel finds these linear relations by plotting the calibration results found from each sensor. **Table 4-5** lists the calibration results for all four sensors. Additionally, associated calibration plots are given in Appendix B.

Pressure transducer	Calibration constants	
Name	C0	C1
PT 1	-1.2525	0.6245
PT 2	-1.2543	0.6239
PT 3	-1.2521	0.6248
PT 4	-1.2522	0.6236

Table 4-5*: List of calibration constants for each pressure sensor*

Eq.(59), a 1.order equation calculate the pressure y in the pipe by inserting the calibration constants and replacing x with the measured voltage found in **Table 4-5**. Similarly, implementing the calibration constants into the MATLAB-script corrects the in-data, providing with desired results.

$$y = C0 + C1 * x \qquad\qquad (59)$$

4.5.5 Electromagnetic flowmeter (EMF)

The flow rate and mean velocity in the headrace are measured by an EMF OPTIFLUX 2000F, installed with an IFC 300 signal converter having 0.2 % accuracy [23]. The flowmeter is located

approximately 2.5 m downstream the upper reservoir. The location satisfies the requirement of fully developed flow, as the location is positioned at a gap larger than ten pipe diameters from the nearest flow disturbance.

The IFC 300 signal converter sends current signals in the range from 4-20 mA to the DAQ device, where the DAQ further converts the signal to voltage for further analyses in LabVIEW. The DAQ device produces an output signal between 2-10 V. Comparing this output signal together with the flow rate may the calibration constants be estimated. Given fabricant calibration is chosen to use in the calibration process. The fabricant values corresponded to 0 m^3/s at 2 V and 0.5556 m^3/s at 10 V compared to the DAQ output signal. The function of the trendline between the minimum and maximum flow rate decides the calibration constants, which are found to be C0 = -0.1389 and C1 = 0.0694. Microsoft Excel is used for the trendline calibration. Appurtenant plot diagram from Microsoft Excel is given in Appendix B. Eq.(59) can now be used to calculate the actual flow rate by inserting the voltage readouts from the DAQ device into x.

4.5.6 Particle image velocimetry (PIV)

To collecting PIV measurements, a test section is established. The test section is designed to fit the PIV instrument available in the water power laboratory at NTNU. The planned PIV measurements were chosen not to be performed, due to high demand on the available PIV instrument. This was not critical for the thesis study or final result, as the PIV measurements were thought to be supplementary. The curiosity to conduct PIV measurement was to see how the local velocity and velocity profile was acting in unsteady flow. The lack of PIV measurement was compensated by literature review on similar studies.

The test section is established approximately 8 m downstream the upper reservoir for all test lengths. The tests section is a 1000x250x250 mm Plexiglas box surrounding a part of the headrace that also is of Plexiglas. To decrease distorted optical view and fluctuation, was the box designed to be filled with water. A drawing of the test section is depict in **Table 4-3**. The test section was mainly design and sized in the project work but finalized in this thesis.
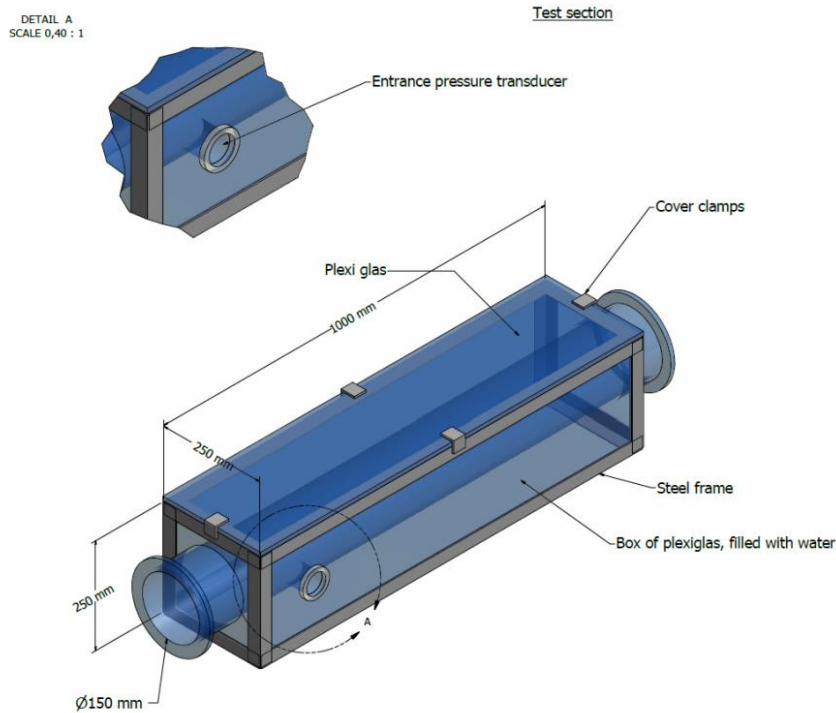
Figure 4-4: *Drawing of the test section for PIV measurements*

4.5.7 Setup – Sensors and DAQ system
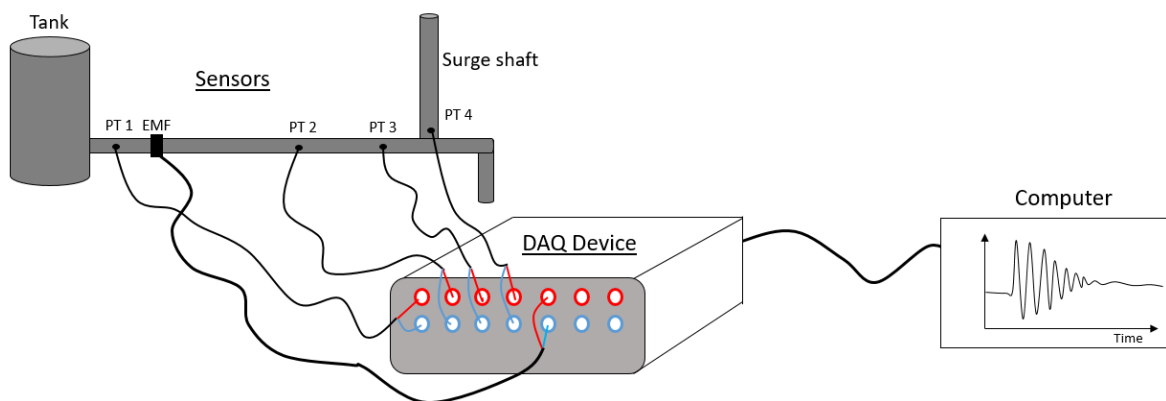
Figure 4-5: *Sketch of the DAQ System setup*

Figure 4-5 shows how the DAQ system is connected and where the sensors are located on the test rig. All sensors seed electrical signal to the DAQ device, which converts the signals to readable output for the specified logging program in the LabVIEW computer application. The data is further converted to enable post-analyze in MATLAB.

4.6 EXPERIMENTAL TEST CAMPAIGN

A test campaign is desired to perform in the dynamic test rig to collect data on harmonic transients, providing with references data on harmonic oscillatory flow. Five specified cases are proposed, considering two different headrace lengths of 11 m and 21 m, and two available head pressures of 1 mWC and 2 mWC. Additionally, both the traditional surge shaft and siphon system is tested. **Table 4-6** lists the different specifications for each case. The initial flow rate before generating the dynamics are specified by the limitation on upswing and downswing in the surge shaft. The time of closure to the dynamics are fully damped out defines the time of inters to study.

Initial/design parameters	Unit	Case 1	Case 2	Case 3	Case 4	Case 5
Surge shaft	-	Traditional	Siphon	Traditional	Traditional	Traditional
Headrace length, L	[m]	11	13.5 *	11	11	21
Roughness, ϵ	[mm]	0.002	0.002	0.002	0.002	0.002
Diameter, D	[mm]	150	150	150	150	150
Flow, Q_0	[m³/s]	0.016	0.016	0.007	0.007	0.007
Velocity, V_0	[m/s]	0.905	0.905	0.395	0.395	0.395
Pressure height, H	[mWC]	1	1	1 mWC	2	2
Dynamic viscosity at 10°C	[Ns/m²]	1.31×10^{-3}	1.31×10^{-3}	1.31×10^{-3}	1.31×10^{-3}	1.31×10^{-3}

*Table 4-6: Specification for all five test cases *Total length from the upper reservoir to the point of column separation (The top of the siphon)*

The siphon system test is thought to be supplementary study on the water behavior where the initial water in the surge shaft is in motion at the initial phase of the generated dynamics. The case will be tested and discussed but not analyzed in detail. The results from the experimental test campaign considering both measurements and simulation are given and discussed in the next chapter.

5 RESULTS AND DISCUSSION

All five test cases were utilized in the dynamic test rig as planned, give satisfying and expected results. Similarly, five friction models were simulated and compared up against the measured data. Several test runs for each case has been performed to ensure good and reliable results by preventing spurious errors in the measurements. In this thesis, only one test run for each case will be treated. The selected test run represents the closest average of all runs with similar specification, after removing outliers. All calculations and related plots are made in MATLAB R2015a. All assumptions with influence on the friction modeling are addressed in Chapter (3.1).

This chapter provides with the thesis results and discussion. The chapter starts with addressing the signal treatment and uncertainty calculations on the measurements. Even if the uncertainties has a great impact on accuracy on the final results are error limits not presented in figures where measured data is compared with simulation results to increase the readability of the results. Separated figures presents uncertainty plots for the pressure and flow rate measurements. Furthermore, the laboratory measurements and numerical results are depicted and discussed, before a closer study on the flow parameter is presented.

Before starting the experimental test, the flow had to reach its steady state flow. Using Eq.(49) by considering the values from **Table 4-6** and **Table 5-6**, the time to steady state was found. **Table 5-1** depicts the result of each case.

	Unit	Case 1	Case 2	Case 3	Case 4	Case 5
Time to steady state	[s]	49.6	49.6	94.7	94.7	94.7

Table 5-1: *Time to steady state after start-up for each test case*

5.1 SIGNAL TREATMENT

To display good and readable measurement without losing vital information, are all measurements recorded with frequency fulfilling the required Nyquist sampling frequency. All sensors use a sampling frequency with 5000 samples per second. The relatively high frequency gave a sensitive and undesirable noisy plot, as all small deviations and instabilities are visible. To increase the readability was it chosen to present the measured results with mean points, where each point is given by an interval of 500 samples. The raw data from all sensors are in MATLAB sorted by the functions `cell2mat` and `arrayfun`, and further averaged by using

the function `mean`. The mean function uses the principle of Eq.(53) for the calculation. **Figure 5-1** depicts the difference between the original raw data and the averaged signal.
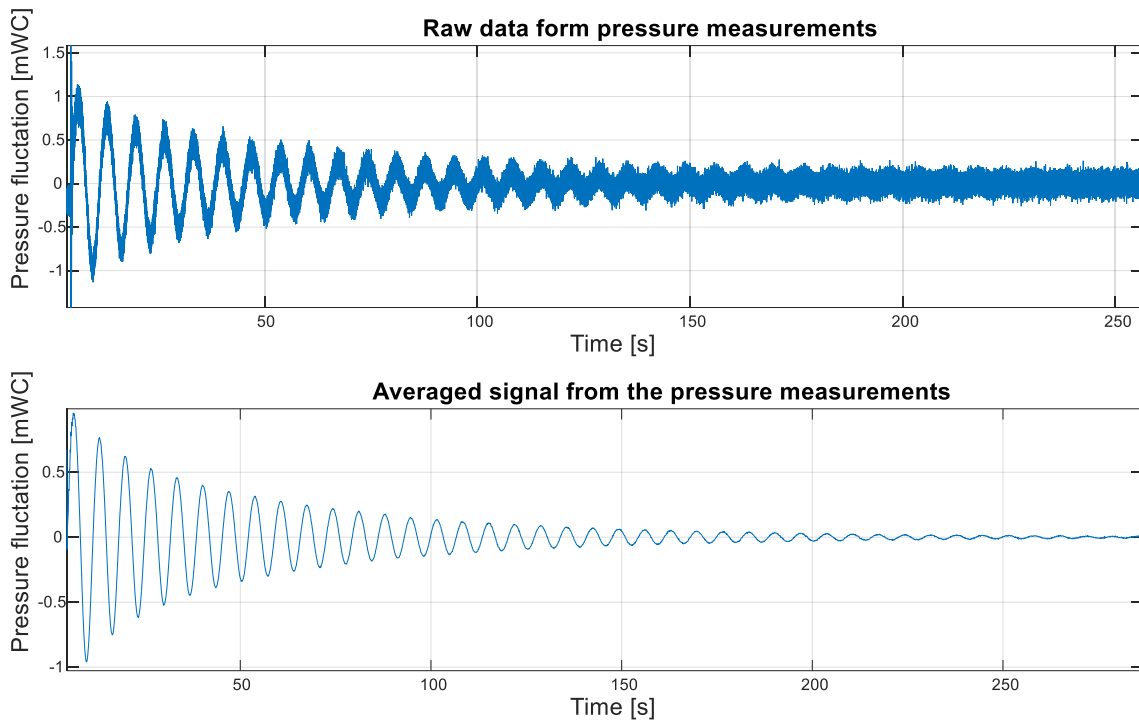
Figure 5-1: Original raw data from measurements compared to averaged signal

By averaging the sampling data with 500 samples per averaging point, the frequency decreases from 5000 Hz to 10 Hz. The relatively large decrease in frequency will still fulfill the Nyquist sampling requirement for mass oscillations at all test lengths. The water hammer, seen has the high fluctuation in the initial phase of the raw data, will, on the other hand vanish as the sampling frequencies are too low to detect the amplitudes of the water hammer after averaging the raw data. **Table 5-2** depicts the required sampling frequencies for mass oscillations considering all test cases.

	Unit	Case 1	Case 2	Case 3	Case 4	Case 5
Required sampling frequency on mass oscillations	[Hz]	63.21	63.21	63.21	63.21	44.91

Table 5-2: *Required sampling frequency Considering all test cases*

Averaging the raw data will influence the uncertainty of the results, this effect is implemented in the uncertainty calculation in the following subchapter.

5.2 UNCERTAINTY CALCULATIONS

The total uncertainty in pressure and flow rate measurements counts for uncertainties from calibration, instrument and measurements. Spurious errors are not considered, as no remarkable outliers were found and system conditions were stable, showing reasonable results. All uncertainty calculations considers Case 1 as specification.

The random error depends on the averaged of raw data, MATLAB is used for the uncertainty calculations with the student-t distribution, using the MATLAB-function `tinv` with a confidence level of 95 %. The t-value was found to be 1.960 which corresponds to a t-value matching the degree of freedom found in **Table A-1**.

In the two next subchapters (5.2.1) and (5.2.2), are the systematic errors from calibration and instruments presented together with the mean random errors from averaged measurements. The estimated error limits are plotted together with the measured result as dotted lines.

5.2.1 Uncertainty in the static pressure transducers

The digital pressure calibrator DPI 601 comes with documentation for the accuracy of $\pm$ 0.05 % at full-scale, where the lack of linearity, hysteresis and repeatability are included. Likewise, are the static PT`s documented by the fabricant to have an accuracy of $\pm$ 0.04 % full-scale. **Table 5-3** lists the errors related to the static PT`s where the full-scale systematic errors from the calibration and instrument are listed together with the mean value of the random measurement errors.

Errors	Description	Full-scale pressure [mWC]	SPT 1 [mWC]	SPT 3 [mWC]	SPT 4 [mWC]
e_{cals}	Systematic error in the calibration	10	±0.05	±0.05	±0.05
e_{SPTs}	Systematic error in the instrument	5	±0.02	±0.02	±0.02
$mean(e_{SPTm})$	Mean random error in the measurements	-	±0.0043	±0.0044	±0.0042

Table 5-3: *Uncertainty in the static pressure measurements*

Results and Discussion

The systematic error, as shown in **Table 5-3**, are relatively larger than the random error from the measurements. Using the systematic uncertainty given by the fabricant, which is often set with high safety margin, is this uncertainty distribution reasonable.

The total uncertainty, f_{SPTT}, in each point is calculated by the RSS method as given in Eq.(56). **Figure 5-2** shows the measured pressure in PT 4 considering test Case 1 with estimated upper and lower error limits. Drawn dotted lines shows the error limits from the calculated error in each mean point.
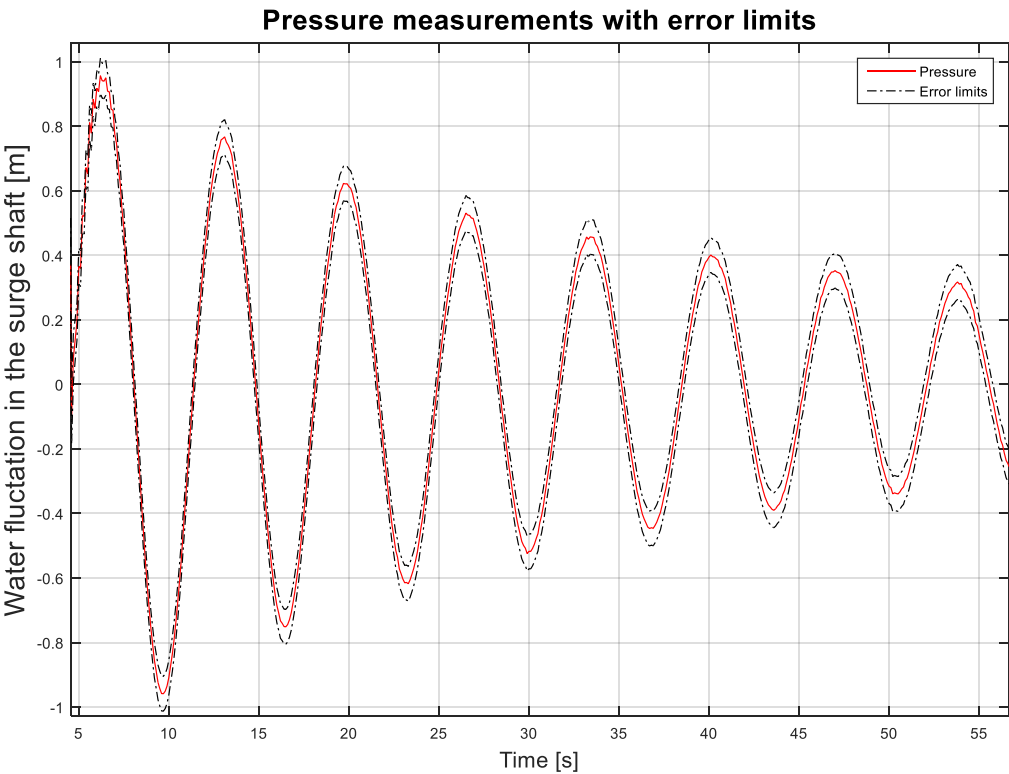
Figure 5-2: Pressure measurements with error limits for Case 1

The maximum deviation between the measured pressure and the error limit shown in **Figure 5-2** is found to be 0.054 mWC by implementing the deviation into the MATLAB-function `max`. The water hammer area is neglected in the uncertainty representation.

5.2.2 Uncertainty in the electromagnetic flowmeter

The total uncertainty from calibration and instrument for the EMF was given by the fabricant to be 0.2 % of full-scale. **Table 5-4** lists the uncertainties for the resulting flow rate measurements.

Uncertainty	Description	Full-scale flow $\left[\frac{m^3}{s}\right]$	Uncertainty in the EMF $\left[\frac{m^3}{s}\right]$
e_{fs}	Systematic error	0.5556	± 0.0011
$\mathbf{mean}(e_{fm})$	Mean random error in the measurements	-	± 0.0000018

Table 5-4: *Uncertainty in the flow rate measurements*

In the same way as for the pressure measurements was the systematic error in the EMF dominant. The quite high systematic error is sourced from the relatively high full-scale flow of 0.5556 m³/s compared to the specific flow measured in the test rig. Additionally, as mention is the uncertainty from the fabricant typically set to have a high safety margin.

Figure 5-3 shows the measured flow rate over time with the estimated upper and lower error limit found in each mean point from Eq.(56), considering Case 1.
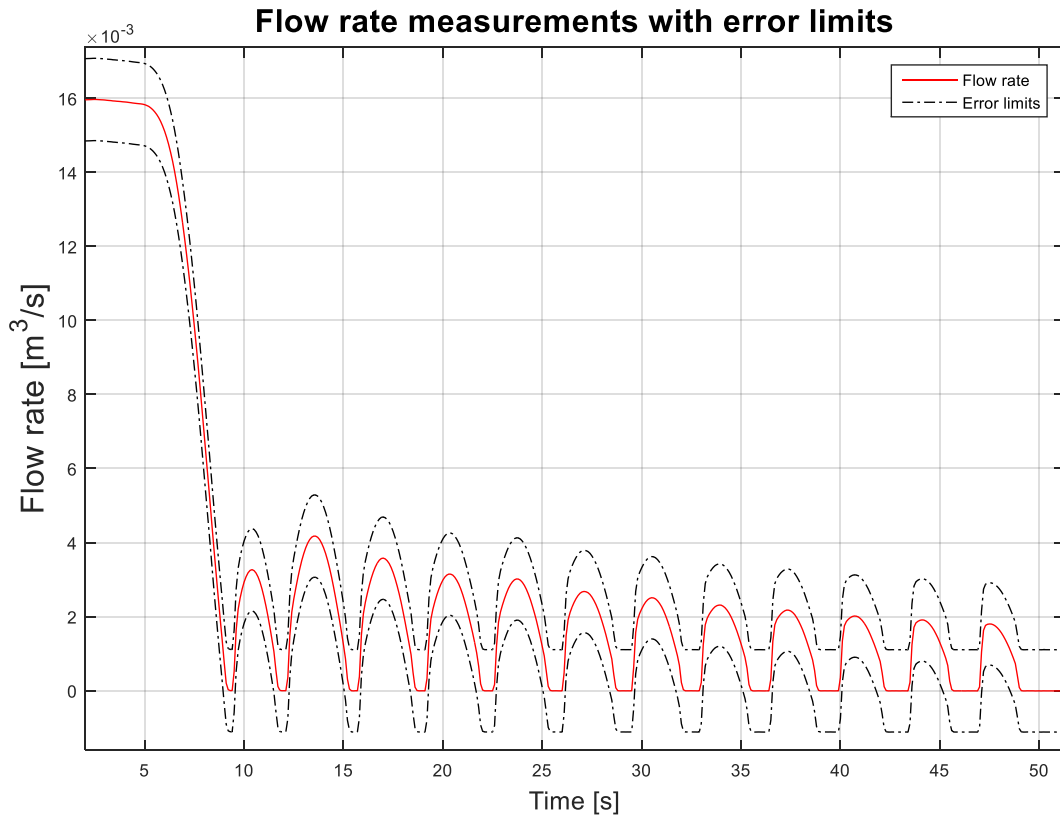
Figure 5-3: *Flow rate measurements with error limits considering Case 1*

The maximum deviation between the measured flow rate and the error limit shown in **Figure 5-3** is found to be 0.0012 m³/s by implementing the deviation into the MATLAB-function `max`. This corresponds and supports the large impact from systematic error discussed previously.

5.3 MEASUREMENTS FROM THE DYNAMIC TEST RIG

The behavior of a sudden closure of a downstream valve is tested for both traditional surge shaft and siphon system. All five cases described in Chapter (4.6) are tested in the dynamic rig. **Figure 5-4** to **Figure 5-8** displays the measurement. Comments on the result are given subsequently.
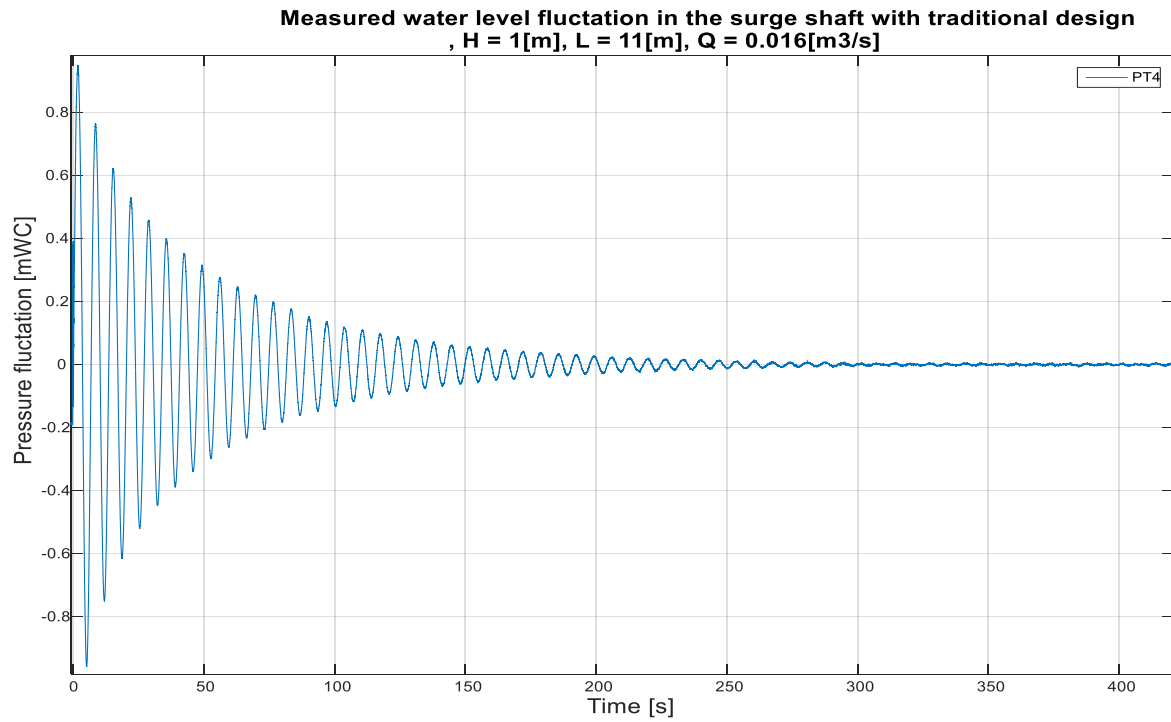
Figure 5-4: *Water fluctuation in the surge shaft Case 1 - Traditional surge shaft*
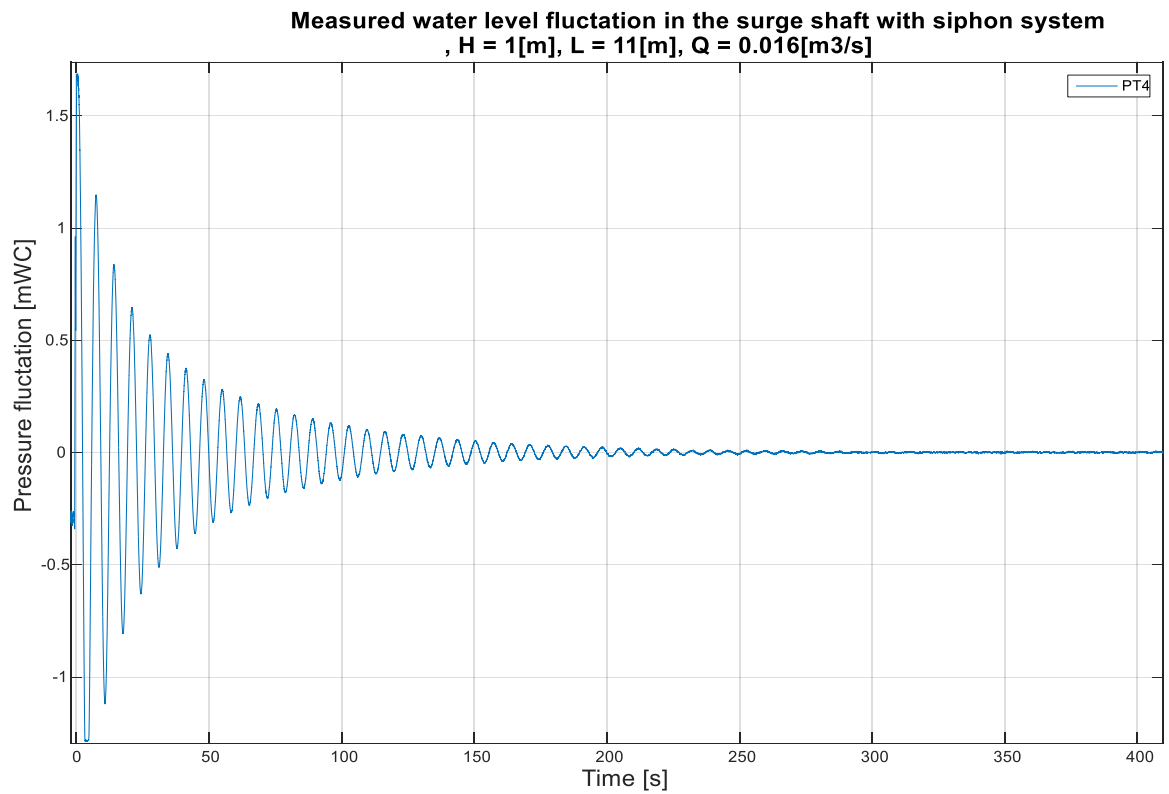
Figure 5-5: *Water fluctuation in the surge shaft for Case 2 - Siphon system*

**Measured water level fluctation in the surge shaft with traditional design
, H = 1[m], L = 11[m], Q = 0.007[m3/s]**
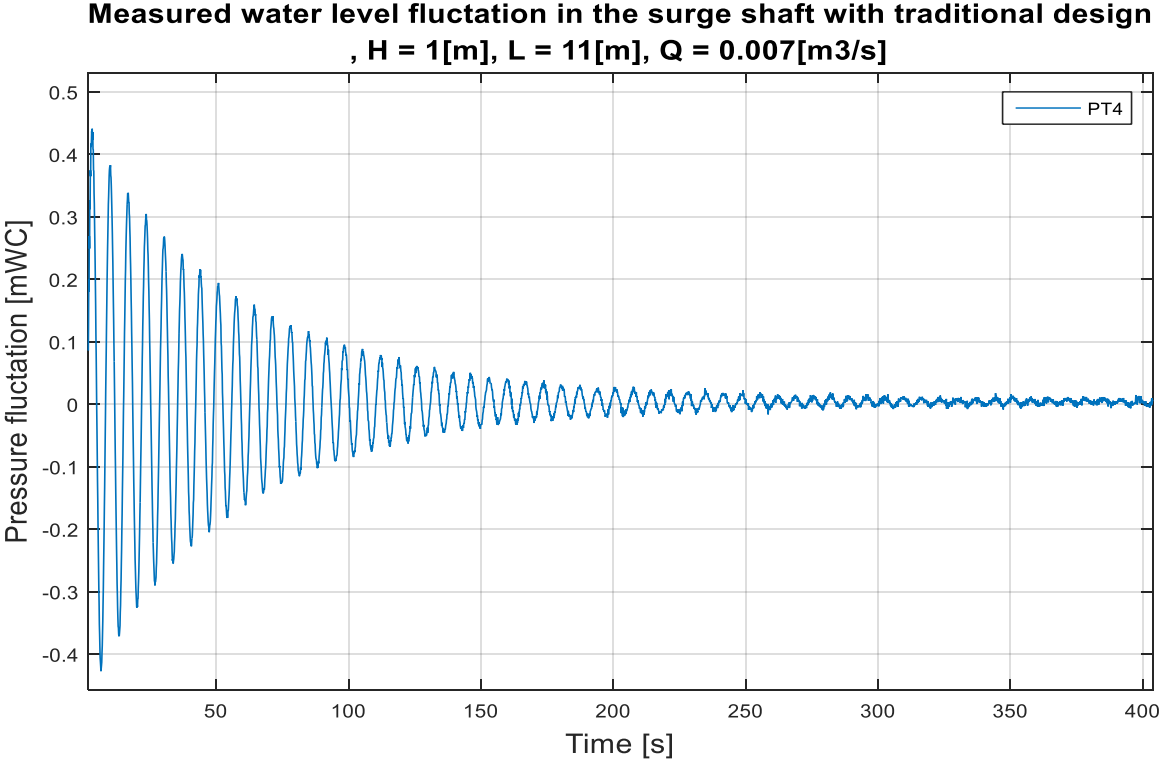
Figure 5-6: *Water fluctuation in the surge shaft for Case 3 - Traditional surge shaft*

**Measured water level fluctation in the surge shaft with traditional design
, H = 2[m], L = 11[m], Q = 0.007[m3/s]**
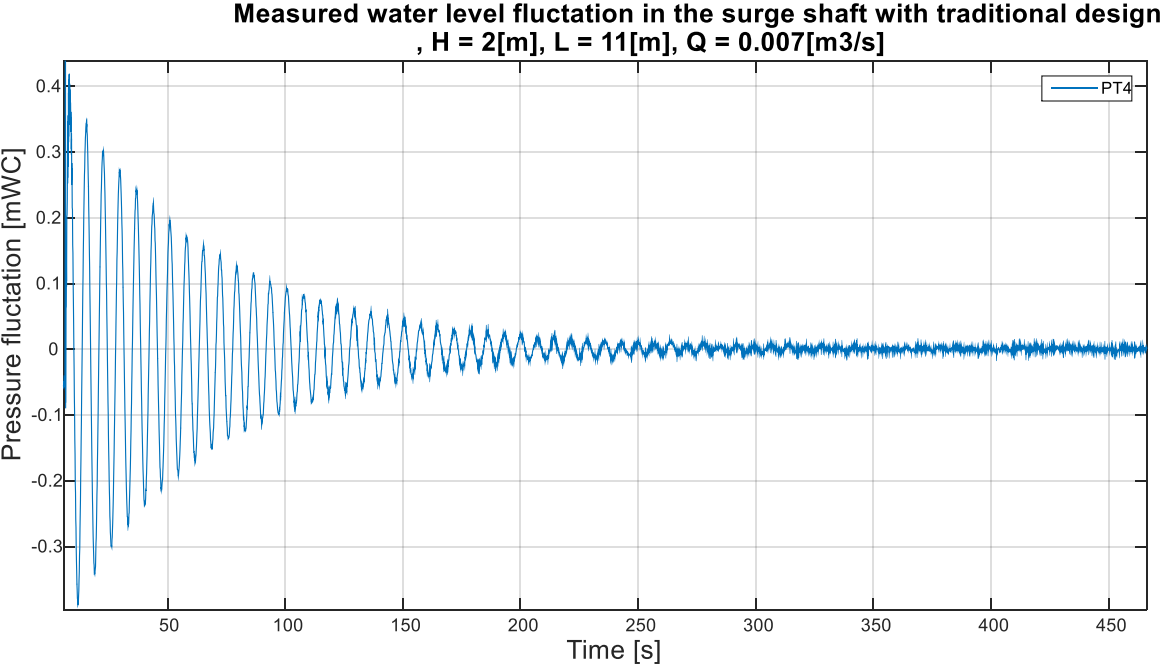
Figure 5-7: *Water fluctuation in the surge shaft for Case 4 – Traditional surge shaft*
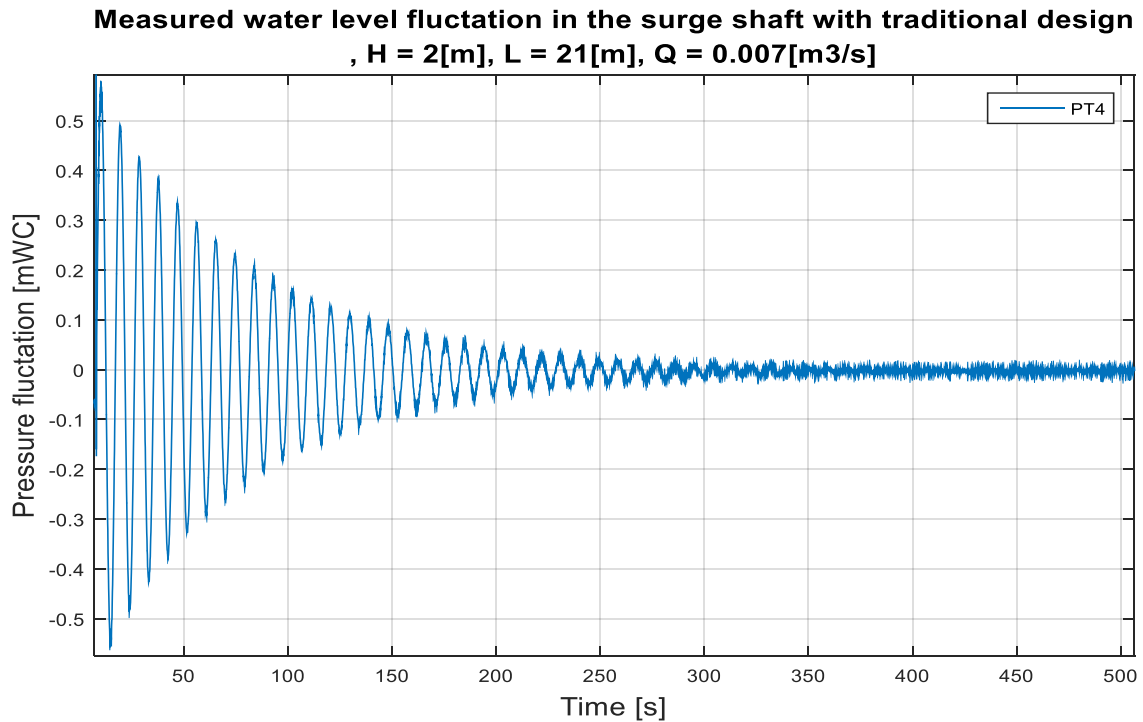
Figure 5-8: *Water fluctuation in the surge shaft Case 5 - Traditional surge shaft*

Figure 5-5, considering Case 1 and Case 2, presents how the oscillations between the two different surge systems develop from start to stationary flow. The measurements show equal frequency, but different time to reach stationary flow. The first peak for the siphon system shows a significantly higher peak than the traditional surge shaft. Hence, the siphon system has a higher damping ratio since the oscillations are damped out faster for the siphon case.

	Unit	Traditional	Damped [%]	Siphon	Damped [%]
Time period	[s]	6,8	-	6,8	-
Peak number 1	[mWC]	0,951	0	1,68	0
Peak number 6	[mWC]	0,278	70,77	0,282	83,21
Peak number 11	[mWC]	0,119	87,49	0,121	92,79
Peak number 22	[mWC]	0,029	96,95	0,021	98,75
Fully damped	[s]	400	-	300	-

Table 5-5: *Comparing the damping in the traditional surge shaft and the siphon system. Readouts from Case 1 and Case 2, depict in Figure 5-4 and Figure 5-5 respectively*

Results and Discussion

Considering Case 1 and Case 3, the impact from different flow rate are illustrated. Higher flow rate seems to give higher oscillations and faster damping. Both cases use approximately the same time to reach stationary flow. The results show reasonable measurements as water oscillations are highly depending on the flow velocity.

The difference between Case 3 and Case 4 illustrates the impact from changed water level in the upper tank. The change of water level in the upper tank should preferably not have any effect on the measurements, since an infinitely large volume in the upper tank may be assumed equal as a solid wall. Hence, the stationary water level in the upper reservoir. The fact that the velocity in the conduit does not depend on the height, but rather the downstream valve, is also a main reason why the height should not have any affect. If the volume of the upper tank is designed too small, relatively to the system, will the mass oscillations, on the other hand, be experienced in the tank, affecting the flow behavior.

The test with an increased water level in the upper tank shows unfortunately slightly reduced frequency, making it necessary to implement the height of the tank in the total headrace length. It is, therefore, reasonable to think that the tank was designed too small compared to the system flow. The increased water level was counted for in the friction modeling, by performing a frequency analyses showing that an increased water level of 1 mWC in the upper tank corresponded to 0.5 mWC increased headrace tunnel. The time to reach stationary flow has a trivial change to increased water level in the upper tank, giving marginally raised damping with 2 m compared to the 1 m water level.

The change in surge shaft design and flow rate shows no significant impact on the frequency. The frequency is as expected mainly depending on the headrace length, as depicted in Case 5 and some tendency in Case 4. The increased headrace tunnel in Case 5 shows additionally impact on the water fluctuation in the surge shaft, generating higher oscillations. It may be reasonable to assume that the increased water fluctuation is a result of a higher inertia.

5.4 FRICTION MODELLING – MASS OSCILLATION SIMULATION

In this chapter, the resulting simulation from the transient modeling using the Euler method is presented. The first subchapter depicts the steady state model considering no friction, followed by the results and discussion of the five friction models. Furthermore, flow parameters, such as velocity and frequency are investigated closer at the end of the chapter. Appendix D provides with the MATLAB-script related to calculation and simulation.

5.4.1 Steady state flow

In steady state condition, the calculations related to flow behavior are found by the known initial values depicted in **Table 4-6**. The minor loss coefficient k_i is estimated by the values depicted in **Table 5-6**. Minor losses includes all disturbance in the waterway after the transient dynamics are generated. In the traditional case is the system demarcated by the free water surface in the upper reservoir and the free surface of the surge shaft. In the siphon, the demarcated area after water column separation can be assumed similar, as the water surface in the siphon system will oscillate in the same pipe section as in the traditional case. If considering the system from the upper reservoir to the sump, which is the natural point of implementing a turbine, the minor losses would be greater due to change in the flow path and total disturbance from additional objects in the path.

Coefficient for minor losses after generated transient dynamics, k	
Operation situation	Traditional surge shaft and Siphon pipe system
Gate Valve, Fully Open	0.12
Tee, Flanged, Dividing Branched Flow	0.61
Inlet, Conus	0.35
Sum	**1.08**

Table 5-6: *Loss coefficient for the minor losses for the traditional surge shaft and the siphon system [6]*

Results and Discussion

Table 5-7 lists some interesting parameter results for all five cases. The head loss is calculated at an assumed steady state flow, using the basic principle of the Darcy-Weisbach head loss equation. Associated equations are given the theory Chapter (2).

Parameters	Unit	Case 1	Case 2	Case 3	Case 4	Case 5
Reynolds number	-	103880	103880	45450	45450	45450
Steady state friction factor	-	0.0177	0.0177	0.0212	0.0212	0.0212
Total head loss	[m]	0.0805	0.0805	0.0176	0.0176	0.0282
Time period of water hammer	[s]	0.0316	0.0316	0.0316	0.0316	0.0573
Time period of mass oscillations	[s]	6.83	6.83	6.83	6.83	9.2
Frequency water hammer	[Hz]	31.6	31.6	31.6	31.6	17.5
Required sampling frequency on water hammer dynamics	[Hz]	63.21	63.21	63.21	63.21	44.91
Frequency mass oscillations	[Hz]	0.92	0.92	0.92	0.92	0.68
Required sampling frequency on mass oscillations	[Hz]	1.84	1.84	1.84	1.84	1.37
Hydrodynamic entry length	[m]	3.66	3.66	2.98	2.98	2.98
Highest upswing	[m]	0.958	0.958	0.455	0.455	0.570
Lowest downswing	[m]	-0.993	-0.993	-0.433	-0.433	-0.583

Table 5-7*: Estimated flow parameters from initial conditions*

All cases are found turbulent at the initial condition. **Table 5-7** show how the head loss is dependent on the flow rate, resulting in a greater loss at a higher velocity for the equal cross-section. The time period of the mass oscillations are considerably larger than the time period of the water hammer, as expected. Hence, assumptions given on the mass oscillations are not valid for water hammer calculation. The water deviation in the shaft is found satisfying for all cases, giving the limitation of not spilling water over the top or letting air into the horizontal headrace tunnel. Required sampling frequency is found from Nyquist sampling theorem, for water hammer and mass oscillations the highest required sampling frequency was 63.21 Hz and 1.84

Hz respectively. Before the signal was averaged down to 10 Hz were all measuring devices fulfilling both frequency requirements, and thus the water hammer may be observed in the raw data from the measurements.

Figure 5-9 depicts the time simulations of the water fluctuations in the surge shaft for 11 m and 21 m with equal velocity. The simulation consider constant friction and confirms the findings from **Table 5-7**. The frequency will decrease as the water string increases, and the combination of the flow rate and initial friction losses determines the size of the water fluctuation.
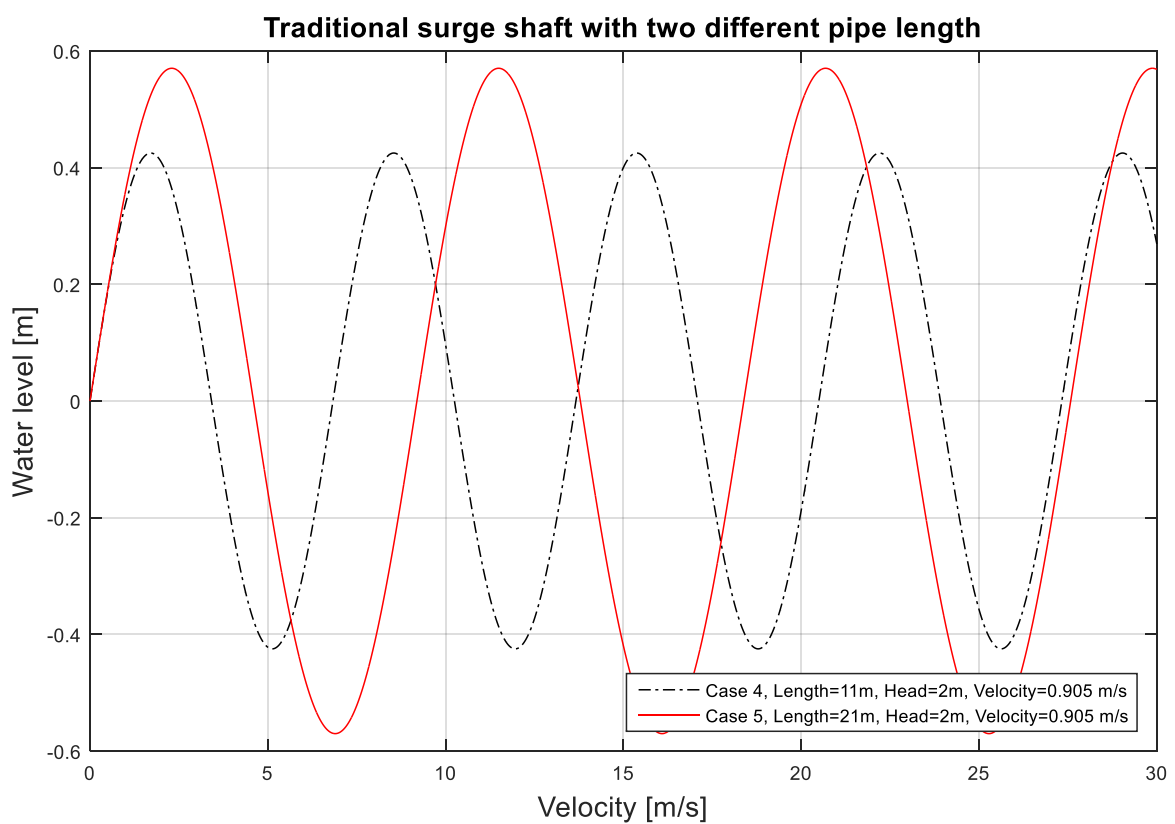
Figure 5-9: *Result from steady state simulation of Case 4 and Case 5*

5.4.2 Unsteady flow simulation - Traditional surge shaft

In contrast to the steady state simulation above will real behavior be slowly damped out as time goes. Hence, friction has to be considered in the modeling process. Following is the results of the four selected transient friction models presented and subsequently discussed in separated subchapters.

5.4.2.1   The Quasi-steady friction model

The Quasi-steady friction model uses the described quasi-steady friction term to calculate the friction by updating the parameters at each time step. **Figure 5-10** to **Figure 5-13** depicts the simulation results considering the cases with traditional surge shaft.
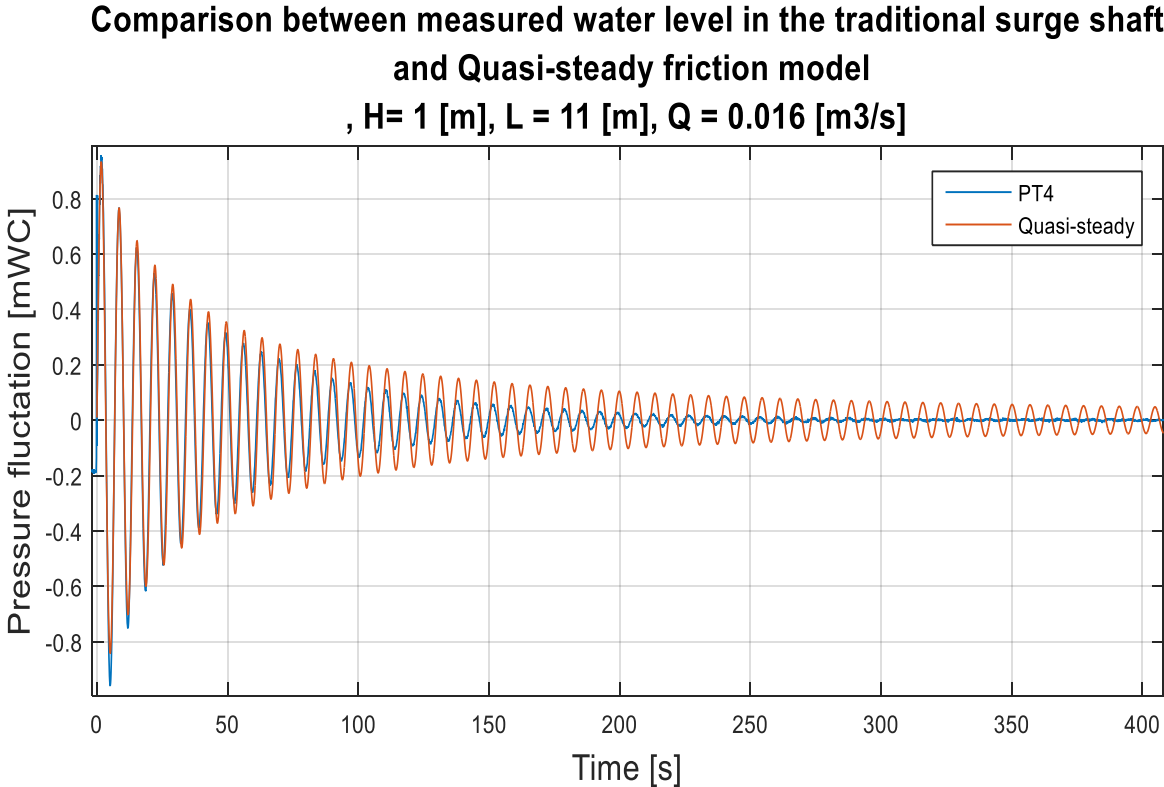
Figure 5-10*: Quasi-steady friction model compared against measured data for Case 1*

**Comparison between measured water level in the traditional surge shaft
and Quasi-steady friction model
, H= 1 [m], L = 11 [m], Q = 0.007 [m3/s]**
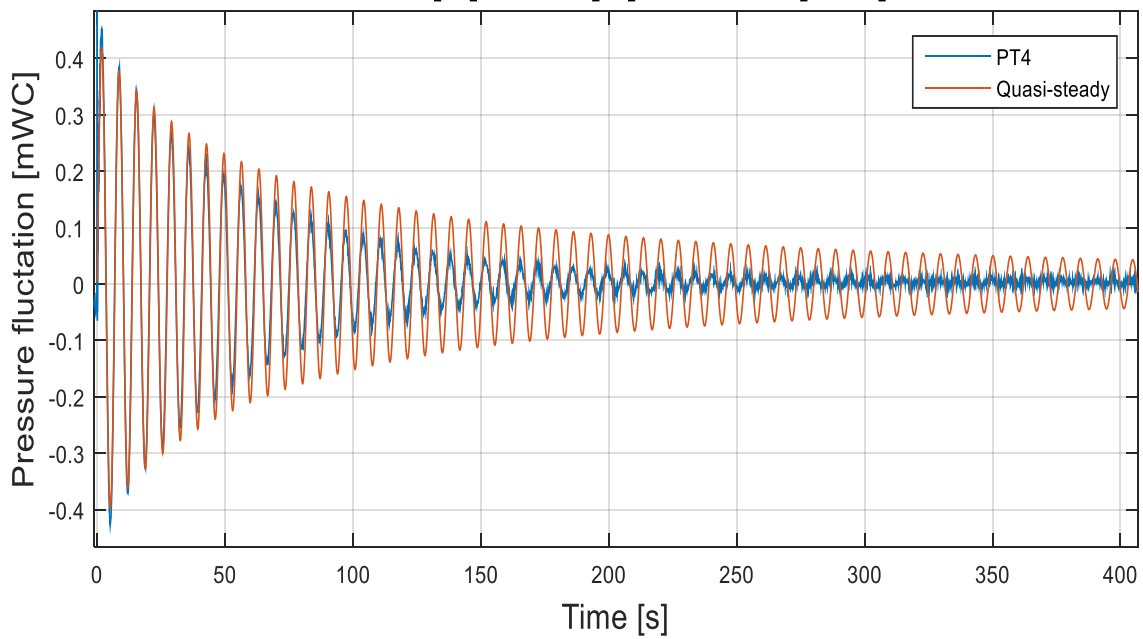
Figure 5-11: *Quasi-steady friction model compared against measured data for Case 3*

**Comparison between measured water level in the traditional surge shaft
and Quasi-steady friction model
, H= 2 [m], L = 11 [m], Q = 0.007 [m3/s]**
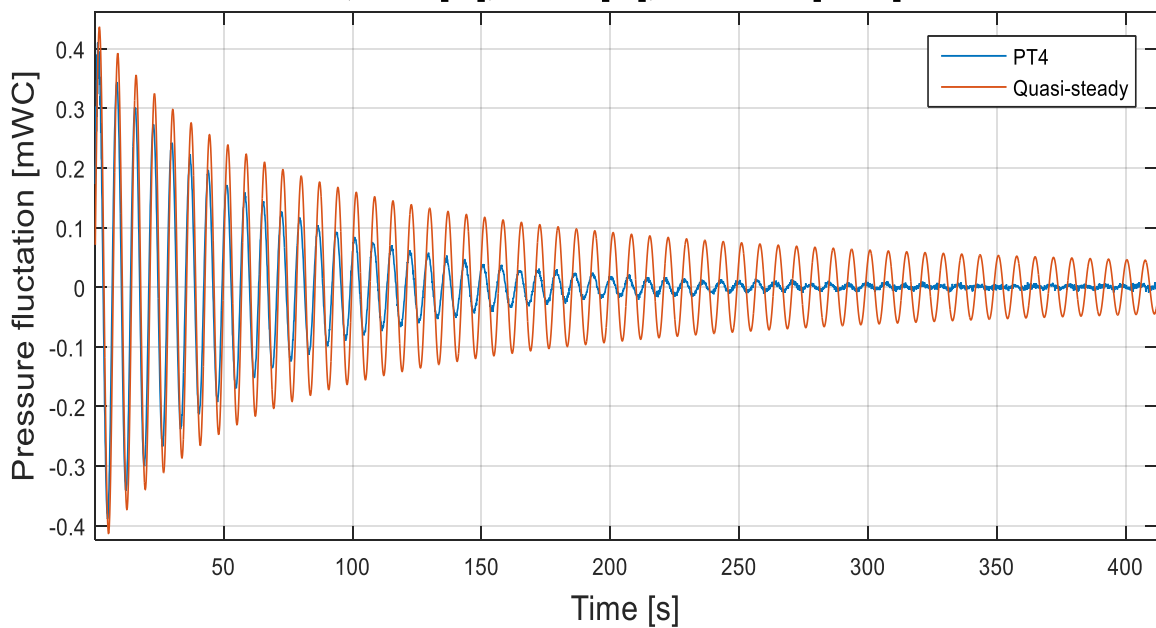
Figure 5-12*: Quasi-steady friction model compared against measured data for Case 4*

Comparison between measured water level in the traditional surge shaft and Quasi-steady friction model
, H= 2 [m], L = 21 [m], Q = 0.007 [m3/s]
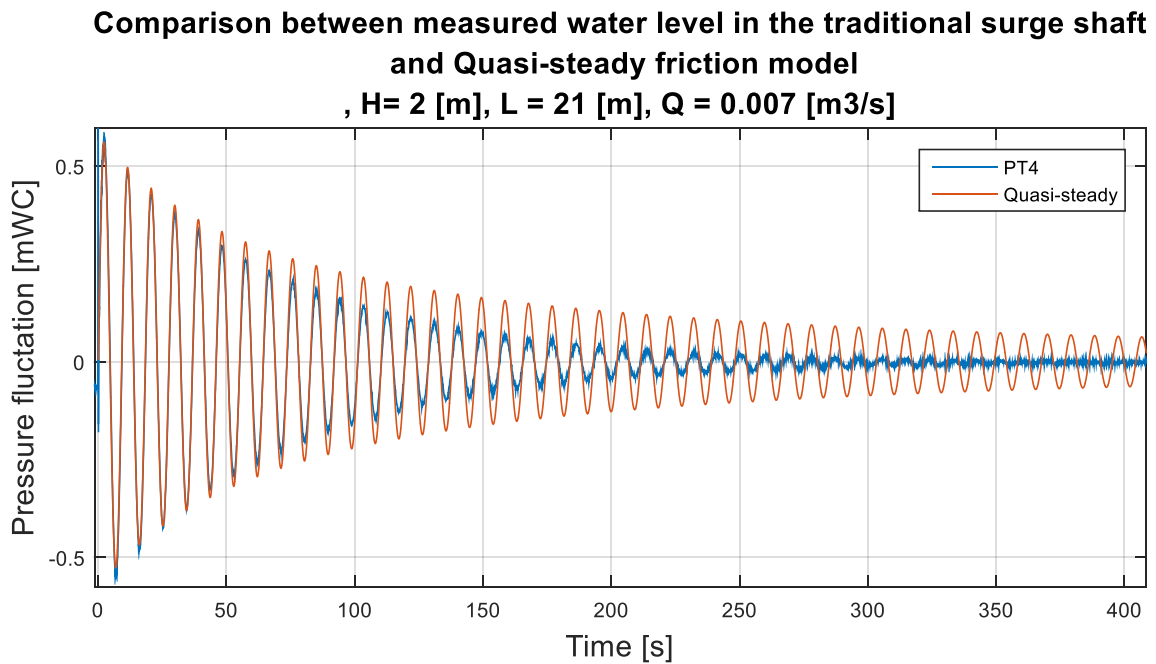
Figure 5-13: Quasi-steady friction model compared against measured data for Case 5

The above results for the Quasi-steady friction model show great correspondents to measurements in the first three to four wave peaks. On the other hand, as time goes, predicts the model too low damping, and additionally give a constant oscillating amplitude when reaching the stationary flow as the frictional losses are disappearing when the average velocity goes to zero.

Results for Case 3 and Case 4 depicts how the deviation between measured value and simulation increases with increasing head in the upper tank. The increased deviation is a result of the change in the measurements, as the model predicts the same response for both water levels as the length is equal. Hence, the model does not take care of the change in the volume of the upper reservoir if just considering headrace length, and performance will, thereby, be decreased with increased water level in the tank.

From **Figure 5-12** to **Figure 5-13**, respectively Case 4 and Case 5 is the headrace length increased from 11 m to 21 m. The length increase show improved performance for the Quasi-steady model, as the deviation from the measurements are reduced. Considering all test cases is the wave propagation quite similar where the oscillations are never completely damped out when reaching the stationary condition.

5.4.2.2   Ogawa et al. friction model

Simulations from the Ogawa et al. friction model compared against measured data is depicted in **Figure 5-14** to **Figure 5-17**.
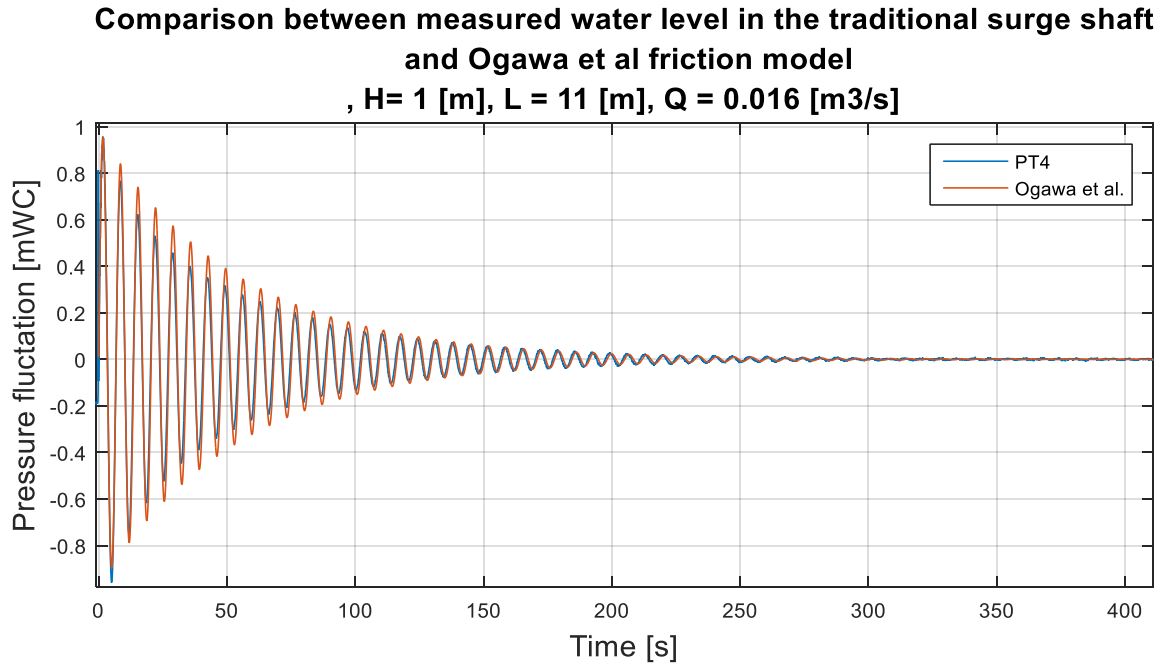
Figure 5-14*: Ogawa et al. friction model compared against measured data for Case 1*
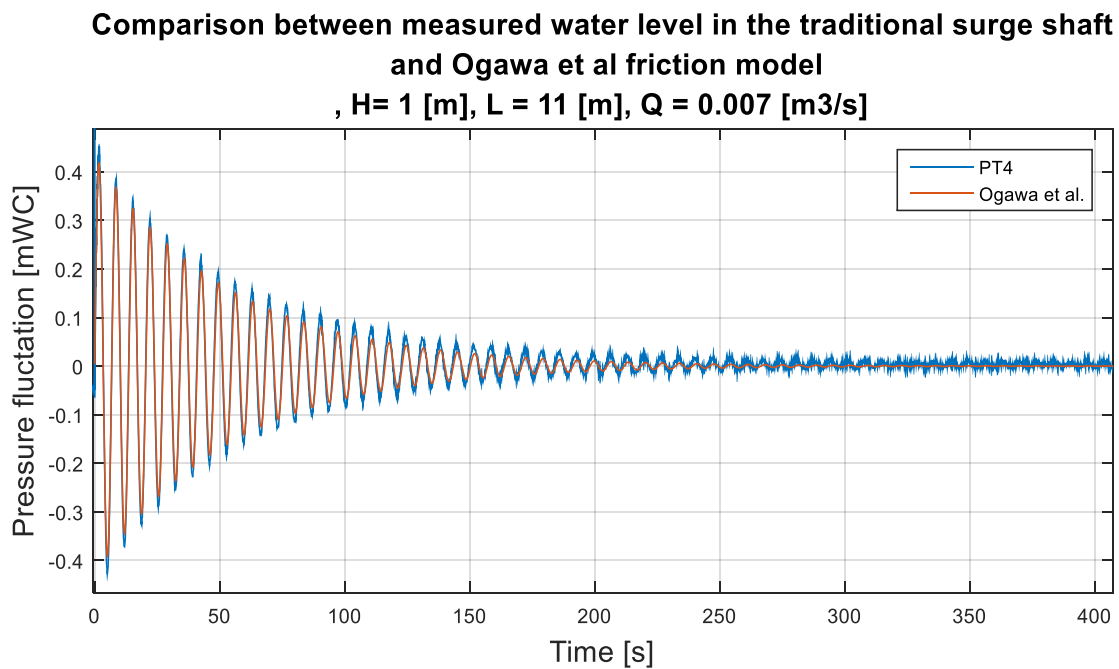
Figure 5-15: *Ogawa et al. friction model compared against measured data for Case 3*

Comparison between measured water level in the traditional surge shaft and Ogawa et al friction model
**, H= 2 [m], L = 11 [m], Q = 0.007 [m3/s]**
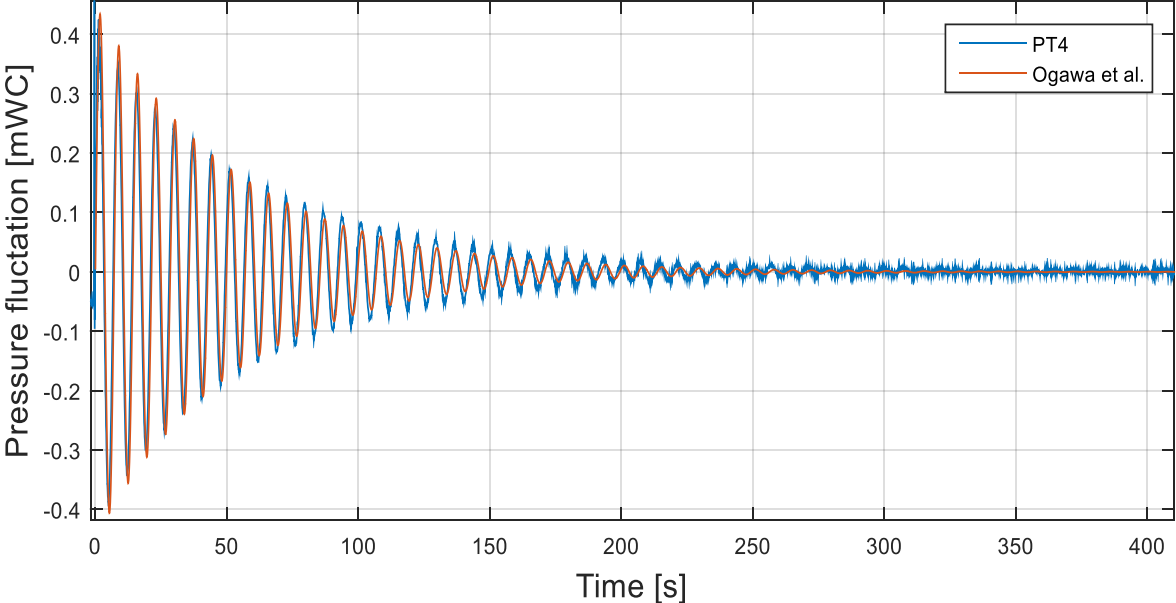
Figure 5-16: Ogawa et al. friction model compared against measured data for Case 4

Comparison between measured water level in the traditional surge shaft and Ogawa et al friction model
, H= 2 [m], L = 21 [m], Q = 0.007 [m3/s]
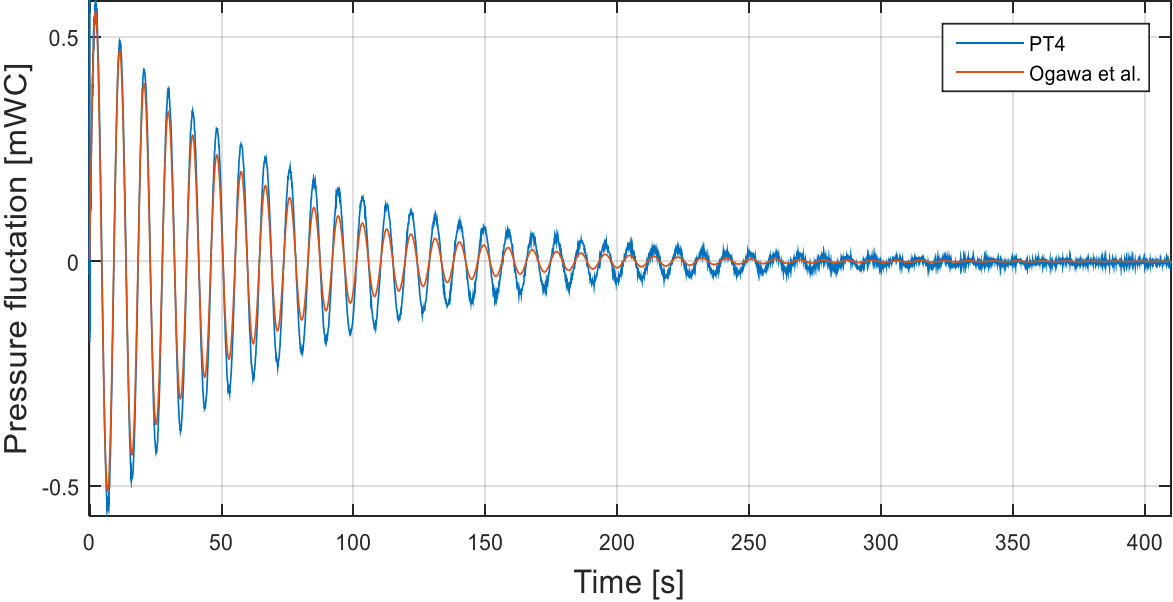
Figure 5-17: *Ogawa et al. friction model compared against measured data for Case 5*

The above simulations show good accordance with measurements in both time period and time to reach complete rest. The model by Ogawa et al. predicts stationary flow after approximately 450 s and 320 s, respectively for 11 m and 21 m. The distribution of the dampening is showing some deviation from the laboratory measurements for all cases. It can be seen that the model predicts less dampening in the initial time periods where the Re number is relatively high, and comparatively larger dampening at the end, where the Re number is low.

The model by Ogawa et al. has reduced performance for an increased headrace length. **Figure 5-16** and **Figure 5-17** displays this reduction, where the headrace tunnel is increased from 11 m to 21 m, giving an increased deviation compared to measurements. The model simulation has no influence of the change in water level in the upper tank, and thereby, similarly as the Quasi-steady model, will the performance be depending on the resulting change in measurements only, if water level change in the upper reservoir is considered. Performance from the model by Ogawa et al. may additionally be reduced by the test rig design since the model is derived from U-tube specific cases and not a hydropower plant design.

5.4.2.3 Vitkovsky's friction model

The fast transient friction model by Vitkovsky is simulated and tested likewies on slow mass oscillations. The result is displayed in **Figure 5-18** to **Figure 5-21**, showing how the simulations are compared against real measurements. Since the water is assumed to move with equal velocity throughout the whole water string is it valid and thus performed simulations with the Euler method. The k coefficient in the Vitkovsky model can be found from the Vardy shear decay coefficient C.

Figure 5-18: *Vitkovsky friction model compared against measured data for Case 1*

Comparison between measured water level in the traditional surge shaft and Vitkovsky friction model
, H= 1 [m], L = 11 [m], Q = 0.007 [m3/s]
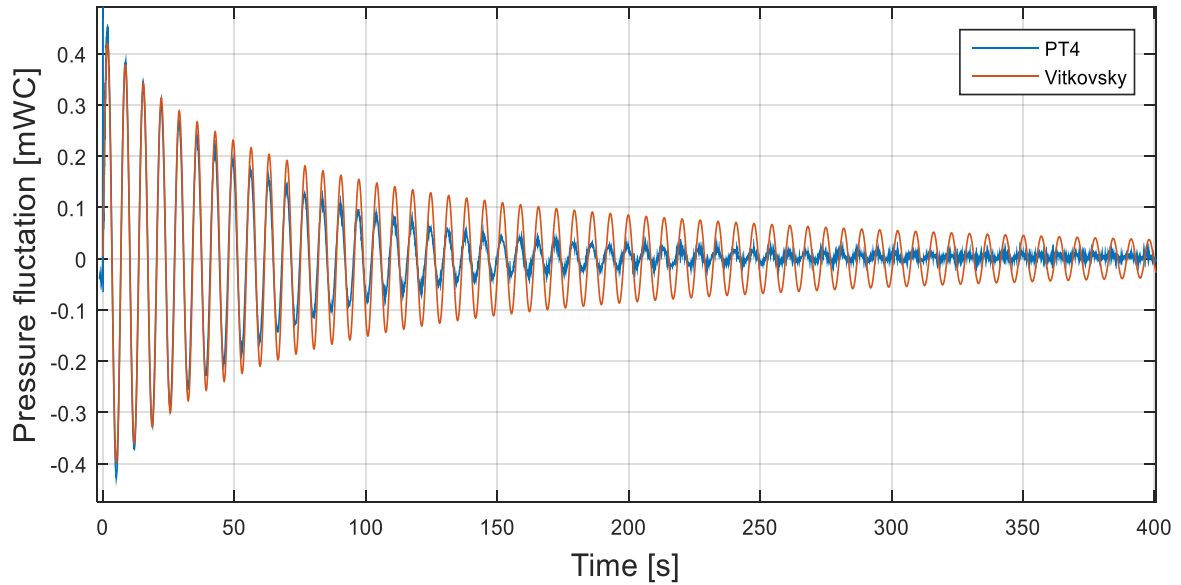
Figure 5-19: *Vitkovsky friction model compared against measured data for Case 3*

Comparison between measured water level in the traditional surge shaft and Vitkovsky friction model
, H= 2 [m], L = 11 [m], Q = 0.007 [m3/s]
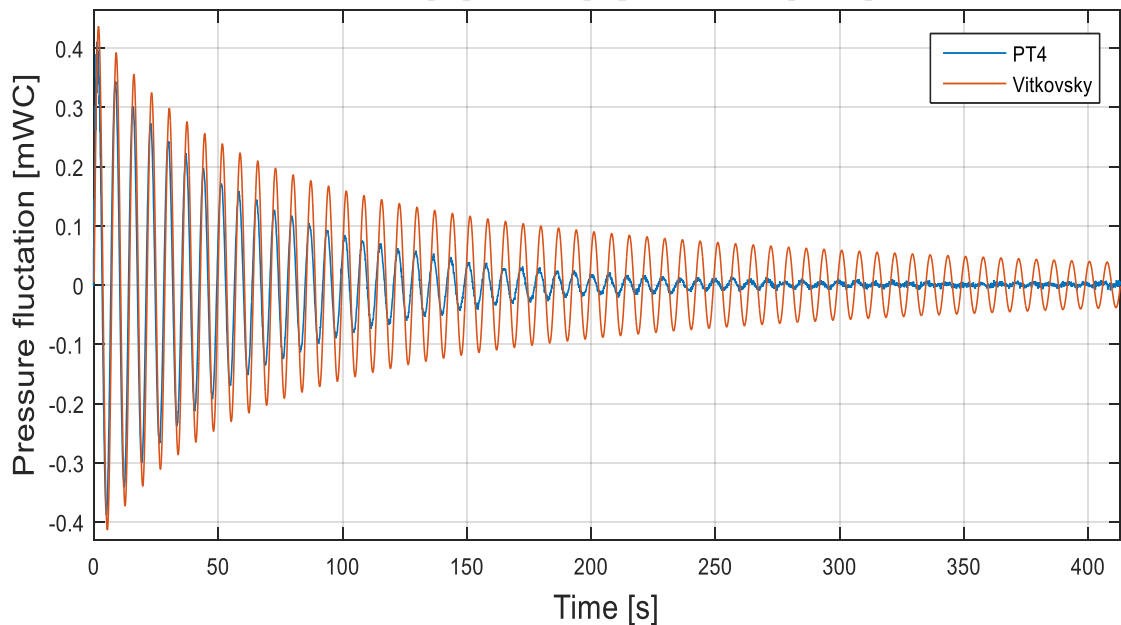
Figure 5-20: *Vitkovsky friction model compared against measured data for Case 4*

Comparison between measured water level in the traditional surge shaft and Vitkovsky friction model
**, H= 2 [m], L = 21 [m], Q = 0.007 [m3/s]**

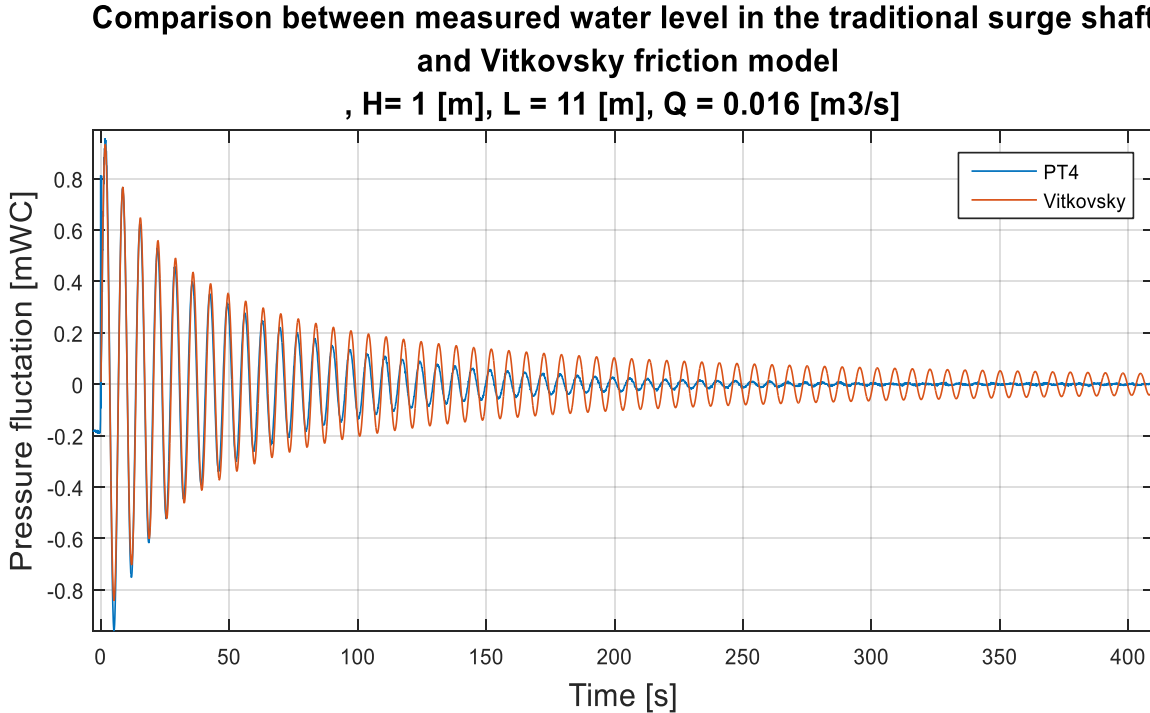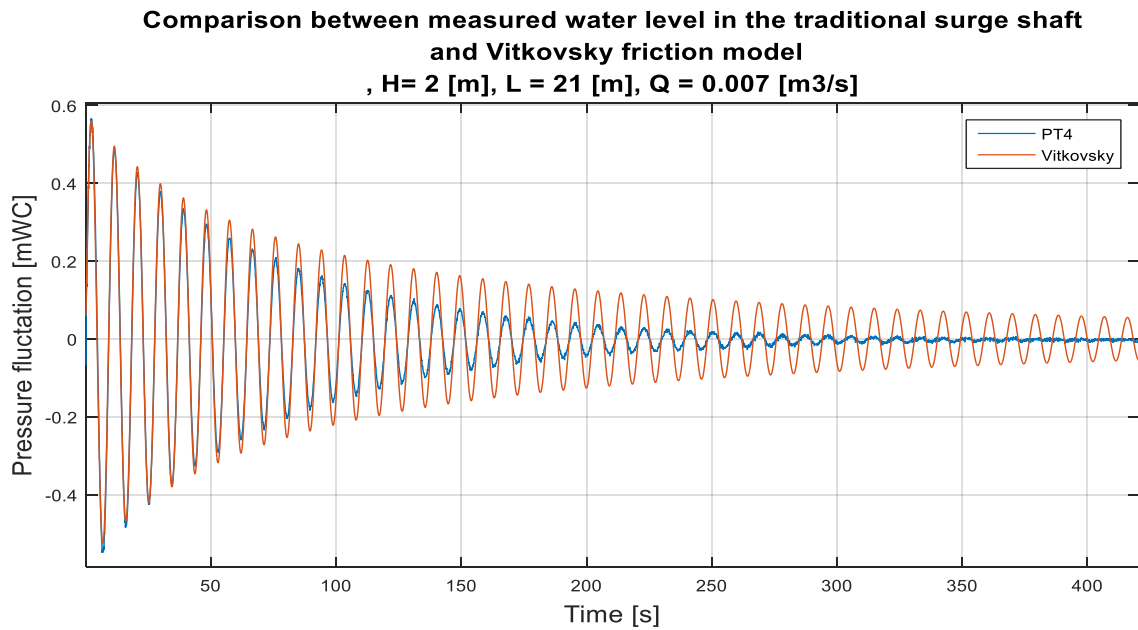***Figure 5-21:*** *Vitkovsky friction model compared against measured data for Case 5*

The model by Vitkovsky is relatively similar in performance for all cases with 11 m headrace and traditional surge shaft. The tendency of the results show best performance for the first two-three time periods, where it estimates an amplitude slightly beneath the results from the measurements in the laboratory. Considering Case 1, Case 3 and Case 4 are the deviations between the measurement and simulation increasing as time develops. The deviation is a result of predicting too low dampening at unsteady flow conditions. The model by Vitkovsky estimate the oscillations to be completely damped out after approximately 1500 s for the 11 m cases, which is 1100 s after the real behavior. With the increased headrace tunnel of 21 m, is the model, on the other hand, showing an improved performance for the first amplitudes, where the deviation between the simulated result and the real behavior is less than for the 11 m cases. As time goes, does also Case 5, with the 21 m headrace predict too low damping compared to measurements, and additionally propagate similar as the 11 m cases but having an even larger deviation to reach stationary condition. Case 5 is approximately damped out after 2500 s, which is over 2000 s slower than the measurements. The frequency, considering all cases are found equal compared to the measurements. The difference in water level in the upper reservoir have no impact on the simulation. The change in performance is thus only depending on the change in the real behavior, like the other models. Hence, increased water level in the tank produces relatively higher damping, giving the model a reduced performance if the water level is increased.

5.4.2.4 One-term friction model

The purposed one-term friction model is tested. The basic idea is presented in chapter (2.7) and utilized through Eq.(32). The correction constant, B, in the model equation is calibrated for steady state flow valid for cross-section extension limited by the backflow angle of 5 degrees, as justified earlier. The correction constant is found to be 308.7, valid at steady state flow for the specification given in **Table 2-1**. It is now of interest to see how this model will perform for unsteady flow conditions, and how the parameters in the model equation affect the results. In this subchapter, will the simulation for the one-term model be evaluated and discussed. Appurtenant MATLAB-script is found in Appendix D.

The length of the pipe not effecting the constant B after calibration. Hence, the model will estimate the same time period as the Darcy-Weisbach head loss equation. The one-term model and Quasi-steady model is equal if there is no velocity change. However, if velocity change is present will the model give different result. Velocity change may be sourced from geometry change, $\left(\frac{\partial V}{\partial x}\right)$, or time dependent oscillations, $\left(\frac{\partial V}{\partial t}\right)$.

The response of increased cross-section between two pipe sections, as depicted in **Figure 2-10** change from the one-term model is a decreased friction. If acceleration or deceleration is present, will the model predict an increased friction. These facts correspond to the theory of frictional forces in pipe flow.

Figure 5-22 shows the one-term model compared against real data measured in the dynamic test rig considering Case 1. The result is quite similar to the simulation with the Quasi-steady model, as shown in **Figure 5-23**. The only difference between these models is the small increase in friction at acceleration and deceleration.
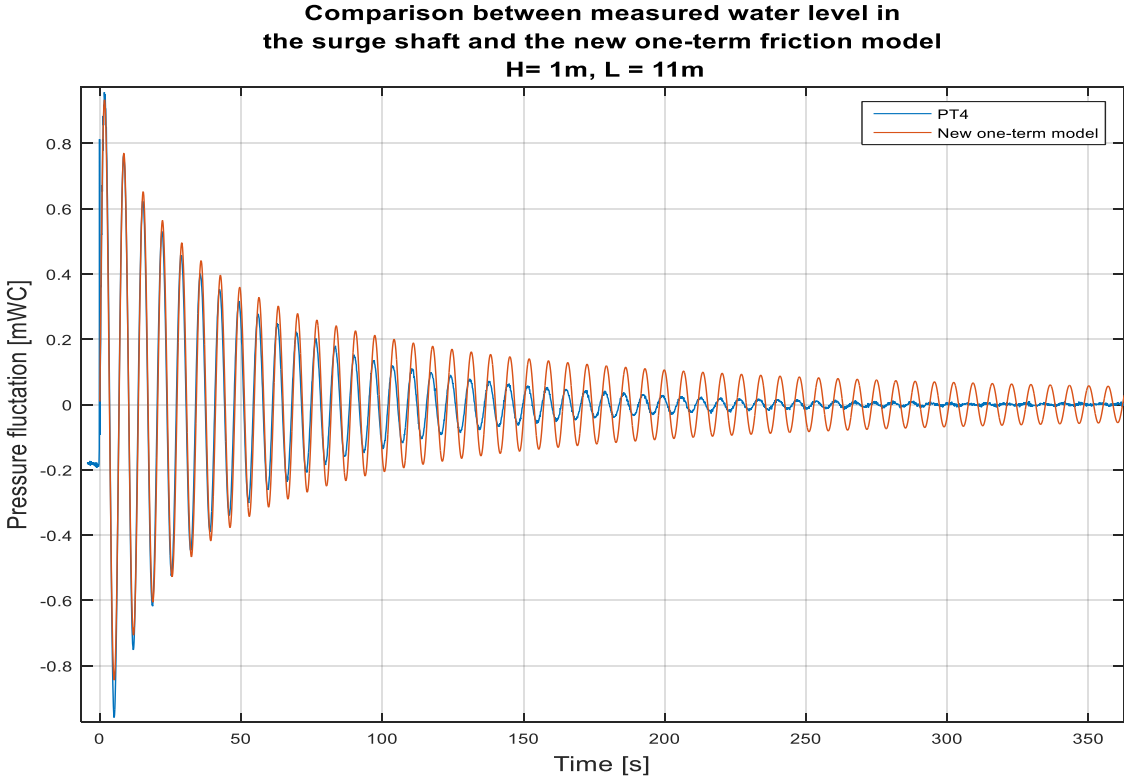
Figure 5-22: *The one-term friction model compared against measured data for Case 1*

Figure 5-23 depicts the simulation of Case 1 where only the time-dependent velocity change is present. In the curiosity to see how the model will behave if the velocity is changing in both time and position, is a simulation with geometrical change simulated. **Figure 5-24** shows the result between the Quasi-steady and the one-term friction model at combined velocity change due to unsteady flow (Time dependent velocity change) and cross-section increase (Position dependent velocity change). The case specification simulated in **Figure 5-24** is given in **Table 2-1**.
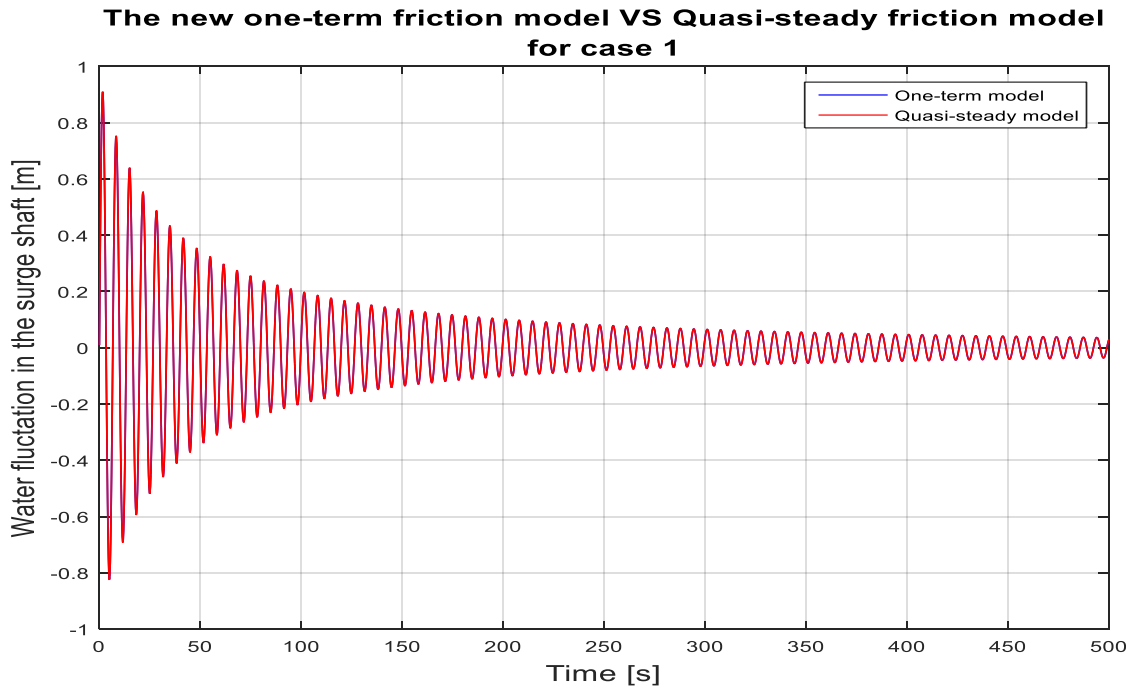
Figure 5-23: *Comparing the one-term model and the Quasi-steady model for Case 1*
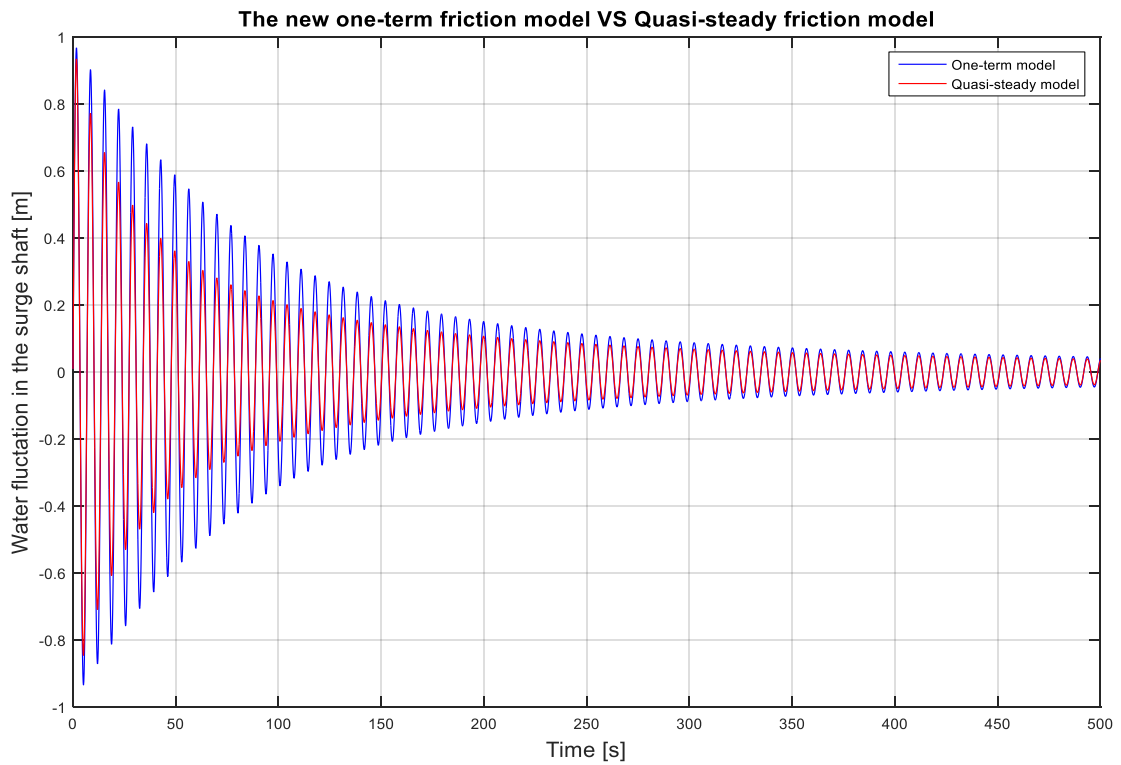
Figure 5-24: *The one-term model VS Quasi-steady model at combined velocity change , considering change in time and position*

Results and Discussion

To evaluate the rate of impact from each of the two sources of velocity change, time and space, is a simulation with just geometrical change performed. **Figure 5-25** depicts the result where the one-term model is compared against the Quasi-steady friction model. How the constant B in the one-term model will be affected by the increased cross-section is shown in **Figure 5-26**.
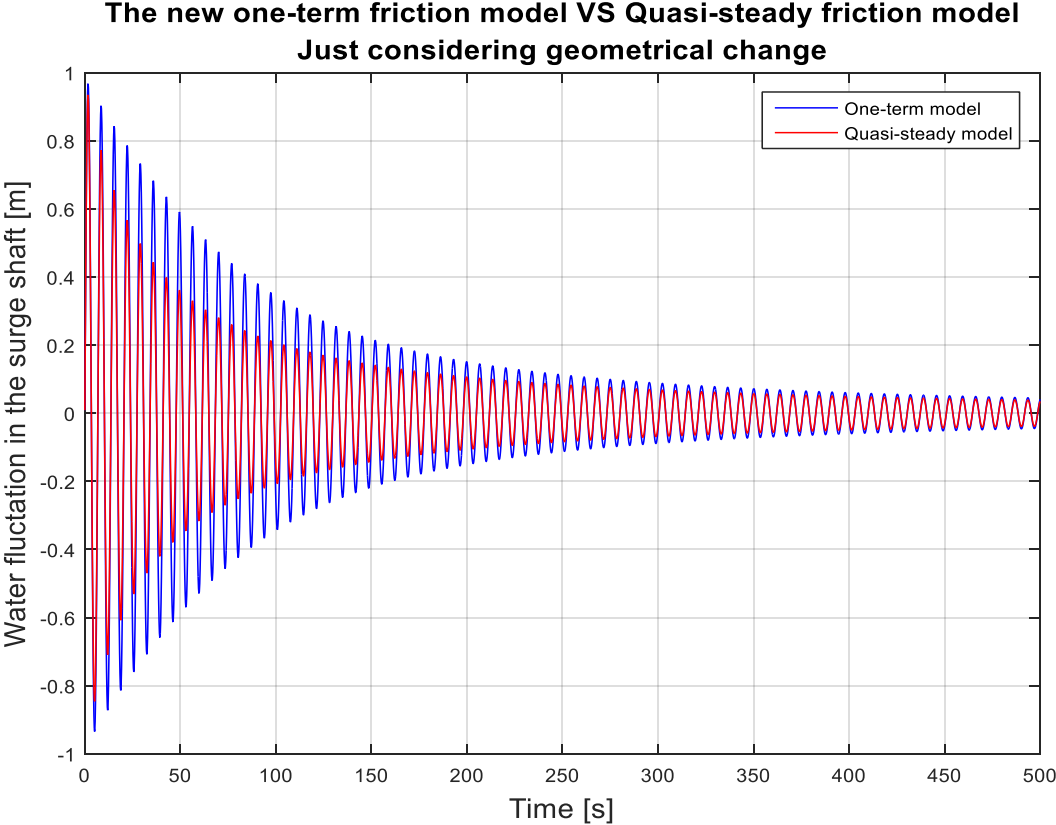
Figure 5-25: The one-term model VS the Quasi-steady model at geometrical change
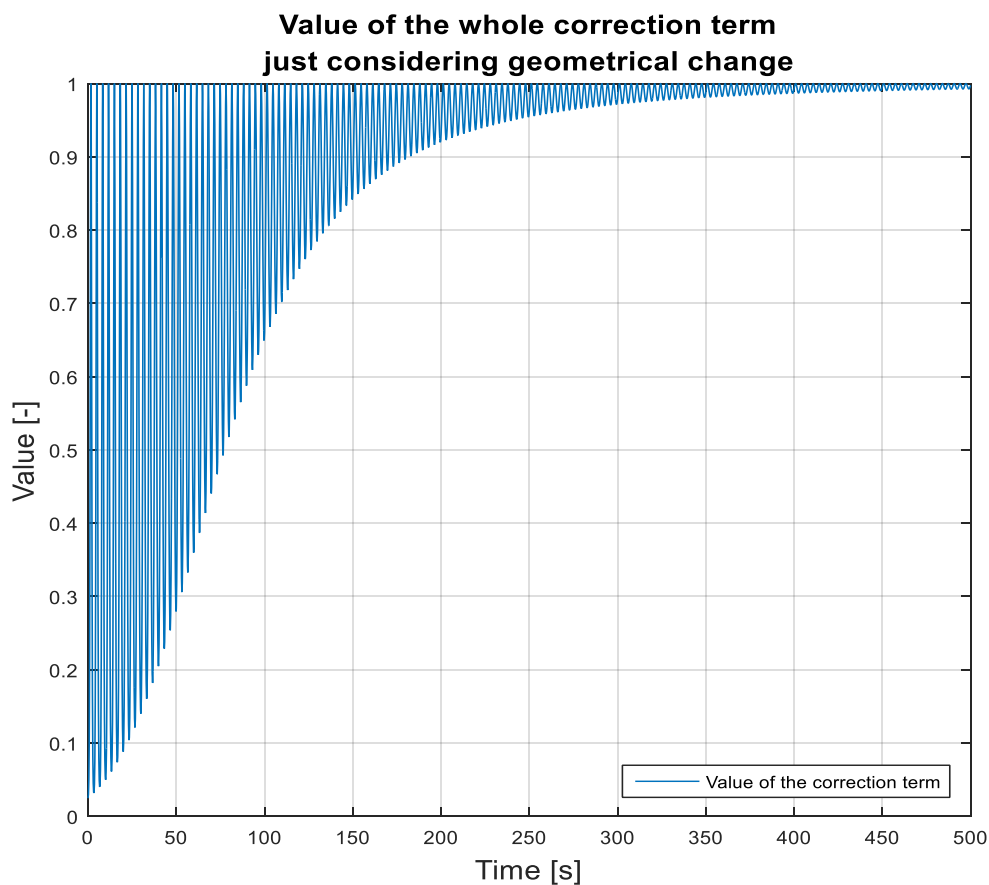
Figure 5-26: *Value of the correction term, considering just geometrical change*

As shown from **Figure 5-25** and **Figure 5-26** above, predicts the one-term model a lower friction due to cross-section increase. This corresponds to the theory on reduced friction at increased cross-section.

If now considering unsteady flow but disregard cross-section change may the effect from unsteady flow be found, and additionally display how this will affect the estimated friction. The result is shown in the previously simulation depict in **Figure 5-23**, where the one-term model with just time dependent velocity change (unsteady flow) is compared against the Quasi-steady model. In **Figure 5-27** is a close-up picture of the randomly selected third peak, depicting the increased frictional impact from the acceleration term in the one-term model. This trend is similar at all peaks. At the top point of the oscillations are both models estimating zero friction, as the average velocity is zero. When the oscillations proceed to the acceleration area, will the system again experiencing friction. **Figure 5-27** depicts a point in the acceleration area, illustrating how the one-term friction model predict an additional friction of approximately

0.0006 mWC compared to the Quasi-steady model. The additional friction is a direct result of the contribution from the correction term, as the acceleration, $\left(\frac{\partial V}{\partial t}\right)$, is greater than zero. The absolute correction of the acceleration in the model equation makes the additional friction from the acceleration to act against the flow at both acceleration and deceleration, which corresponds to earlier investigations on friction [10].

Compering calculated head loss in the one-term friction model and the Quasi-steady model considering case 1 at peak number thre
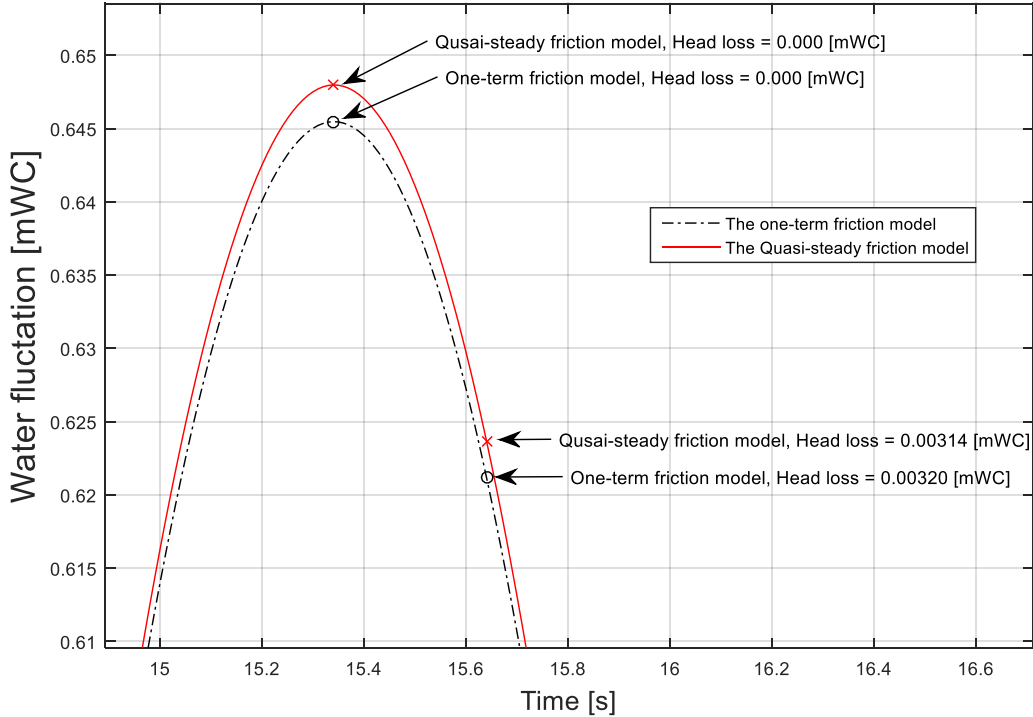
Figure 5-27: The one-term model VS the Quasi-steady model at the third peak

The change in the total value of the correction term considering only unsteady flow is depicted in **Figure 5-28**, and will change in relation to the size of the oscillations, giving largest damping at the highest amplitudes, and further prorogate down as the oscillations are damped out. The deviation ratio between the one-term model and the original Darcy-Weisbach head loss equation for steady state is found to be equal throughout the transient period.
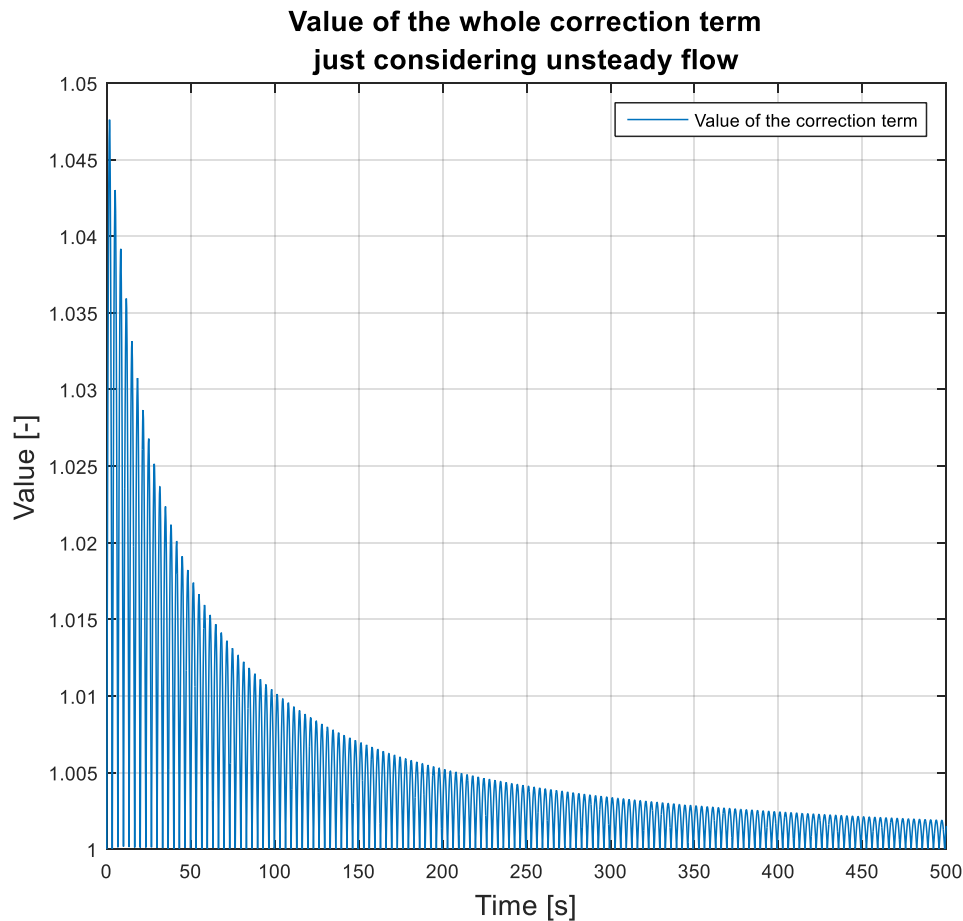
Figure 5-28: *Value of the correction term, considering time dependent velocity change (Unsteady flow)*

The simulation results for the one-term model shows how the idea responds to unsteady flow. The model is not counting for the rate of frictional impact but shows the direction of impact. Hence, the result is not valid for direct use without scaling the impact from the acceleration term first. Since the model acts and adjusts the friction in the desired direction in unsteady flow is it reasonable to think that the one-term model idea could be further developed to deliver accurate results for both steady and unsteady flow conditions.

The fact that the size and thus the contribution on friction from the correction constant is depending on the calibration is something that cannot be ignored. The choice of geometrical specifications of the pipe sections determines the correction constant value, and is thus essential for the end result. As the model is presented now, is the geometrical dimension based on the extension angle where backflow is not generated. This choice is made based on preventing additional losses generated by backflow, which is a additional loss the model do consider.

5.4.3 Unsteady flow simulation - Siphon system

Unsteady flow simulations with siphon system instead of a traditional surge shaft are made for all four transient friction models tested in Chapter (0). A study of how the mass oscillations will behave and how the friction models will perform in a siphon system is issued. As mention does the siphon system introduce the subject on a moving water string in the surge shaft, giving the opportunity to investigate the system without the acceleration phase of the initial stagnant water in the traditional surge shaft. The initial water fluctuation in the surge shaft is set to 1.5 mWC for the siphon system simulation, as this is the height difference between the neutral balance point and the point of water separation in the top of the siphon. This statement shows good correspondence to measured data. The friction modeling compared against measurements, considering siphon shaft, is depicted in **Figure 5-29** to **Figure 5-32**. **Figure 5-29** presents the result for the Quasi-steady friction model. From this result may it be observed that the model estimate too low damping throughout the whole simulation. The model predicts approximately the same propagating behavior as for the traditional surge shaft. Likewise, is the oscillations not completely damped out when reaching stationary flow. The main difference between the two surge shaft designs, using the Quasi-steady model, is the expected friction in the first three-four time periods, where the Quasi-steady model estimates too high friction in the traditional design and too low friction in the siphon shaft.
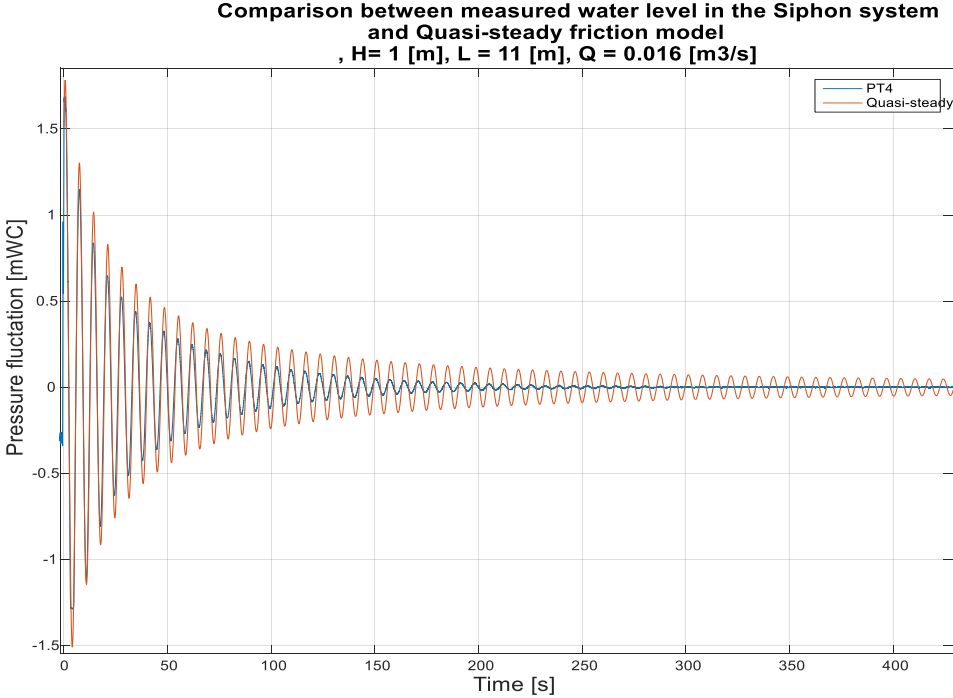
Figure 5-29*: Quasi-steady model compared to measured data for – Siphon system*

When looking at the simulation result from the model by Ogawa et al., depicted in **Figure 5-30**, does this model as well decay in performance for the siphon system. The model predicts too low friction in the start, before it retrieves the measured data at the end of the transient period. Similar to the simulation results with a traditional surge shaft is the oscillations completely damped out when reaching the stationary condition.
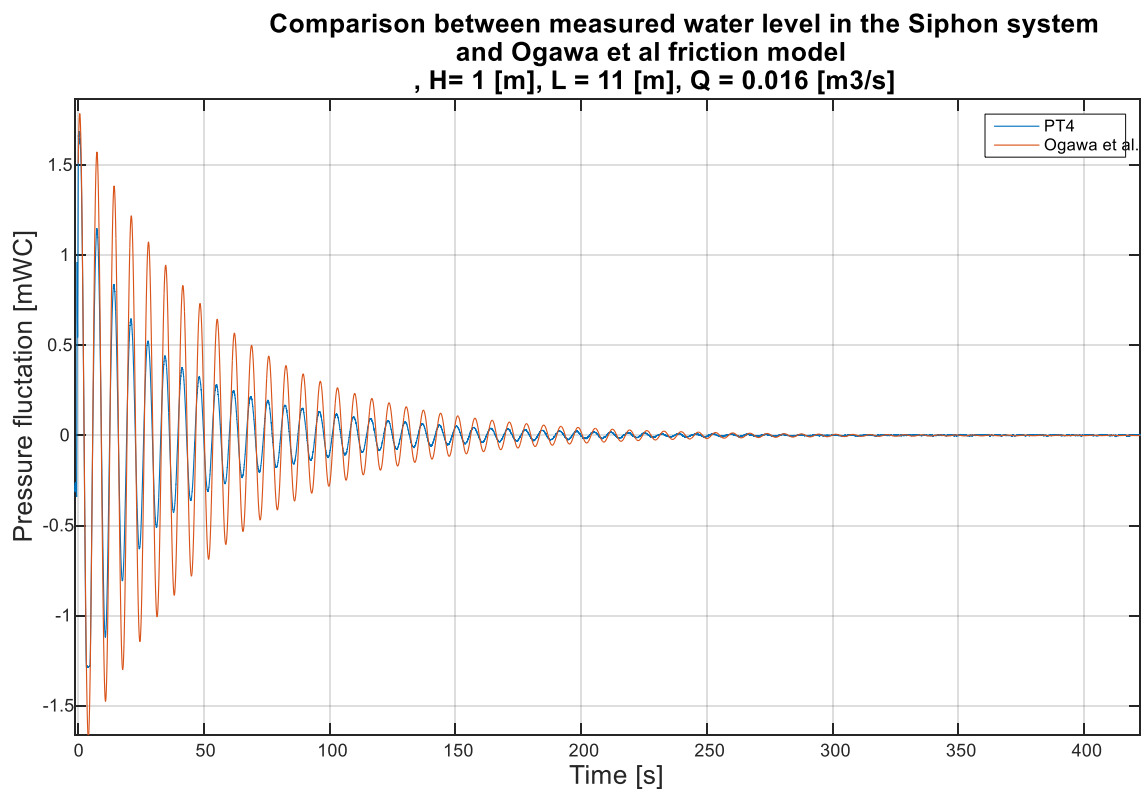
Figure 5-30: *Ogawa et al. model compared to measured data for – Siphon system*

Results and Discussion

The Vitkovsky model, as depicted in **Figure 5-31** obtain the best simulation result considering siphon system, and shows significant improvement from the simulation tests with traditional surge shaft. The result has decent correspondence to the real measurements in approximately the first ten time periods, but after passing this area the friction decreases and the performance decays. This propagation is similar as for the results obtained with the traditional surge shaft simulation.
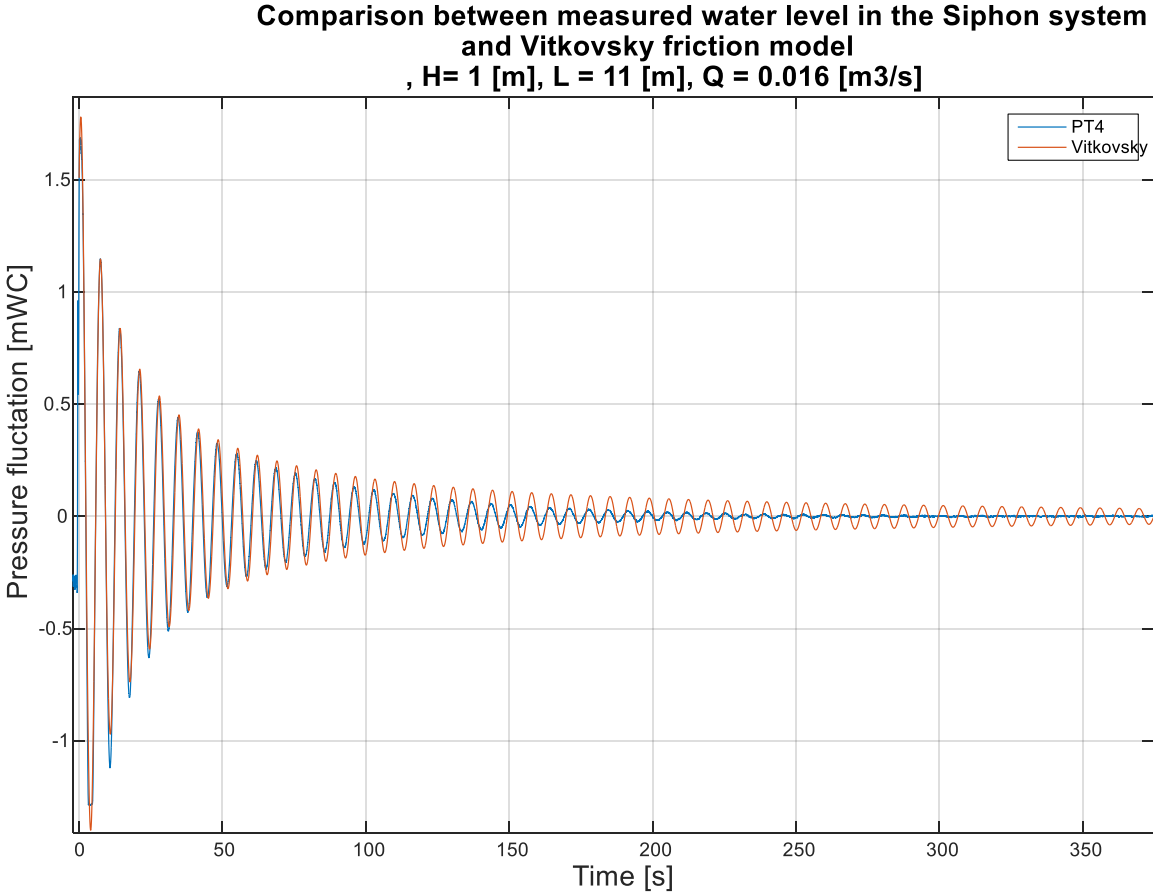
Figure 5-31: *Vitkovsky's model compared to measured data for – Siphon system*

The siphon simulation with the new one-term friction model is depicted in **Figure 5-32**. The model simulation shows respectively too low damping throughout the simulations. The correlation between the one-term model and the Quasi-steady model is similar as experienced for the traditional surge shaft. The correlation is expected since the steady flow parameters in both models are equal, and additionally, is the one-term model calibrated on the Quasi-steady model for steady flow conditions. The difference between these models, likewise as

experienced in the traditional surge shaft is the additional friction estimated by the one-term model when acceleration and deceleration are present.
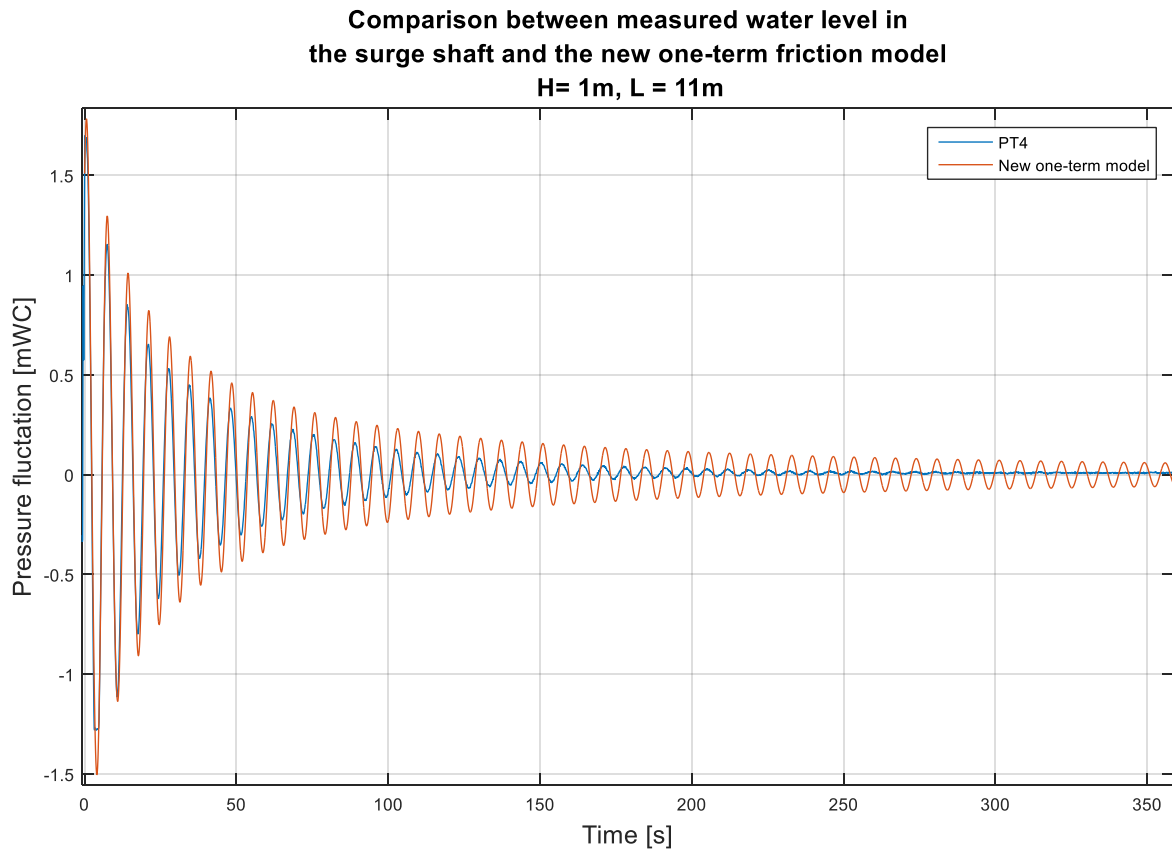
Figure 5-32: *The one-term model compared to measured data for – Siphon system*

To summarize the siphon simulations performs the model by Vitkovsky the best simulation and the tendency for all models are a reduced friction compared to measurements. The Vitkovsky model performs as well better for siphon system than for the traditional surge shaft, as the only model. All models predict approximately the same stationary results after the dynamics are died out for siphon and traditional surge shaft design, in view of both time propagation and size of the stationary estimation.

5.5 FLOW PARAMETER ANALYSES

In this chapter are effects from the flow parameters on the friction modeling investigated. The approach have been on observing how the parameters are acting in unsteady flow and evaluating the rate of impact from parameter change in the friction model. The chapter starts with evaluating the Re number before acceleration and frequency are studied closer.

Eq.(13) estimate the Re number and is specified by the velocity and density. Since the density is assumed to be constant at slow transients, will the velocity be the main deciding parameter. The velocity is depending on the phase of the oscillating dynamics. It can either be positive, negative, zero or accelerating. The phase of the oscillations has shown vital impact on the head loss calculation in unsteady flow. It may be equitable to relate the friction estimated by the quasi-steady term to how the Re number is implemented, as the Re number is significantly dependent on the velocity. The Re number oscillates in phase with the velocity, and since the velocity due to the absolute correction is always positive, will the Re number likewise be positive. If the generated dynamics are large enough is it possible to have an oscillating flow that fluctuates between all regimes. **Figure 5-33** depicts these facts above, showing the simulation result for the Re number in Case 1.
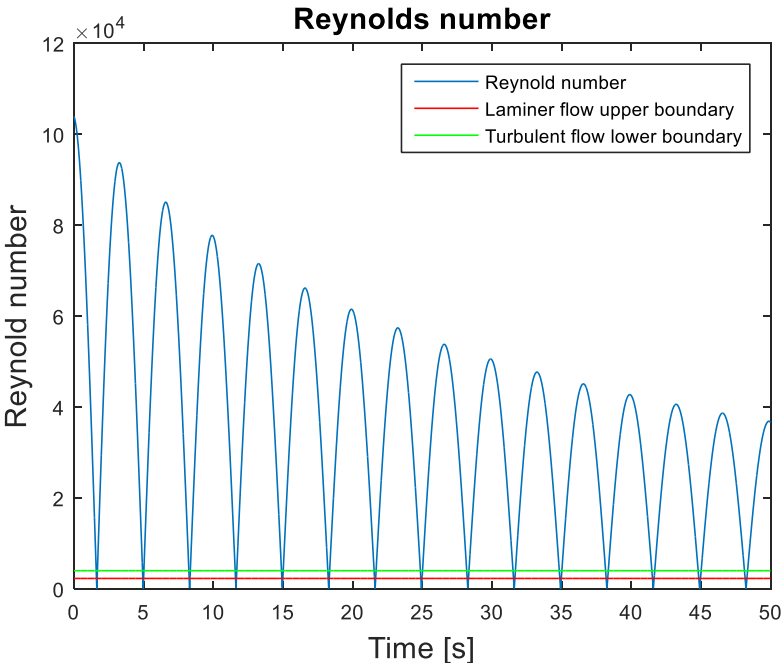
Figure 5-33*: Illustration of the variating Reynolds number for Case 1*

As velocity moves toward zero (In the turning of the oscillations), will the Re number behave likewise, making the laminar friction factor vanish. **Figure 5-34** shows how the friction factor gets a sudden drop as the velocity acts around a Re number equal to 2300. Further, as the velocity goes towards zero, the friction factor is heavily decreased. Hence, the relation between the velocity and the steady state friction factor is changing as the velocity acts around zero. This implies the importance of finding a method more suitable for predicting the frictional effect in the area of turning.
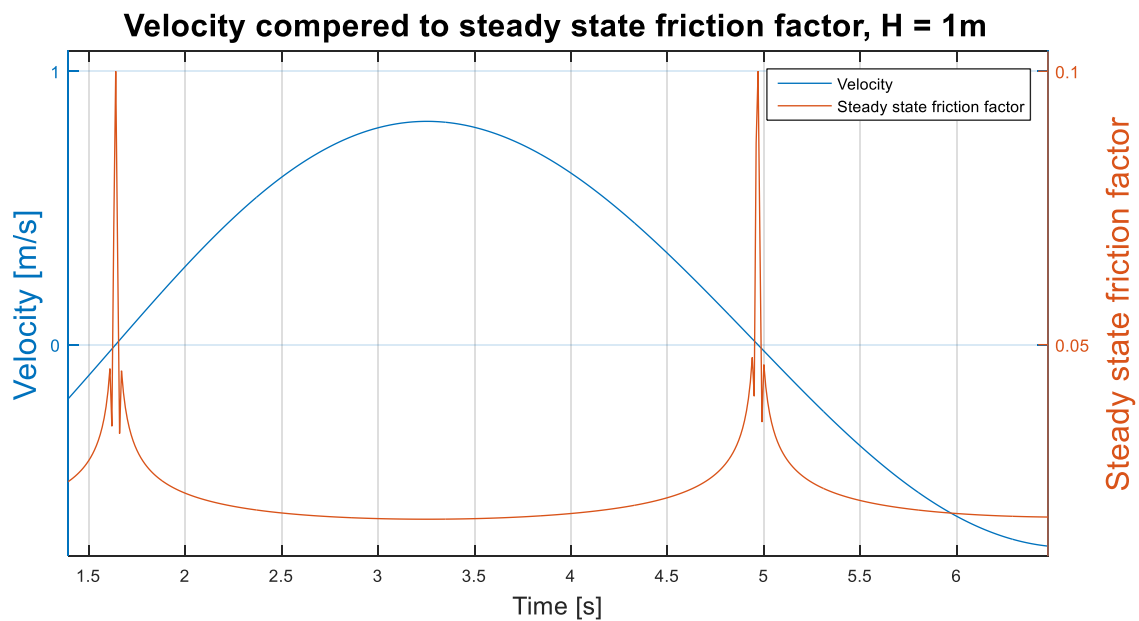
Figure 5-34: *Relationship between velocity and steady state friction factor*

Two main challenges in the area of turning have been detected from the simulation results. The fact that the frictional force is physically larger in this area, and that zero average velocity give zero friction in the quasi-steady term. Thus, a correction or replacement is necessary to achieve a suitable result for the estimation of the actual frictional force. The size of the friction factor show great relation to the implementation of the Re number in the different friction models. The model by Ogawa et al. and Vitkovsky solve this challenge better as the oscillations are fully damped out when reaching stationary flow using two separate terms to describe the friction.

The decrease in performance from the Quasi-steady and one-term model, as time goes, is expected as the mass oscillation propagates with a constant time period, as shown in **Figure**

5-35. The reason of decreased performance is the increased time of turning, as the time period is constant with a decreasing amplitude. This fact indicates that the velocity will stay in and closer to zero for a longer time interval as time goes. **Figure 5-36** and **Figure 5-37** depicts respectively point A and B in **Figure 5-35**, presenting how the time of turning increases with time.
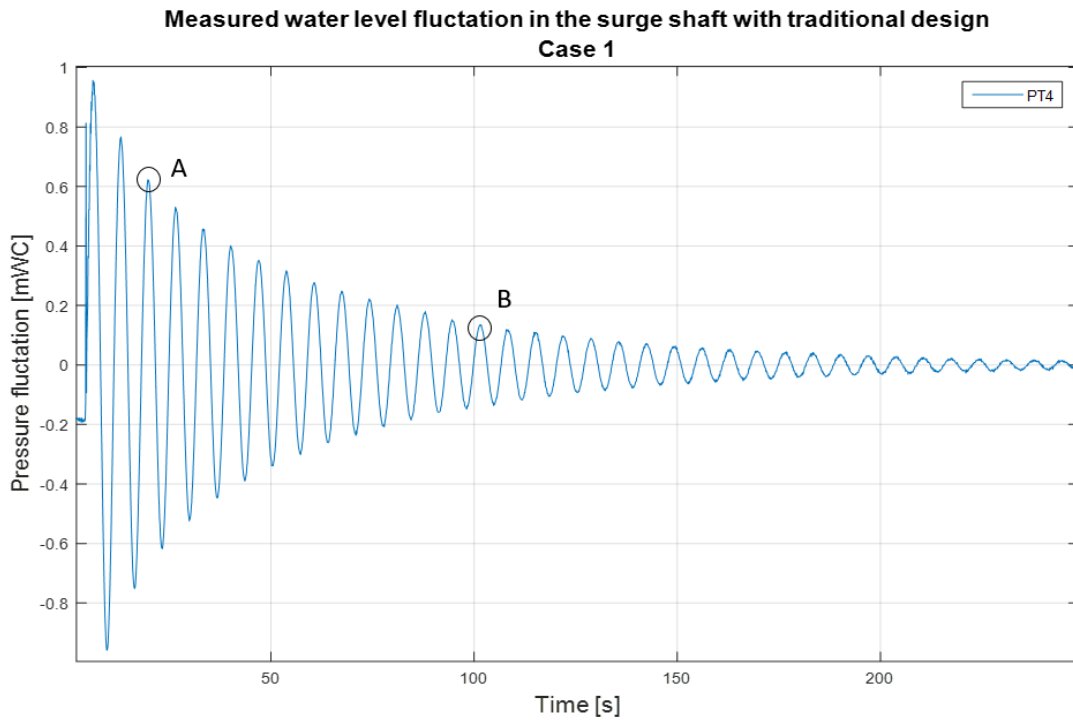
Figure 5-35: *Illustration of the increased turning time as the oscillations propagates*
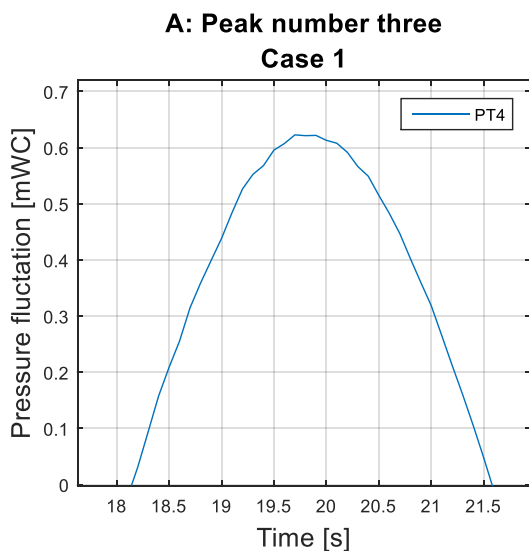
Figure 5-36: *Showing the time of turning for the third peak in Case 1*
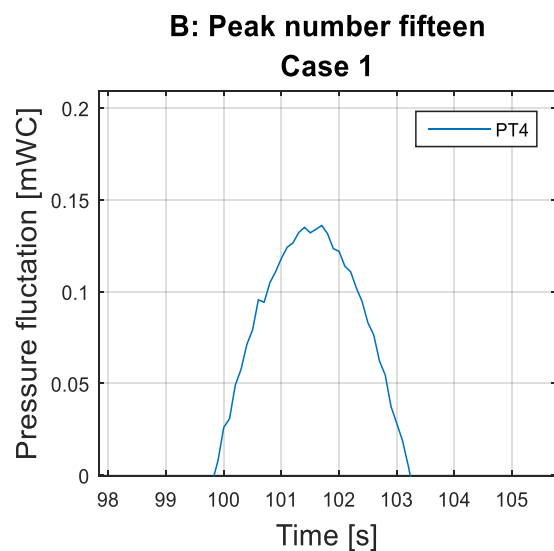
Figure 5-37*: Showing the time of turning for the 15 peak in Case 1*

A study on the velocity profile by Ove Bratland showed how the frictional force increases in the point of turning [24]. He illustrated how the liquid profile acts as the flow turns and how the liquid in the center of the pipe had a higher velocity than the liquid closer to the pipe wall since the water closer to the wall was more affected by the wall friction. From this discovery is it equitable to assume that the time of turning will increase with increasing velocity. Hence, the turning time will increase with the length from the pipe wall. The increased friction in the turning may then be reasonable to relate to the massive flow change experienced by the water. Diverse velocity over the cross-section does similarly make the local velocity greater than zero, contradicting the estimated zero friction at zero average velocity. It is evident that such facts may be a vital reason for the deviation from the simulated friction with the steady state models. Acceleration and deceleration generates as mention extra friction. This friction is natural to link to the high change in velocity gradients when the water is oscillating between zero and maximum flow.

How does frequency influence the damping? Simulations and laboratory tests on two different lengths are evaluated for the frequency study. The aim is to observe how the friction models perform for increasing headrace length. The natural behavior of an increased pipe length is a decrease in the oscillating frequency. **Figure 5-38** to **Figure 5-41** depicts the performance plot considering equal flow rate at 11 m and 21 m headrace length for each friction model. The performance is given in percentage of the measured real data. Positive value means that the friction model is more damped than the real measurements. Associated values may be found in Appendix D.
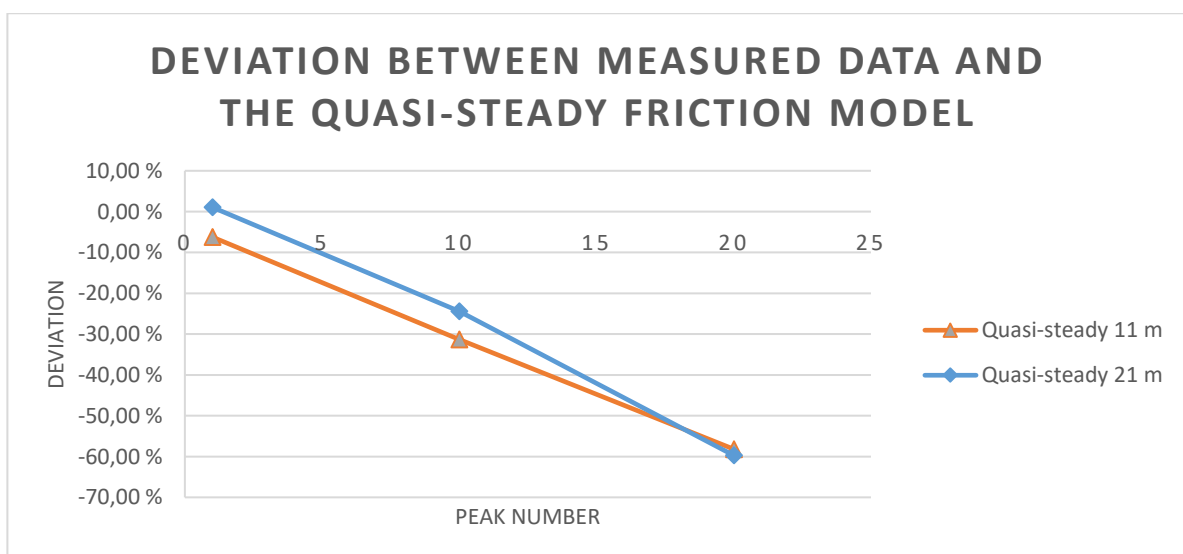
Figure 5-38: Performance plot for the Quasi-steady friction model
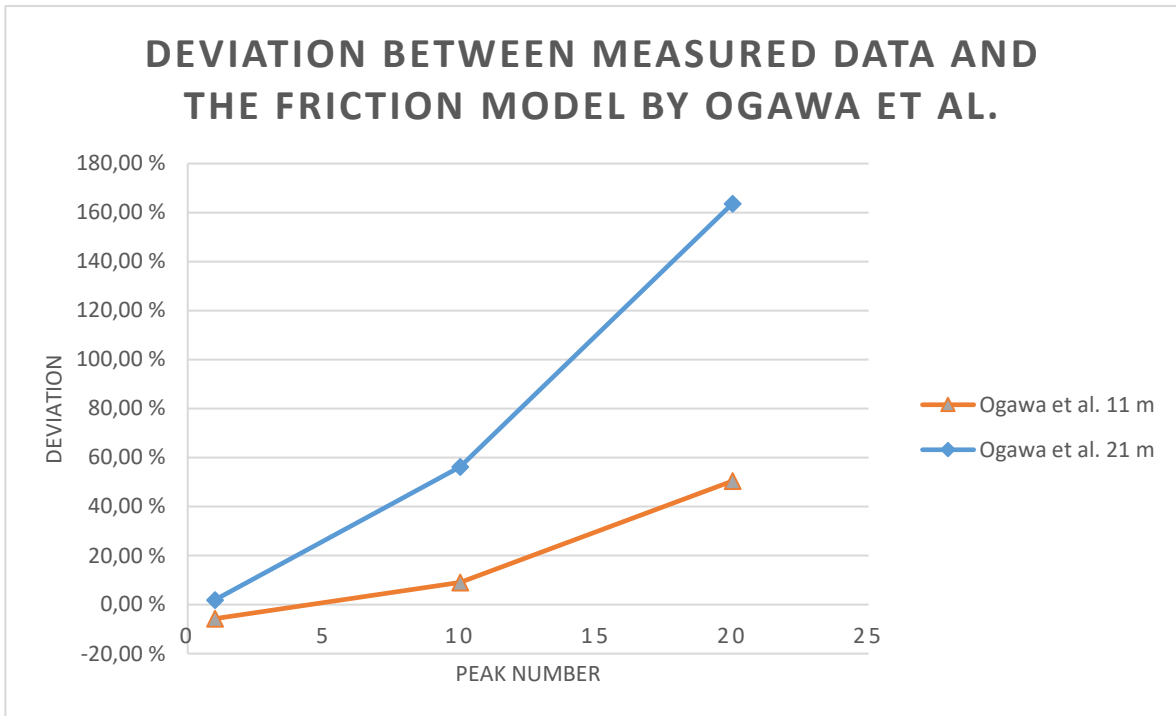
Figure 5-39: *Performance plot for the model by Ogawa et al.*
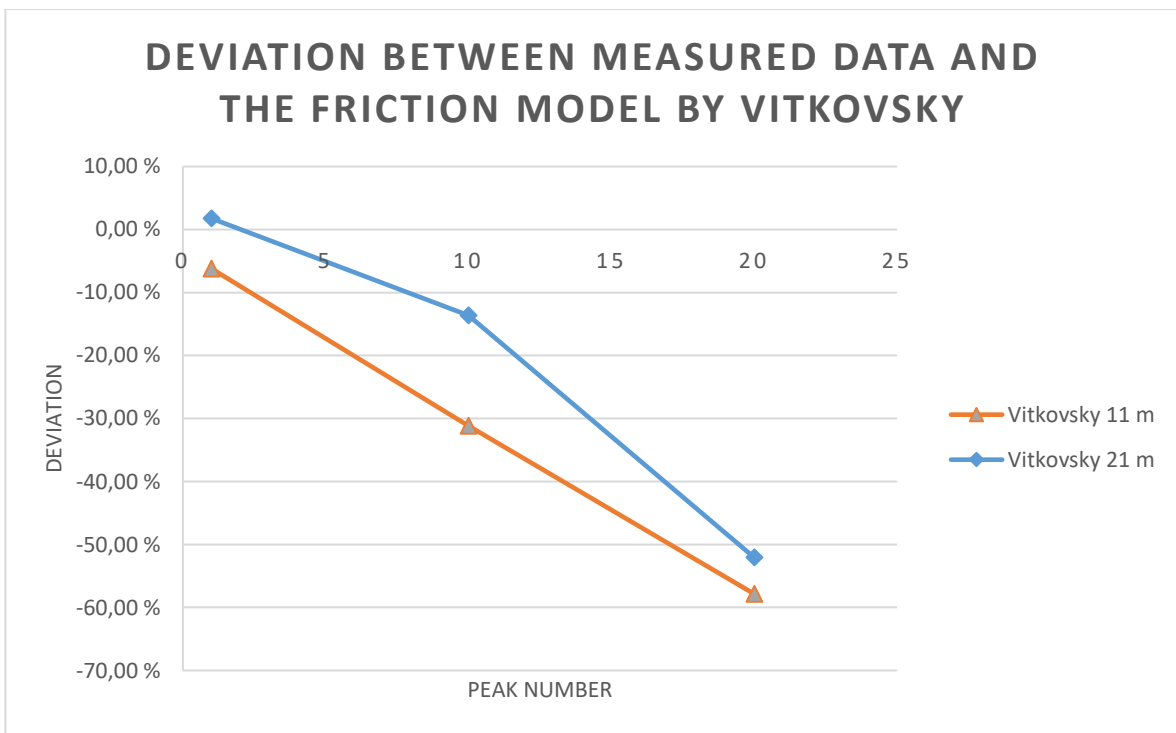
Figure 5-40: *Performance plot for the model by Vitkovsky*
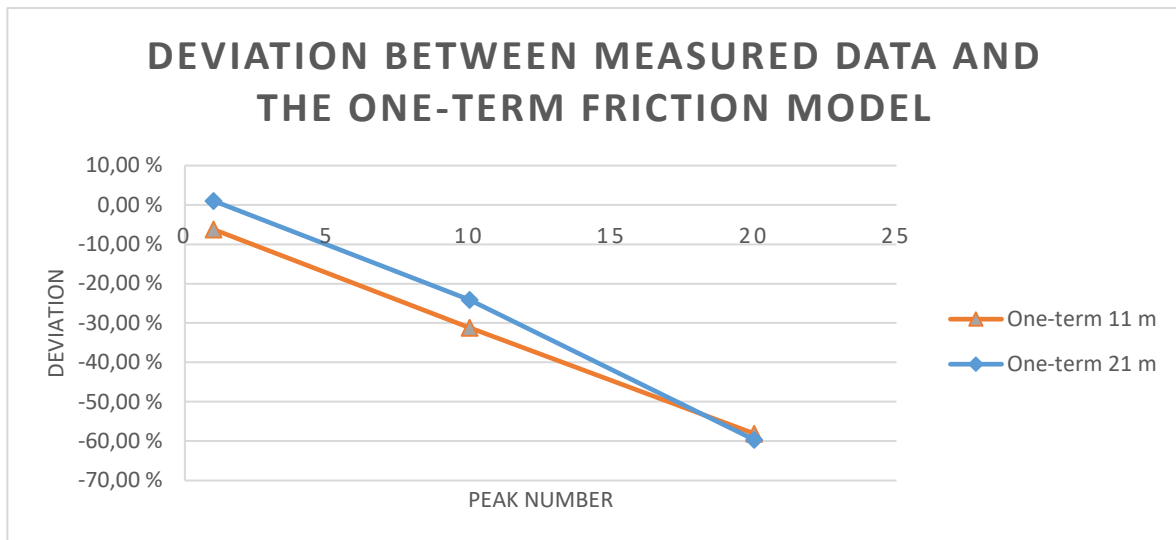
Figure 5-41: *Performance plot for the one-term friction model.*

The above performance-plots depict the case of decreased frequency between Case 4 and Case 5 for all four transient friction models. The plots show an increased performance for the three models based on the Darcy-Weisbach head loss equation in the transient period where the Re number is high. However, the performance on these three models decays faster for the case with increased headrace. The model by Ogawa et al., on the other hand, decreases in performance and decline faster for the increased headrace.

The performance from each model may be studied closer by splitting the equations and evaluate each parameter. The major change to the system from Case 4 to Case 5 is an increased length from 11 m to 21 m. The initial velocity and available head are equal in both cases.

Considering the model equation by Ogawa et al. should an increased headrace length give a decreased change in flow rate, since the length is implemented in the denominator of the velocity independent term. The velocity independent term will be more dominate as the change in velocity is reduced. Hence, the oscillations will decay faster as time goes. This fact is observed in the simulation depicted in **Figure 5-39**.

If now considering the three other models based on the Darcy-Weisbach head loss equation the length parameter is implemented in the nominator, giving an expectation of increased friction from the length parameter. Simulation results correspond to this expectation showing increased friction. These models show additionally improved results for increased headrace length. However, as the time goes are the performance-plots illustrating a faster decaying performance

Results and Discussion

with the increased headrace. This seems to be related to a lower estimated friction at decreased frequency as the acceleration is decreasing and time spent in the turning increased.

The one-term model and the model by Vitkovsky show improved results on the Quasi-steady model by implementing acceleration in the friction calculation. Both models estimate additional damping to the Quasi-steady model when acceleration is present. The size of the acceleration will determine the rate of impact. Hence, decreased frequency provides with less additional friction from acceleration. If counting for the increased time in the turning as well, a steeper deviation in performance as observed in simulations is expected.

In review, the common challenge in transient modeling using simple one-dimensional models is experienced to be sourced from the zero velocity in the turning, sizing the additional friction from acceleration and compensate for frequency change. Transient friction models designed to take care of the extra friction showed large deviates in performance, as experienced from four different models tested. Transient friction models are typically designed to fit specific cases or have different influence from equal parameter specification. Both the model by Ogawa et al. and the model by Vitkovsky showed the advantage of having an extra unsteady friction term, making the oscillation die completely out. The model by Ogawa showed best results as it was approximately in line with the measurements. The challenge with simple one-dimension friction modeling will always be the sizing of the impact from the unsteady term. The size of the term depends strongly on how the changing parameters is implemented, and of course the design of the system. It is not easy to foresee the motion if not all impacts are considered, which may be difficult to achieve with the assumptions simplifying the calculations down to one-dimensional analyses. The system design will additionally have impact on the results, since the models could as mention be derived from tests in specific pipe systems. It is reasonable to think that the performance e.g. the model by Ogawa et al. designed specific for U-tube oscillations, may get reduced performance in modified conditions since the model is derived on ideal U-tube design and not a hydropower plant system. Hence, performance from each model may variety depending on the system analyzed.

It is surely not easy to reach the goal for the future within friction modeling, presenting a model counting for the additional unsteady friction in a simple, correct and low demanding approach. However, designing a model to be valid in specific systems seems from the divers modeling result to be a good and trustful approach to develop valid models on specific cases, such as the hydropower system.

6 CONCLUSION

The work of this thesis was divided into two main parts. First, a literature study on closed conduit flow, followed by accomplish the establishment of the dynamic test rig and performing an experimental test campaign on the rig. Secondly, perform friction modeling on exixtiong models and a new one-term friction model. It as additionally been written and presented a paper on the preliminary work given by in a previous project work by the author.

The establishment of the dynamic test rig was finalized with minor changes from the original plan, achieving good results and impeccable operation. No unpredicted errors or system leakages was found. Both the traditional surge shaft and the siphon system behaved as desired. The laboratory measurements showed excellent correspondence to expectations, displaying the fluid and transient motion satisfyingly.

Five different friction models have been simulated and compared against measured data

1) Darcy-Weisbach head loss equation at steady state flow
2) Quasi-steady model for unsteady flow
3) Model by Ogawa et al. for unsteady flow
4) Model by Vitkovsky for unsteady flow
5) The purposed One-term model for unsteady flow

Simulation results obtained from the different friction models were quite diverse. The comparison between fluid modeling and measurements illustrated how important it is to implement additional friction to describe the motion correctly. Three challenges considering one-dimensional friction modeling where found,

1) The case of zero average velocity in the area of turning
2) Additional friction at acceleration and deceleration
3) Reduced performance at increased headrace tunnel

The thesis presents interesting findings on the one-term model described, giving an improved performance by introducing the acceleration term in the quasi-steady friction term, predicting increased friction at acceleration and deceleration. The one-term model was calibrated to achieve similar results as the stationary model at steady flow conditions with cross-section change, showing satisfying results. The rate of frictional impact at unsteady flow was not counted for in the one-term model as it is purposed but modified with an absolute sign making

the additional friction at acceleration always acts against the flow direction. Even if the one-term model did not handle the challenge with zero velocity in the turnings, did it show interesting results that could be interesting to develop further.

Simulations show how the steady state models predict an incorrect result by using the average velocity to decide the velocity term in the head loss estimation, since the time spent in the turning decreased the modeling performance as the quasi-steady term vanished. Hence, the Quasi-steady model, built on the steady state friction model was never damped out.

Two models designed for unsteady flow was tested, based on these results was the importance of implementing extra friction due to acceleration and zero average velocity illustrated as the performance was significantly improved by introducing an extra friction term independent of the quasi-steady friction term. The specified model on U-tube oscillations from Ogawa et al. performed with best results, showing how the flow modeling may be improved by deriving the model equation counting for the system design, as mass oscillations in the dynamic test rig are quite similar to the motion of U-tube oscillations.

7 FURTHER WORK

Investigation on harmonic oscillatory flow is a relevant subject today, having several unsolved issues that in the future are necessary or in a way desired to solve, an additionally, new and more complex issues to handle. Concerning this thesis may it be natural to take advantage of the opportunity to use the already established test rig to pursue these issues. In this chapter will a twofold further work be purposed.

The first task considers work on the dynamic test rig. At the end of the laboratory work was it, unfortunately, two planned subtasks that were not accomplished, due to lack of time and high demand of the technical crew in the laboratory. These tasks were PIV measurements, for inspection of the velocity profile at unsteady flow, and the test with 29 m headrace tunnel, for further frequency investigation. Both assignments are ready to be performed, as the test section for PIV measurements described in Chapter (4.5.6) is installed, and the extra headrace length is prepared and ready to be established.

The second task considers work on pursuing a new simplified one-term model that counts for the rate of damping in the acceleration term, and additionally the frictional impact at zero velocity in the turnings. The natural approach would be to work further with the challenges observed and presented in this thesis, followed by a more comprehensive test campaign with the aim of proposing a new one-term model scaled and valid in both steady and unsteady flow conditions. Supplementary work of interest could be a closer study on other similar friction models, and see how they would perform and how they solve the diverse challenges. One interesting model is the model presented by Bjørnar Svingen, using the Rayleigh-dampening to establish a specific model for U-tube oscillations considering instantaneous mean flow velocity and diffusion [16].

There are as mentioned countless of unsolved topics to study within harmonic oscillatory flow. Hopefully, would the dynamic test rig contribute to further or new research on this subject matter since the rig now is realized and ready for operation. The dynamic test rig is both simple to run and easy to modify for other designs and subjects, if necessary.

8 REFERENCES

[1]. Bergset, I., *Establishing a test rig for investigations of flow transient*. 2016, NTNU.

[2]. NVE, N.v.-o.e., *Forskrift om leveringskvalitet i kraftsystemet.* 2004.

[3]. Nielsen, T.K., *Dynamisk dimensjonering av vannkraftverk*. SINTEF rapport (SINTEF. Avdeling for strømningsteknikk : trykt utg.). Vol. STF67 A 90038. 1990, Trondheim: SINTEF, Strømningsmaskiner.

[4]. Rikstad, L., *Design of a Test Rig for Investigations of Flow Transient.* 2016.

[5]. Tullis, J.P., *Hydraulics of pipelines : pumps, valves, cavitation, transients*. 1989, New York: Wiley.

[6]. White, F.M., *Fluid Mechanics*, ed. Seven. 2011: McGraw-Hill Higher Education.

[7]. Storli, P.-T., *Closure to "Transient Friction in Pressurized Pipes. III: Investigation of the EIT Model Based on Position-Dependent Coefficient Approach in MIAB Model" by Pål-Tore Storli and Torbjørn K. Nielsen.* Journal of Hydraulic Engineering, 2013. **139**(5): p. 567-568.

[8]. Çengel, Y.A., J.M. Cimbala, and M. Kanoğlu, *Fluid mechanics : fundamentals and applications*. 2nd ed. in SI units. ed. 2010, Boston: McGraw-Hill.

[9]. Li, P., *An Experimental Investigation of Velocity Distribution and Head Loss of Oscillatory Flow in a Rectangular Duct with Sand Roughness*. 2004, Fakultet for ingeniørvitenskap og teknologi.

[10]. Brekke, H., *[Doktoravhandling] : [141] 1 : A stability study on hydro power plant governing including the influence from a quasi nonlinear damping of oscillatory flow and from the turbine characteristics*. Vol. [141] 1. 1984, Oslo: H. Brekke.

[11]. Zidouh, H. and L. Elmaimouni. *Wall shear stress in transient turbulent pipe flow*. in *2013 International Renewable and Sustainable Energy Conference (IRSEC)*. 2013.

[12]. Ogawa, A., et al., *Damped oscillation of liquid column in vertical U-tube for Newtonian and non-Newtonian liquids.* Journal of Thermal Science, 2007. **16**(4): p. 289-300.

[13]. Bergant, A., A. Ross Simpson, and J. Vìtkovsk, *Developments in unsteady pipe flow friction modelling.* Journal of Hydraulic Research, 2001. **39**(3): p. 249-257.

[14]. Zarzycki, Z., *Improved method for simulating transients of turbulent pipe flow.* Journal of Theoretical and Applied Mechanics 49, 2011.

[15]. Vitkovsky, J.S., M. Bergant, A. Simpson, A. Lambert, M., *Numerical Error in Weighting Function-Based Unsteady Friction Models for Pipe Transients.* Journal of Hydraulic Engineering, 2006. **132**(7).

[16]. Svingen, B. and R. Vennatrø, *Transient og oscillerende hydraulisk demping i rør*. SINTEF rapport (SINTEF. Termisk energi og vannkraft). Vol. STF84 A96441. 1996, Trondheim: SINTEF, Energi, Termisk energi og vannkraft.

[17]. Sellevold, M.O.D., *Demping av U-røyrsvingingar i vasskraftverk.* 2013.

[18]. Munson, B.R., *Fundamentals of fluid mechanics*. 6th ed. ed. 2009, Hoboken, N.J: Wiley.

[19]. IEC, T.I.E.C., *Field acceptance tests to determine the hydraulic performance of hydraulic turbines, storage pumps and pump-turbines.* 1991(The International Electrotechnical Commission).

[20]. Solemslie, B.W., *Compendium in Instrumentation, Calibration & Uncertainty Analysis.* 2013.

[21]. instuments, N. *Aliasing*. Available from: http://zone.ni.com/reference/en-XX/help/370051P-01/cvi/libref/analysisconcepts/aliasing/.

[22]. Eldar, Y.C., *Sampling theory : beyond bandlimited systems*. 2014, Cambridge University Press.

[23]. Krohne, *OPTIFLUX 2000 Technical Datasheet*. 2014, Bagges: http://krohne.com/en/dlc/product-related-downloads/flowmeters/electromagnetic-flowmeters/optiflux-2000/.

[24]. Bratland, O., *Single phase flow assurance.* 2009.

[25]. Kvaløy, J.T., H. Tjelmeland, and s. Norges teknisk-naturvitenskapelige universitet Institutt for matematikk og, *Tabeller og formler i statistikk*. 2000, Trondheim: Tapir akademisk forl.

Appendix A. UNCERTAINTY

Table A-1 list the values of t_α given by $P(T > t_\alpha) = \alpha$. Where T is student t-distributed with degree of freedom, v.

v ↓	α						
	0,1000	0,0500	0,0250	0,0100	0,0050	0,0010	0,0005
1	3,078	6,314	12,706	31,821	63,657	318,309	636,619
2	1,886	2,920	4,303	6,965	9,925	22,327	31,599
3	1,638	2,353	3,182	4,541	5,841	10,215	12,924
4	1,533	2,132	2,776	3,747	4,604	7,173	8,610
5	1,476	2,015	2,571	3,365	4,032	5,893	6,869
6	1,440	1,943	2,447	3,143	3,707	5,208	5,959
7	1,415	1,895	2,365	2,998	3,499	4,785	5,408
8	1,397	1,860	2,306	2,896	3,355	4,501	5,041
9	1,383	1,833	2,262	2,821	3,250	4,297	4,781
10	1,372	1,812	2,228	2,764	3,169	4,144	4,587
11	1,363	1,796	2,201	2,718	3,106	4,025	4,437
12	1,356	1,782	2,179	2,681	3,055	3,930	4,318
13	1,350	1,771	2,160	2,650	3,012	3,852	4,221
14	1,345	1,761	2,145	2,624	2,977	3,787	4,140
15	1,341	1,753	2,131	2,602	2,947	3,733	4,073
16	1,337	1,746	2,120	2,583	2,921	3,686	4,015
17	1,333	1,740	2,110	2,567	2,898	3,646	3,965
18	1,330	1,734	2,101	2,552	2,878	3,610	3,922
19	1,328	1,729	2,093	2,539	2,861	3,579	3,883
20	1,325	1,725	2,086	2,528	2,845	3,552	3,850
21	1,323	1,721	2,080	2,518	2,831	3,527	3,819
22	1,321	1,717	2,074	2,508	2,819	3,505	3,792
23	1,319	1,714	2,069	2,500	2,807	3,485	3,768
24	1,318	1,711	2,064	2,492	2,797	3,467	3,745
25	1,316	1,708	2,060	2,485	2,787	3,450	3,725
26	1,315	1,706	2,056	2,479	2,779	3,435	3,707
27	1,314	1,703	2,052	2,473	2,771	3,421	3,690
28	1,313	1,701	2,048	2,467	2,763	3,408	3,674
29	1,311	1,699	2,045	2,462	2,756	3,396	3,659
30	1,310	1,697	2,042	2,457	2,750	3,385	3,646
40	1,303	1,684	2,021	2,423	2,704	3,307	3,551
50	1,299	1,676	2,009	2,403	2,678	3,261	3,496
60	1,296	1,671	2,000	2,390	2,660	3,232	3,460
70	1,294	1,667	1,994	2,381	2,648	3,211	3,435
80	1,292	1,664	1,990	2,374	2,639	3,195	3,416
100	1,290	1,660	1,984	2,364	2,626	3,174	3,390
120	1,289	1,658	1,980	2,358	2,617	3,160	3,373
∞	1,282	1,645	1,960	2,326	2,576	3,091	3,291

Table A-1: *Student t-distribution[25]*

Appendix B.   CALIBRATION

The static PT`s and the EMF is calibrated by comparing voltage readouts from the sensor against a known reference value. The calibration constants are then found from the trendline formed by the plots on a pressure-voltage diagram and a flow rate-voltage diagram, respectively for the static PT`s and the EMF. A DPI 601 digital pressure indicator sets the pressure reference. The flow boundaries of maximum and minimum flow for the EMF is set by the fabricant. The measured points on the calibration diagrams form a trendline function, giving the calibration constants C0 and C1 in Eq.(59). **Figure B-1** to **Figure B-5** depicts the calibration diagrams.
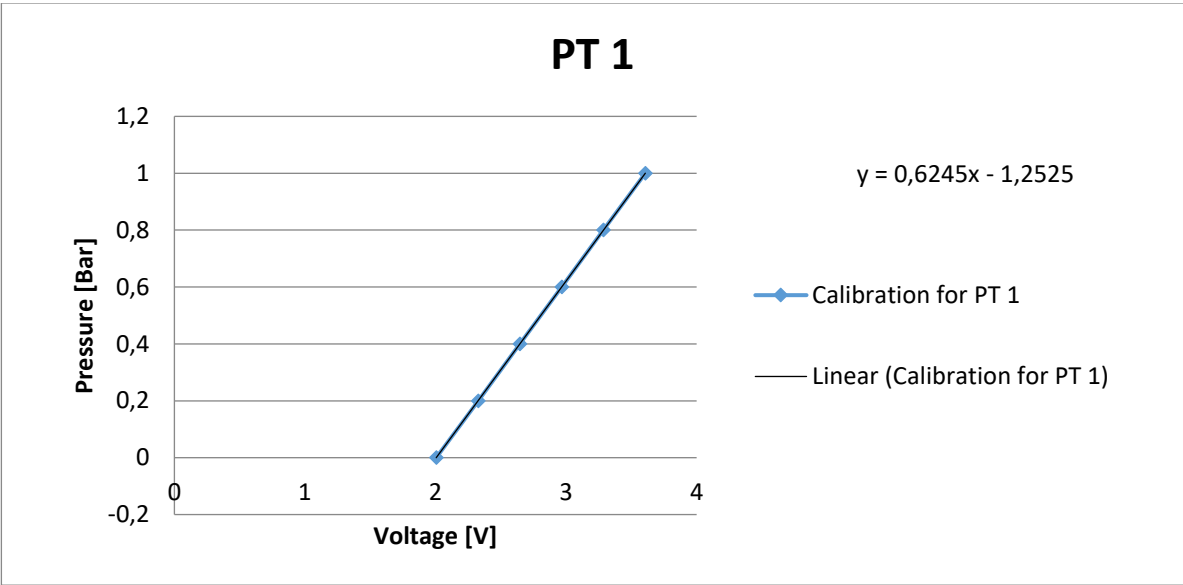
Figure B-1: Calibrating results for pressure transducer 1
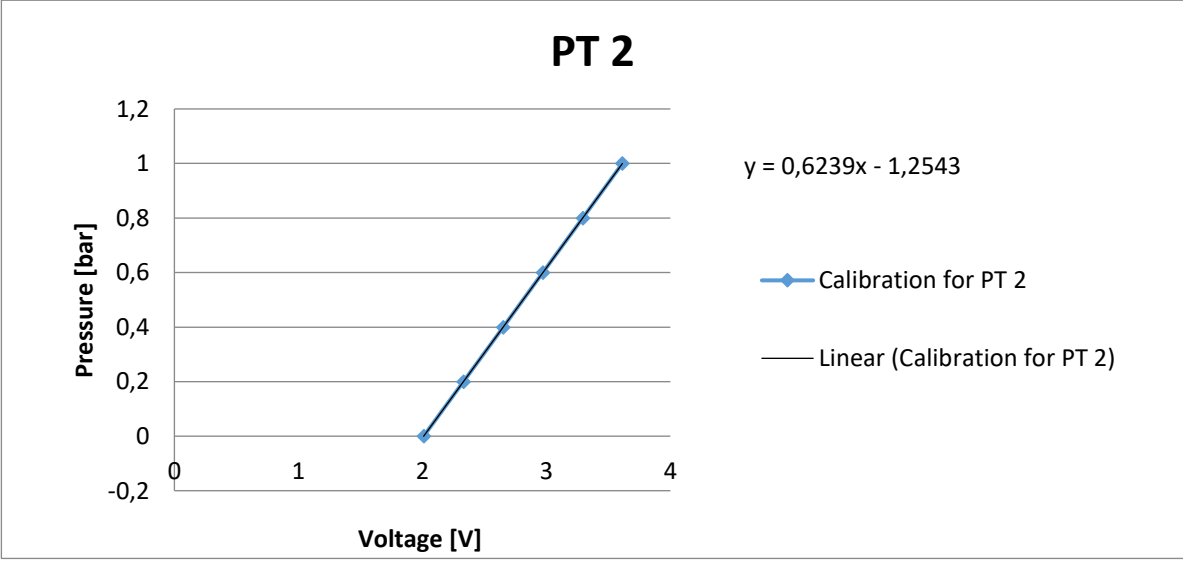
Figure B-2: Calibrating results for pressure transducer 2
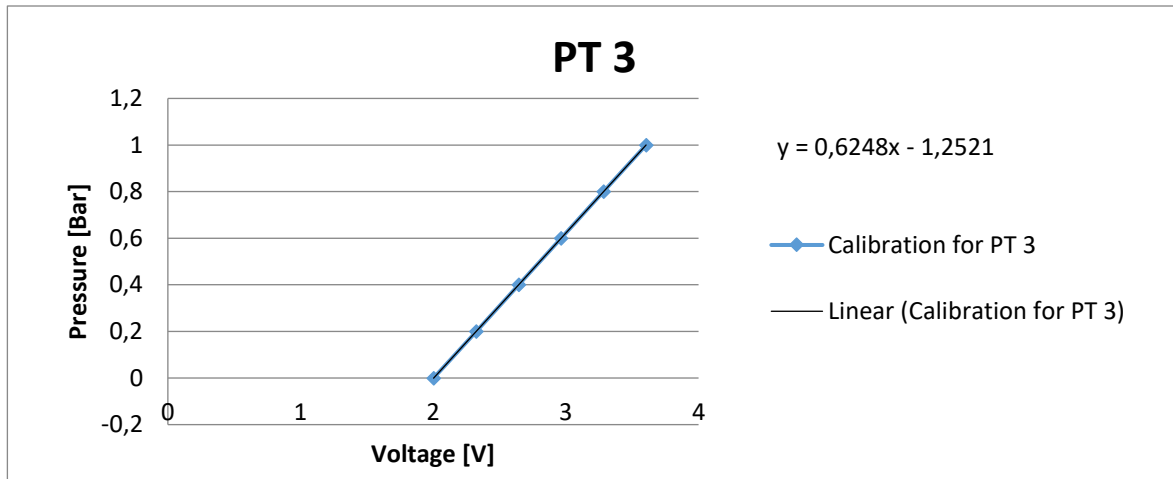
Figure B-3: *Calibrating results for pressure transducer 3*
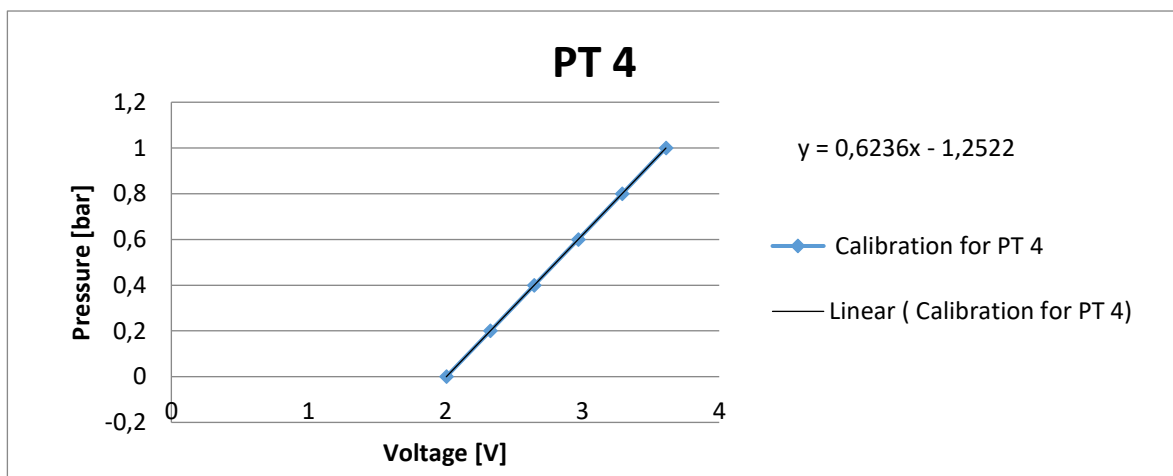
Figure B-4: *Calibrating results for pressure transducer 4*
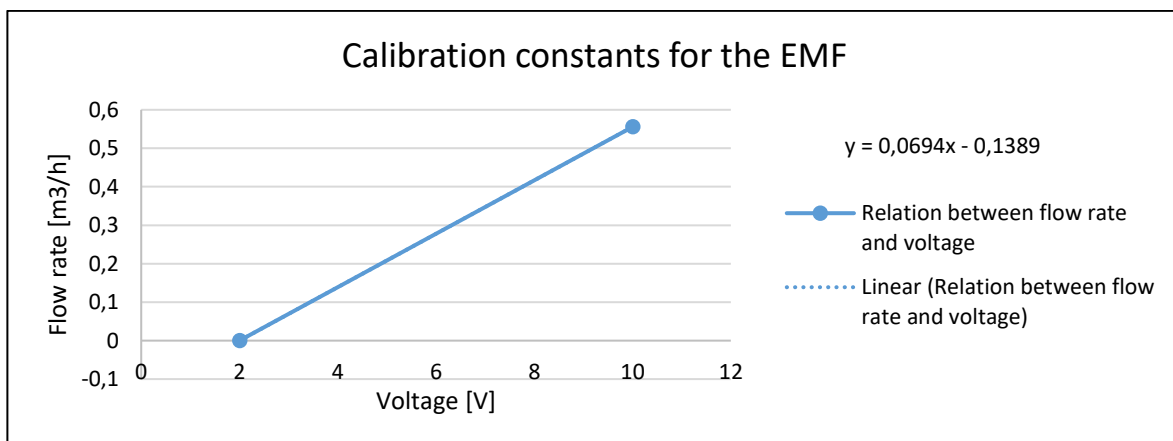
Figure B-5: *Calibration constants for the electromagnetic flowmeter*

The pressure and flow rate can now be found by implement the voltage readouts from the DAQ device into x in Eq.(59).

Appendix C. CALCULATION - ESTIMATION OF THE B CONSTANT

The calibration of the correction constant, B, is made from the case described in **Table 2-1**. The parameter values in pipe section two are found by the limited extension degree on the diffuser of 5 degrees, given by the length of the conical diffuser and the diameter in pipe section one [6]. The estimation of the correction constant is shown in Eq.(60) to Eq.(64).

$$B^{\left(\left|\frac{\partial V}{\partial t}\right|\right)+V_1\left(\frac{\partial V}{\partial x}\right)} * f_1 * \left(\frac{L}{D_1}\right) * \left(\frac{|V_1| * V_1}{2 * g}\right) = f_2 * \left(\frac{L}{D_2}\right) * \left(\frac{|V_2| * V_2}{2 * g}\right) \tag{60}$$

$$B^{\left(\left|\frac{\partial V}{\partial t}\right|\right)+V_1\left(\frac{\partial V}{\partial x}\right)} * f_1 * \left(\frac{\cancel{L}}{D_1}\right) * \left(\frac{|V_1| * V_1}{\cancel{2 * g}}\right) = f_2 * \left(\frac{\cancel{L}}{D_2}\right) * \left(\frac{|V_2| * V_2}{\cancel{2 * g}}\right) \tag{61}$$

$$B^{V_1\left(\frac{\partial V}{\partial x}\right)} = \frac{f_2}{f_1} * \left(\frac{D_1}{D_2}\right) * \left(\frac{|V_2| * V_2}{V_1^2}\right) \tag{62}$$

$$B = \sqrt[V_1*\left(\frac{V_1-V_2}{\Delta x}\right)]{\frac{f_2}{f_1} * \frac{D_1}{D_2} * \frac{|V_2| * V_2}{|V_1| * V_1}} \tag{63}$$

$$B = \sqrt[0.905*\left(\frac{0.1929-0.905}{1}\right)]{\frac{0.0209}{0.0177} * \frac{0.15}{0.3250} * \frac{0.1929^2}{0.905^2}} = 308.7 \tag{64}$$

Appendix D. FREQUENCY ANALYSES

Headrace length	11 m					21 m				
Friction model of interest	Quasi-steady	Ogawa et al	Vitkovsky	One-term	Lab-results	Quasi-steady	Ogawa et al	Vitkovsky	One-term	Lab-results
Readouts										
Peak number 1 [m]	0,4365	0,4344	0,436	0,436	0,4109	0,5610	0,5560	0,557	0,561	0,5670
Peak number 10 [m]	0,2097	0,1321	0,209	0,209	0,1440	0,2480	0,1200	0,217	0,247	0,1874
Peak number 20 [m]	0,1270	0,0353	0,126	0,126	0,0531	0,1440	0,0220	0,121	0,143	0,0580
Time to steady state [s]	Never	450	1500	Never	400	Never	320	2500	Never	400
Calculated deviation between model simulation and laboratory measurements										
Peak number 1 [%]	-6,23	-5,72	-6,21	-6,21	0,00	1,06	1,94 %	1,76	1,06	0,00
Peak number 10 [%]	-31,33	9,01	-31,1	-31,1	0,00	-24,44	56,17	-13,6	-24,1	0,00
Peak number 20 [%]	-58,19	50,42	-57,8	-58,0	0,00	-59,72	163,64	-52,0	-59,6	0,00

Table D-1: *Comparing the damping propagation for all four friction models , considering Case 4 and Case 5, with 11 m and 21 m headrace*

Appendix E. MATLAB SCRIPT

Flow simulation and measurement treatment

Below is the MATLAB script used to calculate flow parameters, interesting numbers, simulation results and measurement treatment. Additionally, at the end of the script is the main plots used in the thesis described.

```matlab
clear all

load('master.mat')


%--------------Stationery flow calculation-----------%

%----------Flow Parameters:

%Diameter
D = 0.150; %m
%Pipe roughness
e = 0.000002; %m
%Density
rho = 999.7; %kg/m^3
%bulk modulus
K = 2.15*10^9;
%Cross section
A = pi*(D^2)/4; % m^2 cross section
%Length
L=11;
%Initial velocity
V = 0.905;
%flow
Q = V*A;
%Dynamic viscosity at 10 C
my = 1.307*10^-3; %Ns/m^2

%----------Calculations:

%Pressure wave speed
a = sqrt(K/rho);

%Reynolds number
Re = (rho*V*D)/my;

%Friction factor
if Re < 2300
    f = (64/Re); % Laminar
else
    f=(1/(1.8*log10((6.9./Re)+((e*D)/3.7)^1.11))^2); % Turbulent
end

hf_f = f.*(L/D)*((V^2)/(2*g)); % Friction loss

%Minor losses
```

```matlab
k_loss = 1.08;
hf_m = k_loss*((V^2)/(2*g)); %Head loss from minor losses

%Total head loss
hf_loss = hf_f + hf_m;

%Time periode of water hammer
TpW = (4*L)/a;


%Frequensy of water hammer
omegaW = 1/TpW;

%Frequency of mass oscillations
omegaM = sqrt(g/(A*(L/A)));

%Time period of mass oscillations
TpM = (2*pi)/omegaM;


%Hydrodynamic entry length
if Re < 2300
    Lh = 0.005*Re*D; %Laminar
else
    Lh = 1.359*D*Re^(1/4); %Turbulent
end


%Fully developed shock wave
Hmax = (a*V)/g;

%time to steady state
tsteady = (L/(V*f*(L/D)))*(log((V+(0.99*V))/(V-(0.99*V))));

%Highest upswing
dz_max = Q* sqrt((L/A)/(g*A))-(1/3)*hf_loss;

%Lowest downswing
dz_min = -Q* sqrt((L/A)/(g*A))-(1/9)*hf_loss;

%------------Simulation

tmax=15;
dt=0.01;
t0=0:dt:tmax;

dz = dz_max.*sin((2*pi*t0)/TpM);

figure(1)
plot(t0,dz);
title ('Velocity and laminar friction factor, H = 1m', 'fontsize', 14);
xlabel ('Velocity [m/s]', 'fontsize', 14);
ylabel ('Laminar friction factor', 'fontsize', 14);


%---------------SLOW TRANSIENT SIMULATION------------------%
clear all
```

Appendix E

```matlab
g=9.81; %Gravitational acceleration [m/s^2]
v=1.307e-6; %Kinematisk viskositet water at 10 C [m^2/s]
R=0.075; %Pipe radius [m]
D=R*2; %Pipe Diameter [m]
rho = 999.7; %[kg/m^3] Density
my = 1.307*10^-3; % [Ns/m^2] Dynamic viscosity at 10 C
A=pi*(D^2)/4; %Pipe-section [m]
L=11; %Pipe length [m]
eps=2e-5; %Pipe roughness [m]
H0=1; %Water level in the upper reservoir [m]
Z=0; %initial water fluctation [m]
Z1=Z; % Quasi-steady
Z2=Z; % Ogawa et al.
Z3=Z; % Vitkovsky
Z6=Z; % One-term model
Q=-0.016; %Volume flow at start Q=(Qs-Qv) [m^3/s]
Q1=Q;% Quasi-steady
Q2=Q;% Ogawa et al.
Q3=Q;% Vitkovsky
Q6=Q;% One-term model
dQ3=0; % change in volume flow vitkovsky
dQ6=0;% change in volume flow one-term model
Vm=abs(Q)/A; %inital velocity [m/s]

%----------Ogawa et al. constants:

Rei=(Vm*D)/v; %Imaginary Reynolds number [-]
Kvm=Rei/(8.75+0.0233*Rei); %Water
Kv=25*D*(1+(4.5e-9/D^4))*Kvm; %velocity factor [-]
phi=atand(1/(sqrt((2*g/L)*(((R^2)/(Kv*v))^2)-1)));

%-----------Unsteady flow Simulation:
tmax=600; %Simulation time
dt=0.01; %Time step


Qa = zeros(1,tmax/dt);
Z1a = Qa;
Z2a = Qa;
Z3a = Qa;
Z6a = Qa;
Rea = Qa;
Va = Qa;
dV = Qa;
V6a=Qa;
f=Qa;
f6=Qa;
hf_f=Qa;
hf_f6=Qa;
acca = Qa;
ta = Qa;
Ba=Qa;


t2=0:dt:tmax;
l=1;


for t=0:dt:tmax
```

```matlab
%velocity
V=Q1/A;
%acceleration
acc=diff(Va);




%---------Quasi-steady state:

%updating the Reynold number:
Re = (D*abs(Q1))/(A*v);


%Calculation of the quasi stationary friction factor:
 if Re<2300
     f = (64/Re); %Laminer
 else
     f =(1./(1.8.*log10((6.9./Re)+((eps*D)/3.7).^1.11))).^2); % Turbulent
 end
if f>0.1
    f=0.1;
end


 %friction losses
 hf_f = f*(L/D)*(((Q1*abs(Q1))/(2*g*A^2))); %Head loss from friction

 %Minor losses
 k_loss = 1.08; % Total loss coefficient
 hf_m = k_loss*(((Q1*abs(Q1))/(2*g*A^2))); % Head loss from minor losses

 %Total head loss
 hf_loss = hf_f + hf_m;

 %Flow change in the u-tube
 dQ1 = dt*((g*A/L)*(Z1-hf_loss));
 Q1ny = Q1 + dQ1;

 Q1 = Q1ny;

 Z1ny=Z1-(dt*(Q1/A));
 Z1=Z1ny;




%------------Ogawa et al. friction model:

dQ2 = dt*(((g*A*2*Z2)/L)-2*v*Kv*Q2/(R^2))/2;
Q2ny = Q2 + dQ2;

Q2=Q2ny;

Z2ny=Z2-(dt*(Q2/A));
Z2=Z2ny;
```

Appendix E

```matlab
%----------------------Vitkovsky friction model:
% Updating the Reynolds number:
Re3 = (D*abs(Q3))/(A*v);

dv = (dQ3/A);

%friksjonsfaktor
 if Re3<2300
     fv = 64/Re3; %Laminer
 else
     fv =(1./(1.8.*log10((6.9./Re3)+((eps*D)/3.7).^1.11)).^2); %Turbulent
 end
 if fv>0.1
     fv=0.1;
 end

 %Calculating C_star
 if Re3<2300
     C_star=0.00476;
 else
     C_star=7.41/(Re3^(log(14.3/(Re3^0.05))));
 end

 % Brunone friction coefficient k:
 k=sqrt(C_star)/2;

 %Quasi-steady friction term
 f_fq3 = fv;
 hf_fq3 = fv*(L/D)*((Q3*abs(Q3))/(2*g*A^2));

 %Unsteady friction term, head loss
 f_fu3 = ((k*D)./((Q3/A)*abs(Q3/A)))*abs((dV/dt))*sign(Q3/A);
 hf_fu3 =
((k*D)./((Q3/A)*abs(Q3/A)))*abs((dV)/dt)*sign(Q3/A).*(L/D).*(((Q3*abs(Q3))/(2*g*A^2)));


 %Minor losses
 k_loss3 = 1.08; % Loss coefficient

 hf_m3 = k_loss*(((Q3*abs(Q3)))/(2*g*A^2)); % Head loss from minor losses

 %Total head loss
 hf_loss3 = hf_fq3 + hf_fu3 + hf_m3;

 %Loss term

 R_loss =(((fv+f_fu3).*L)/(2*g*(A^2)*D))+(k_loss3/(2*g*A^2));

 %flow change in the u-tube
 dQ3 = dt*((g*A/L)*(Z3-R_loss*Q3*abs(Q3)));
 Q3ny = Q3 + dQ3;

 Q3 = Q3ny;

 Z3ny=Z3-dt*(Q3/A);
 Z3=Z3ny;
```

X

```matlab
%------------------new one-term friction model

% Updating the Reynolds number:
Re6 = (D*abs(Q6))/(A*v);

dV6 = dQ6/A;

%Quasi-steady friction term, head loss
if Re6<2300
    f6 = (64/Re6); % Laminer
else
    f6 =(1./(1.8.*log10((6.9./Re6)+((eps*D)/3.7).^1.11)).^2); %Turbulent
end

%%If conical cross-section change is present

%(Canceled, when just considering unsteady flow(Velocity change in time))

% dx = 1; %Length of the conical pipe
%Dx=D+(2*(dx*tand(5))); % Diameter pipe section two
%A2=(pi/4)*Dx^2; % Cross-section pipe section two

%dVx = (Q6/A2)-(Q6/A); %Change in velocity due to geometrical change

dV6 = (dQ6/A); %Change in velocity due to change in time


B=308.7^(abs(dV6)); %+((Q6/A)*(dvx/dx))); % Correction constant

V6=(Q6/A); %velocity

%friction losses
hf_f6 = B*f6*(L/D)*(((Q6*abs(Q6))/(2*g*A^2)));

%Minor losses
k_loss6 = 1.08; % Loss coefficient
hf_m6 = k_loss6*(((Q6*abs(Q6))/(2*g*A^2)));

%Total head loss
hf_loss6 = hf_f6 + hf_m6;

%flow change in the u-tube

dQ6 = dt*((g*A/L)*(Z6-hf_loss6));
Q6ny = Q6 + dQ6;

Q6 = Q6ny;

Z6ny=Z6-(dt*(Q6/A));
Z6=Z6ny;
%--------------------------------------------------------------%

Qa(l)=Q;
Z1a(l)=Z1;
Z2a(l)=Z2;
Z3a(l)=Z3;
Z6a(l)=Z6;
```

```matlab
    Rea(l)=Re;
    Va(l)=V;
    dVa(l)=dV;
    fa(l)=f;
    f6a(l)=f6;
    hf_fa(l)=hf_f;
    hf_f6a(l)=hf_f6;
    Ba(l)=B;
    ta(l)=t;


    l=l+1;
end

Lam = ones(size(ta)) * 2300;
Turb = ones(size(ta)) * 4000;




%----------------------Simulation-----------------------------%

%-------Quasi-steady simulation----%

figure(1)
plot(ta,Z1a);
title ('U-tube oscillations','fontsize', 14);
xlabel ('Time [s]', 'fontsize', 14);
ylabel ('Water level fluctation in the surge shaft [m]', 'fontsize', 14);
legend ('Quasi-steady state');

%-------Ogawa et al. simulation-----%

figure(2)
plot(ta,Z2a)
title ('U-tube oscillations','fontsize', 14);
xlabel ('Time [s]', 'fontsize', 14);
ylabel ('Water level fluctation in the surge shaft [m]', 'fontsize', 14);
legend ('Ogawa et al');

%-------Vitkovsky simulation-----%
figure(3)
plot(ta,Z3a);
title ('Vitkovsky damping model, H = 1m', 'fontsize', 14);
xlabel ('Time [s]', 'fontsize', 14);
ylabel ('Water level fluctation in the surge shaft [m]', 'fontsize', 14);
legend ('Vitkovsky');

%---------Reynolds number
figure(4)
plot(ta,Rea,ta,Lam,'r',ta,Turb,'g');
title ('Reynolds number', 'fontsize', 14);
xlabel ('Time [s]', 'fontsize', 14);
ylabel ('Reynold number', 'fontsize', 14);
legend ('Reynold number', 'Laminer flow upper boundary', 'Turbulent flow lower boundary');

%---------Velocity simulation
```

```matlab
figure(5)
plot(ta,Va);
title ('Velocity, H = 1m', 'fontsize', 14);
xlabel ('Time [s]', 'fontsize', 14);
ylabel ('Amplutide', 'fontsize', 14);
legend ('Velocity');

figure(6)
plot(Va,fa);
title ('Velocity and laminar friction factor, H = 1m', 'fontsize', 14);
xlabel ('Velocity [m/s]', 'fontsize', 14);
ylabel ('Laminar friction factor', 'fontsize', 14);


figure(7)
plotyy(ta,Va,ta,fa);
[hAx,hLine1,hLine2] = plotyy(ta,Va,ta,fa);
grid;
title ('Velocity compered to steady state friction factor, H = 1m', 'fontsize', 18);
xlabel ('Time [s]', 'fontsize', 14);
ylabel(hAx(1),'Velocity [m/s]','fontsize', 18) % left y-axis
ylabel(hAx(2),'Steady state friction factor','fontsize', 18) % right y-axis
legend ('Velocity', 'Steady state friction factor', 'location','northeast');




% ------------------- Measurments ------------------- %

[t,Y,S]=loadData;

n = 500; %Number of measurements

%Finding the average of n measurements
Yavg = cell2mat(arrayfun(@(x) mean(Y(1:end,x:x+n-1),2)',1:n:size(Y,2)-n-
1,'UniformOutput',0)')';

%Finding the standard deviation for all sensors
S_PT1 = arrayfun(@(x) std(Y(1,x:x+n-1)), 1:n:size(Y,2)-n-1);% standard deviation SPT 1
S_PT2 = arrayfun(@(x) std(Y(2,x:x+n-1)), 1:n:size(Y,2)-n-1);% standard deviation SPT 2
S_PT3 = arrayfun(@(x) std(Y(3,x:x+n-1)), 1:n:size(Y,2)-n-1);% standard deviation SPT 3
S_EMF = arrayfun(@(x) std(Y(4,x:x+n-1)), 1:n:size(Y,2)-n-1);% standard deviation EMF

%Finding the t-value for a confidence level of 95 % with n measurements
t_value = tinv(0.975,n-2);

%%RANDOM UNCERTAINTY

%Student-t calcualtions

%error
e_pr_PT1 = (t_value*S_PT1)./sqrt(n);
e_pr_PT2 = (t_value*S_PT2)./sqrt(n);
e_pr_PT3 = (t_value*S_PT3)./sqrt(n);
e_fr_EMF = (t_value*S_EMF)./sqrt(n);
e_r = [e_pr_PT1; e_pr_PT2; e_pr_PT3; e_fr_EMF];

%Mean of random error
```

Appendix E

```matlab
e_r_mean = [mean(e_pr_PT1); mean(e_pr_PT2); mean(e_pr_PT3); mean(e_fr_EMF)];

%Uncertainty
f_pr_PT1 = e_pr_PT1./Yavg(1,:);
f_pr_PT2 = e_pr_PT2./Yavg(2,:);
f_pr_PT3 = e_pr_PT3./Yavg(3,:);
f_fr_EMF = e_fr_EMF./Yavg(4,:);
f_r = [f_pr_PT1; f_pr_PT2; f_pr_PT3; f_fr_EMF];



%%%SYSTEMATIC UNCERTAINTY

%Pressure sensors
e_S_CAL = 0.0005*100; % Systematic uncertainty DIgital calibration  DPI 601 Full-scale mWC
e_S_P = 0.0004*50;    % Systematic uncertainty pressure instrument Full-scale mWC

f_S_PCAL = @(P) sqrt((e_S_CAL./P).^2 + (e_S_P./P).^2); %Totat systematic uncertainty in procentage

%Flow meter
e_S_F = 0.002 * 0.55556; % Systematic uncertainty flow meter Full-scale m^3/s
f_S_F = @(Q) sqrt((e_S_F./Q).^2);%Totat systematic uncertainty in procentage

%TOTAL UNCERTAINTY for each point
f_TPT1=sqrt((f_S_PCAL(Yavg(1,:)).^2)+(f_r(1,:).^2));% Total uncertainty SPT 1
f_TPT2=sqrt((f_S_PCAL(Yavg(2,:)).^2)+(f_r(2,:).^2));% Total uncertainty SPT 2
f_TPT3=sqrt((f_S_PCAL(Yavg(3,:)).^2)+(f_r(3,:).^2));% Total uncertainty SPT 3
f_TEMF=sqrt((f_S_F(Yavg(4,:)).^2)+(f_r(4,:).^2));% Total uncertainty EMF


%TOTAT ERROR in each average piont
e_TPT1 = abs(f_TPT1.*Yavg(1,:));
e_TPT2 = abs(f_TPT2.*Yavg(2,:));
e_TPT3 = abs(f_TPT3.*Yavg(3,:));
e_TEMF = abs(f_TEMF.*Yavg(4,:));



%%%PLOT
t1 = 0 : 1/5000 : (length(Y)-1)*1/5000;%Time for original signal
t2 = n/5000: n/5000 : (length(Yavg))*n/5000;%Time for average plot

%Pressure measurements

sensor = 3; %Sensor of interest


figure(8)
clf
plot(t2, Yavg(sensor,:),'r'); %Average signal
hold on
grid
plot(t2, eval(['Yavg(',num2str(sensor),',:) + e_TPT',num2str(sensor)]),'-.k');%upper error limit
plot(t2, eval(['Yavg(',num2str(sensor),',:) - e_TPT',num2str(sensor)]),'-.k');%lower error limit
title ('Pressure measurements with error limits','fontsize', 18);
xlabel ('Time [s]', 'fontsize', 14);
```

```matlab
ylabel('Water fluctuation in the surge shaft [m]','fontsize', 18)
legend ('Pressure', 'Error limits', 'location','northeast');


%------Results of measurements----%
figure(9);
plot(t2,Yavg(sensor,:));
grid
title ({'Measured water level fluctuation in the surge shaft with traditional design',', H =
2[m], L = 21[m], Q = 0.007[m3/s]', 'fontsize', 14);
xlabel ('Time [s]', 'fontsize', 14);
ylabel ('Pressure fluctation [mWC]', 'fontsize', 14);
legend([S(sensor)]);

%------Measurements VS Quasi-steady----%
figure(10);
plot(t2,Yavg(sensor,:),ta,Z1a);
grid
title ({'Comparison between measured water level in the traditional surge shaft',' and Quasi-
steady friction model',', H= 2 [m], L = 21 [m], Q = 0.007 [m3/s]'}, 'fontsize', 14);
xlabel ('Time [s]', 'fontsize', 14);
ylabel ('Pressure fluctation [mWC]', 'fontsize', 14);
legend([S(sensor);'Quasi-steady']);

%------Measurements VS Ogawa et al-----%
figure(11);
plot(t2,Yavg(sensor,:),ta,Z2a);
grid
title ({'Comparison between measured water level in the traditional surge shaft',' and Ogawa
et al friction model',', H= 2 [m], L = 21 [m], Q = 0.007 [m3/s]'}, 'fontsize', 14);
xlabel ('Time [s]', 'fontsize', 14);
ylabel ('Pressure fluctation [mWC]', 'fontsize', 14);
legend([S(sensor);'Ogawa et al.']);

%------Measurements VS Vitkovsky-----%
figure(12);
plot(t2,Yavg(sensor,:),ta,Z3a);
grid
title ({'Comparison between measured water level in the traditional surge shaft',' and
Vitkovsky friction model',', H= 2 [m], L = 21 [m], Q = 0.007 [m3/s]'}, 'fontsize', 14);
xlabel ('Time [s]', 'fontsize', 14);
ylabel ('Pressure fluctation [mWC]', 'fontsize', 14);
legend([S(sensor);'Vitkovsky']);


%--------New one-term friction model----------%
figure(13);
plot(ta,Z6a,ta,Z1a);
grid
title ('H= 2m, L = 21m', 'fontsize', 14);
xlabel ('Time [s]', 'fontsize', 14);
ylabel ('Pressure fluctation [mWC]', 'fontsize', 14);
legend('New one-term','Quasi');

figure(14);
plot(t2,Yavg(sensor,:),ta,Z6a);
grid
title ({'Comparison between measured water level in','the surge shaft and the new one-term
```

Appendix E

```
friction model',' H= 1m, L = 11m'}, 'fontsize', 14);
xlabel ('Time [s]', 'fontsize', 14);
ylabel ('Pressure fluctation [mWC]', 'fontsize', 14);
legend([S(sensor);'New one-term model']);

%---------Signal treatment----------%
figure(15);
subplot(2,1,1);
plot(t1,Y(sensor,:));
grid
title ('Raw data form pressure measurments', 'fontsize', 14);
xlabel ('Time [s]', 'fontsize', 14);
ylabel ('Pressure fluctation [mWC]', 'fontsize', 14);
subplot(2,1,2);
plot(t2,Yavg(sensor,:));
grid
title ('Averaged signal from the pressure measurments', 'fontsize', 14);
xlabel ('Time [s]', 'fontsize', 14);
ylabel ('Pressure fluctation [mWC]', 'fontsize', 14);
```

Published with MATLAB® R2015a

Appendix F.   PICTURE - DYNAMIC TEST RIG

Figure F-1: *Picture of the surge shaft , combination of traditional surge shaft and siphon system*

Figure F-2: *Picture of the test section for PIV measurements*

Appendix F

Figure F-3: *Picture of the upper tank . Showing the outlet for the headrace and spillway*

Appendix G. RISK ASSESSMENT

NTNU		Hazardous activity identification process	Prepared by	Number	Date
			HSE section	HMSRV2601E	09.01.2013
			Approved by	Replaces	
HSE			The Rector		01.12.2006

Unit: Department of Energy and Process engineering

Line manager: Olav Bolland

Participants in the identification process (including their function):

Short description of the main activity/main process: Master project for student Isak Bergset

Project title: Investigations of a harmonic oscillatory flow

Date: 15.01.2017

Is the project work purely theoretical? NO   Answer "YES" implies that supervisor is assured that no activities requiring risk assessment are involved in the work. If YES, briefly describe the activities below. The risk assessment form need not be filled out.

- Signatures: Responsible supervisor: Pål-Tore Selbo Storli   Student: Isak Bergset

ID nr.	Activity/process	Responsible person	Existing documentation	Existing safety measures	Laws, regulations etc.	Comment
01	Operating a dynamic test rig for water flow in pipesystem. - Pressure, velocity and flow measurments	- Isak Bergset - Bård Aslak Brandåstrø	- Attached sketches of the dynamic rig		- HMS course	

Appendix G

		prepared by	Number	Date
NTNU		HSE Section	HMSRV2604	8 March 2010
HSE/KS		approved by	Page	Replaces
	Risk matrix	Rector	4 of 4	9 February 2010

Date: 15.01.2017

Unit: Department of Energy and Process engineering

Line manager: Olav Bolland

Participants in the identification process (including their function):

Short description of the main activity/main process: Master project for student Isak Bergset.

Project title: Investigations of a harmonic oscillatory flow

Signatures: *Responsible supervisor: Pål-Tore Selbo Storli*   *Student: Isak Bergset*

Activity and location	Potential undesirable incident/strain	Likelihood: Likelihood (1-5)	Consequence: Human (A-E)	Environ-ment (A-E)	Economy/ materiel (A-E)	Repu-tation (A-E)	Risk value	Comments/status Suggested measures
Moving heavy objects	-When reestablishing the surge shaft at different lengths the pipe system can be dangers if something falling off. This can injure personnel and equipment.	2	D	B	D	D	2D	-Have a good overview of personnel in the lifting area. -Use approved lifting equipment and techniques. -Use helmet and shoes -Inform relevant personnel about the job.
Welding	-Scatted object hitting and injure the eye. -Sharp damaging light for the eyes. -Burning injurie (contact injurie)	2	E	B	B	C	3E	-Overview of the working place. -Us of recommended safety clothing -Use glasses/goggles -Spare other against possible danger. -Be aware of the how to use the equipment.
Drilling	-Contact with the rotating drill. Can cause damage to	2	B	C	C	B	2B	-Overview of the working place.

xx

NTNU — HSE/KS

Risk matrix

	prepared by	Number	Date
	HSE Section	HMSRV2604	8 March 2010
	approved by	Page	Replaces
	Rector	4 of 4	9 February 2010

Activity		No.						Code	Measures
	equipment, additional items and injure personnel. -Drilling at wrong place -High sound damaging the hearing.	3	B	B	C	C	B	3B	-Use of recommended safety clothing -Use glasses/goggles. -Be aware of the how to use the drill.
Lifting of minor components and material.	-losing small or minor items down can cause danger to personnel. 3. person and the item itself if the height or weight is large enough.	3	D	C	C	B	B	3B	-Have a good overview of personnel in the lifting area. -Use approved lifting equipment and techniques. -Use helmet and shoes.
Sawing	- Cut injuries on personnel or items/material. - Scattered object hitting and injure the eyes. - Some saws can make high sound, which can damage the hearing. - Sawing at wrong place.	3	D	C	C	C		3D	-Clear the area for potential damaging items. -Use safety equipment. (gloves, cap to cover hair) -Be aware of the how to use the drill.
Work on higher plan (above normal ground, 2.floor or similar)	- Fall injuries - Dropping items that can injure personnel around and the item itself.	3	D	A	B	C	B	3D	-Stand on a safety ground. -Use safety equipment if necessary - Have a good overview of personnel in the lifting area. -Use approved lifting equipment and techniques. -Use helmet and shoes.
Water leakage from the pipe system	-Slippery floor -Water stream at high pressure	4	C	B	B	C	B	4C	-Protect eyes whit classes -Beware of slippery floor

NTNU HSE/KS	Risk matrix	prepared by	H3E Section	Number	HMSRV2604	Date	8 March 2010
		approved by	Rector	Page	4 of 4	Replaces	9 February 2010

| Other work in the laboratory | 5 | D | A | B | C | 5D | - Beware of other projects and work in the laboratory |
| -High noise -Moving equipment hitting personnel -Falling items hitting personnel | | | | | | | - Always use safety and protection gear to protect ears and eyes. - Consider to use helmet and other protection gear such as protected shoes and protection/work cloths |

Likelihood, e.g.:
1. Minimal
2. Low
3. Medium
4. High
5. Very high

Consequence, e.g.:
A. Minimal
B. Small
C. Moderate
D. Critical
E. Very critical

Risk value (each one to be estimated separately):
Human = Likelihood x Human Consequence
Environmental = Likelihood x Environmental consequence
Financial/material = Likelihood x Consequence for Economy/materiel
Reputation = Likelihood x Consequence for reputation

Potential undesirable incident/strain
Identify possible incidents and conditions that may lead to situations that pose a hazard to people, the environment and any materiel/equipment involved.

NTNU		prepared by	Number	Date
⊙	Risk matrix	H3E Section	HMSRV2604	8 March 2010
HSE/KS		approved by	Page	Replaces
		Rector	4 of 4	9 February 2010

Criteria for the assessment of likelihood and consequence in relation to fieldwork

Each activity is assessed according to a worst-case scenario. Likelihood and consequence are to be assessed separately for each potential undesirable incident. Before starting on the quantification, the participants should agree what they understand by the assessment criteria:

The likelihood of something going wrong is to be assessed according to the following criteria:

1. **Minimal**
   Once every 50 years or less

2. **Low**
   Once every 10 years or less

3. **Medium**
   Once every year or less

4. **High**
   Once a month

5. **Very high**
   Once a week

Human consequence is to be assessed according to the following criteria:

A. **Minimal**
   Small injury that may require simple first aid, but no medical treatment; insignificant health risk

B. **Small**
   Injury that requires medical treatment. No absence from work other than for treatment. No injury of permanent character.

C. **Moderate**
   Injury that involves absence from work; may produce acute sickness

D. **Critical**
   May result in permanent injury; may produce serious health

Environmental consequences are assessed according to the following criteria:

A. **Relatively safe**
   Insignificant impact on the environment

B. **Small**
   Small impact and short restitution time

C. **Moderate**
   Possibility of undesirable long term effects; some cleanup is to be expected

D. **Critical**
   Undesirable long term effects; cleanup to be expected

E. **Very critical**
   Damaging to living organisms; irreversible impact on the environment; cleanup must be undertaken

The unit makes its own decision as to whether opting to fill in or not consequences for environment, economy/materiel and reputation. It is up to the individual unit to choose the assessment criteria for economy/material and reputation.

Risk = Likelihood x Consequence

Please calculate the risk value for "Human", and if chosen, "Environment", "Economy/materiel" and "Reputation", separately. Then refer to the risk assessment matrix.

Appendix G

NTNU		prepared by	Number	Date
	Risk matrix	H3E Section	HMSRV2604	8 March 2010
H3E/KB		approved by Rector	Page 4 of 4	Replaces 9 February 2010

About the column "Comments/status, suggested preventative and corrective measures":
Measures can impact on both likelihood and consequences. Prioritise measures that can prevent the incident from occurring; in other words, likelihood-reducing measures are to be prioritised above greater emergency preparedness, i.e. consequence-reducing measures.

MATRIX FOR RISK ASSESSMENT at NTNU

		Minimal	Low	Moderate	High	Very High
CONSEQUENCE	Very critical	E1	E2	E3	E4	E5
	Critical	D1	D2	D3	D4	D5
	Moderate	C1	C2	C3	C4	C5
	Small	B1	B2	B3	B4	B5
	Minimal	A1	A2	A3	A4	A5
		LIKELIHOOD				

Principles for accept criteria. Explanation of colours used in the risk assessment matrix.

Colour		Description
Red		Unacceptable risk. Measurements to reduce risk value must be carried out.
Yellow		Matter of judgement. Measurements to reduce risk value must be considered.
Green		Acceptable risk. Measurements may be carried out for other reasons.

xxiv

NTNU			Risk matrix	prepared by	Number	Date
				HSE Section	HMSRV2604	8 March 2010
HSE/KS				approved by	Page	Replaces
				Rector	4 of 4	9 February 2010

Dynamic test rig second section with surge shaft

PARTS LIST	
ITEM	PART
1	Support cane
2	Ring attachment
3	Surge shaft
4	Support
5	Penstock
6	Floor

3160 mm
2700 mm
2500 mm

Siphon pipe
Butterfly valve
Pressure transducer
Gate valve
Flow direction
To the sump

Appendix:

Appendix G

NTNU		Risk matrix	prepared by	Number	Date
			HSE Section	HMSRV2604	8 March 2010
			approved by	Page	Replaces
HSE/KS			Rector	4 of 4	9 February 2010

Dynamic test rig first section

Flow direction

Pressure transducer

Pressure transducer

1200 mm
2000 mm
2000 mm
2000 mm
460 mm
2500 mm
4500 mm
2775 mm
3000 mm
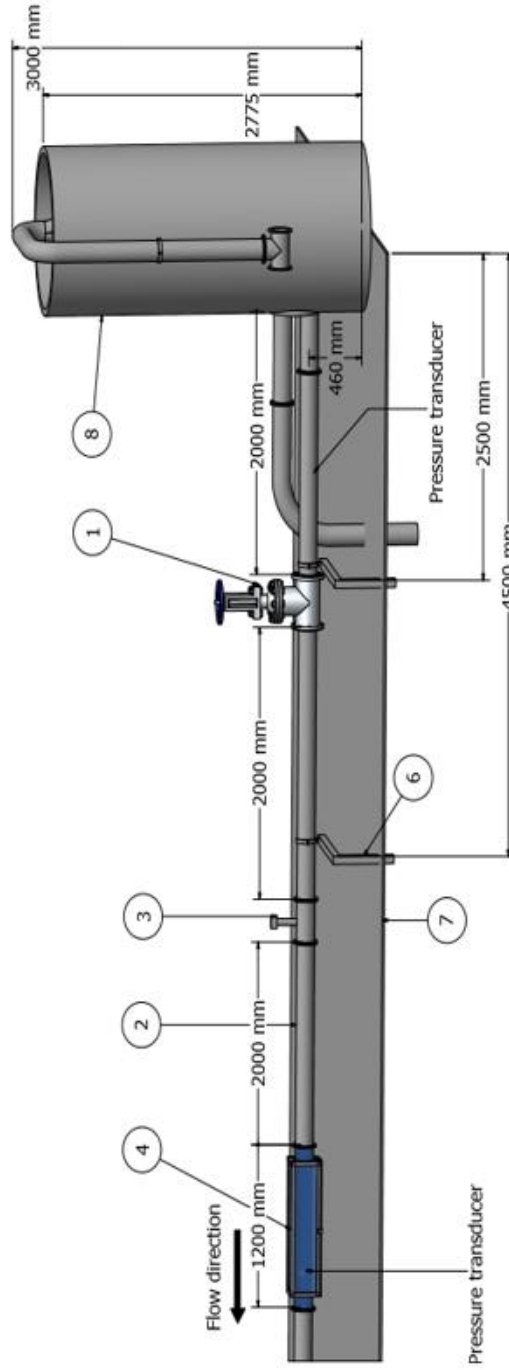
PARTS LIST	
ITEM	PART
1	Gate valve
2	Penstock
3	Electromagnatic flowmeter
4	Test section
5	Surge shaft
6	Support
7	Floor
8	Upper resavoir

Appendix H.   PAPER – CRHT-VII

Proceedings of the International Symposium on Current Research in Hydraulic Turbines

CRHT – VII

Isak Bergset

Investigations of a Harmonic Oscillatory Flow

Isak Bergset[1*]

Pål-Tore Storli[2*]

[1]*Department of energy and process engineering at Norwegian University of Science and Technology, The Waterpower laboratory, Alfred Getz vei 4, 7491 Norway*

[2]*Associate professor, pal-tore.storli@ntnu.no*

** Corresponding author (*isakb@stud.ntnu.no*)*

Abstract

This paper presents a study on frictional losses in closed conduit flow, where the calculations on harmonic mass oscillation is issued. The mass oscillation, also called U-tube oscillations, are applied by a rapid closure of a downstream valve. The aim is to facilitate the opportunity to purpose a new friction model that needs less computational power to solve, making it simpler for power companies to use. Three existing methods of calculating the frictional forces is introduced, simulated and compered. First, is the steady state friction model considered, by using the laminar friction factor by Darcy-Weisbach or the turbulent friction factor by Haaland, depending on the flow regime. Secondly, the damping model by Ogawa et al, and last, the model by Vitkovsky. The basic of the theoretical study is made through the Governing equations, taking the equation of momentum and continuity into consideration. By looking at slow transients, neglecting the elasticity and thermal effects of the pipe system and water, the system oscillations are simulated by use of the Euler method.

A dynamic test rig with a horizontal penstock, an upper reservoir and a surge shaft is established. In addition, valves and measuring instruments are installed to perform an experimental campaign measuring the flow parameters of interest. The rig is constructed to have the possibility to assemble measurements on transient oscillations in both traditional surge shaft and a siphon system. For the measurement in the test rig a static pressures transducers, an electromagnetic flowmeter and a particle image velocimetry are installed.

The results will first present the established dynamic rig with a proposal for an experimental test campaign. Secondly, the frictional models are simulated and evaluated. Validations and evaluations of existing models are made in the interest of defining their accuracy and utility in use. Source of errors and complexity is identified and discussed, giving a basic for the further work towards developing a new friction model.

This paper is based on the project thesis drawn by the author in the spring of 2016, and presents the pre work for the ongoing Master thesis on the subject of develop a new one-term friction model.

Keywords: Harmonic oscillations, Transitional flow, Friction models, Governing equation, Dynamic test rig, New friction model.

1. Introduction

A hydropower plant is rarely, if ever, operating at perfectly steady state conditions. Imbalances in the electrical grid system will cause slight variations in the rotational speed of the runner, and due to the runner characteristics this will change the turbine head and dynamics are induced in the conduits, causing oscillations in pressure and flow. Even bigger oscillations are induced when the operational point of the

turbine is deliberately changed. Associated with all these oscillations are hydraulic losses, losses that are in contrast to steady state losses, difficult to describe using 1D models that is simple enough for implementing in production planning optimization tools, seeking to determine the best time to implement these deliberate changes. Thus, the optimal solution found using these models are based on inaccurate representation of the losses, and the solution is likely suboptimal.

In a hydropower plant, there are mainly generated two dynamic phenomena, due to water regulation; the water hammer and mass oscillation, considering pressure propagation and mass flow change respectively. These two oscillating phenomena propagates in quite large differences in time, making it necessary to investigate them separately and with different assumptions. In general, all cases of flow has to satisfy the basic equations of continuity (Eq.(1)) and momentum (Eq.(2)), where the fundamental laws are satisfied. This equations are called the Governing equation and can be derived in terms of piezometric head $H\ [m]$ and velocity $V\ \left[\frac{m}{s}\right]$ as follows [1].

i.   Continuity:

$$V\frac{\partial H}{\partial x} + \frac{\partial H}{\partial t} + \frac{a^2}{g}\left(\frac{\partial V}{\partial x}\right) = 0 \tag{1}$$

ii. Momentum:

$$g\frac{\partial H}{\partial x} + \frac{fV|V|}{2D} * V\frac{\partial V}{\partial x} + \frac{\partial V}{\partial t} = 0 \tag{2}$$

Where, $x[m]$ = Length of each section, $t[s]$ = time, $a\left[\frac{m}{s}\right]$ = Pressure propagation speed, $g\left[\frac{m^2}{s}\right]$= Acceleration from gravity and f is the friction factor.

The linear momentum considers the Newton second law, stating that all forces acting on a mass of a fluid in a given direction, is equal to the product of mass and acceleration. The equation of continuity deals with the mass, stating that total applied mass into a system must equal the time rate of change of mass inside the system [2]. Existing accurate models to estimate frictional losses in unsteady pipe flow demands high computational power and can be complex in use because of their 3D nature. This is unfavourable for power companies, where optimal operational strategies are made on a daily basis and calculations that are computationally demanding and require highly skilled personnel is not an option. The interest of developing a new and simple 1D model to reduce the required demand is thus desired to find.

The subject of this study is to look closer into the modelling of the slow transients of U-tube oscillations, where the knowledge is undesirable low and methods for predicting the system behaviour are unfit. By investigating existing models, and identify their advantages and disadvantages, a new model with less complexity and less computational demands can hopefully be found. The basic wave equation describing the natural behaviour of the U-tube oscillations can be derived by combining Eq.(1) and Eq.(2), and will thus be of great importance for the further study on the mass oscillation.

Figure 1 illustrates the basic U-tube oscillation in a hydropower plant, where the water level in the upper reservoir is assumed constant throughout the whole sequence. The water level in the surge shaft will on the other hand oscillate with a time step of T and natural frequency ω. The system friction will gradually damp the oscillations back to initial level.
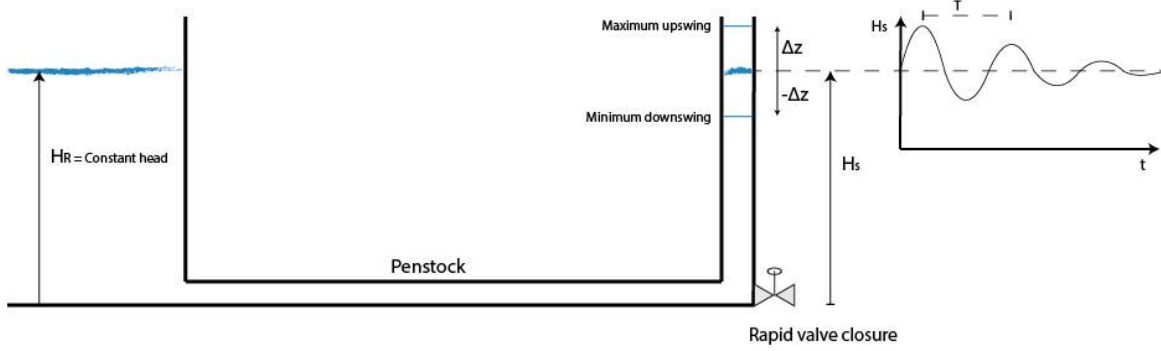
Figure 1. Schematic illustration of mass oscillation

The natural frequency of the oscillation is given by,

$$\omega = \sqrt{\frac{g}{A_s * \left(\frac{L}{A_T}\right)}} \qquad (3)$$

Where, $L\ [m]$ = Pipe length and the subscription s and T refers to the surge shaft and penstock respectively. The time period is found from Eq.(4).

$$T = \frac{2\pi}{\omega} \qquad (4)$$

Considering the Newton second law and the continuity equation, the mass oscillation can now be expressed as an ordinary differential equation. The change in water level in the surge shaft estimates the rate of the mass oscillations. By taking the continuity equation and the given assumptions at slow transients, the flow change $dQ\ [\frac{m^3}{s}]$ is found as expressed in Eq.(5) [3].

$$dQ = dt * \frac{gA}{L}(dH - RQ|Q|) \qquad (5)$$

Where R is the head loss,

$$R = \frac{f * L}{2gDA^2} + \left(\frac{k_i}{2 * g * A^2}\right) \qquad (6)$$

$D\ [m]$ is the diameter of the pipe.

The first term in the Eq.(6) considers the frictional losses, estimated by a friction model. The second term, is the losses from minor disturbances, found by the specified loss coefficient k_i. Water fluctuations in the surge shaft is found by the change in volume. The principle is illustrated in Figure 2 and equation (7).
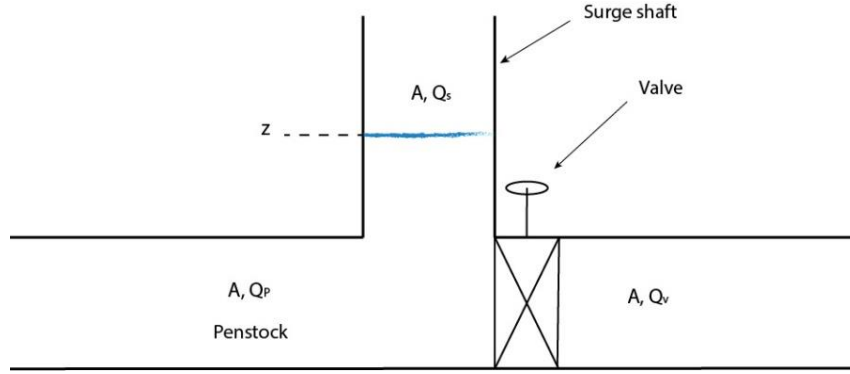
Figure 2. Illustration of the pipe branch at the surge shaft. Depicting the indices of the volume flow

$$\frac{dz}{dt} = \frac{Q_P - Q_v}{A} = \frac{Q_S}{A} \ [m] \tag{7}$$

When the valve is closed, we can assume $Q_S = Q_P = Q \ \left[\frac{m^3}{s}\right]$. To find the rate of volume flow in the surge shaft, is it necessary to find the change in flow rate and add this to the flow rate in the previous time step.

$$Q_{new} = Q_{s,previous} + dQ \tag{8}$$

The new water level $z_{new} \ [m]$ in the surge shaft is then found by Eq. (9) for each time step.

$$z_{new} = z_{old} + dt * \frac{Q_{new}}{A} \tag{9}$$

The interest now, is to look closer into how we can calculate the loss term R, in a most accurate and suitable way, by using different friction models.

Existing models

The study on frictional losses in pipe system has been present for a long time. Julius Weisbach presented in 1845 a further developed equation from Darcy, describing the head loss h_f [m], as depicted in Eq. (10). The equation made it possible to estimate the steady state frictional losses in a pipe system [1].

$$h_f = f\frac{L}{D} * \frac{V * |V|}{2g} = f\frac{L}{D} * \frac{Q * |Q|}{2 * g * A^2} \ [mWC] \tag{10}$$

Where, f is the Darcy-Weisbach friction factor. Eq. (11) depicts the basic Darcy-Weisbach friction factor at laminar steady state flow.

$$f_{lam} = \frac{64}{Re} \tag{11}$$

Where Re is a non-dimensional Reynolds number that indicates the viscous effect compared to the inertia effect. The Re value is found by Eq. (12).

$$Re = \frac{\rho V D_H}{\mu} \tag{12}$$

Where, ρ = Density of the fluid, D_H = Hydraulic diameter and μ = Dynamic viscosity. This number is typically used to determine if the flow is laminar (Re < 2300), turbulent (Re > 4000) or in the transitional flow regime (2300 < Re > 4000) [1]. A method to estimate the friction factor suited for turbulent flow at steady state have been proposed by several. One of the most common equation is the implicit Colebrook equation. Haaland simplified the Colebrook equation in 1983, introducing the following equation,

$$\frac{1}{\sqrt{f}} = -1.8 \log\left[\left(\frac{\frac{\varepsilon}{D}}{3.7}\right)^{1.11} + \frac{6.9}{Re}\right]$$

(13)

Where ε is the roughness of the inner pipe wall.

Steady state friction models has shown good results for steady state flow, but experimental tests has identified erroneous result for unsteady flow [4, 5]. The models tends to undervalue the friction after some time, and in addition, the oscillations are never fully dampened out. The interest of making a model to correct the undesired deviation was first presented by Daily in 1956, where he purposed a model consisting of the sum of the steady state friction using the instantaneous flow properties (so-called quasi-steady friction) and an unsteady term utilising instantaneous acceleration. Other researchers, such as Brunone in 1991 and Vitkovsky in 1998, have since further developed the model. The model that Vitkovsky presented was an improvement of the model by Brunone, implementing a sign, $sign(V)$ to account for the direction on the convective deceleration and acceleration of the flow. If V ≥ 0 the term is +1 and if V ≤ 0 the term is -1. The original equation from Brunone and the improved equation from Vitkovsky`s is depicted in Eq. (14) and (15) respectively [5].

$$f = f_q + \frac{k * D}{V|V|}\left(\frac{\partial V}{\partial t} - a * \frac{\partial V}{\partial x}\right)$$

(14)

$$f = f_q + \frac{kD}{V|V|}\left(\frac{\partial V}{\partial t} + asign(V)\left|\frac{\partial V}{\partial x}\right|\right)$$

(15)

Where f_q is the quasi-steady friction term, which is equal to the steady state friction term, but is updated at each time step, to give a more accurate result. The procedure is to update the Reynold number, considering the change in local velocity at the point of interest.

The second term in Eq. (14) and (15) is called the unsteady friction term, and corrects the deviation that the quasi-steady state has from actual friction. This term is further divided in two acceleration terms, one accounting for velocity change in time and the second considering velocity change in space, referred as the convective acceleration term. k is the Brunone friction coefficient, found by the Vardy`s shear decay coefficient C. Vardy uses the British head loss definition $f = 4f_{BR}$, and thus has to be accounted for.

$$k = \frac{\sqrt{C}}{2}$$

(16)

At laminar flow the Vardy shear decay coefficient is,

$$C = 0.00476$$

(17)

At turbulent flow.

$$C = \frac{7.41}{Re^{\log\left(\frac{14.3}{Re^{0.05}}\right)}} \tag{18}$$

The models above are two of many models for predicting the frictional effect in unsteady flow. Bergant et al. [5]. Presented a list, dividing all common known models into six groups. The different groups are categorized by how each specific model is calculating the unsteady correction term. It is usual to divided the models into two main categories, as follows,

1) Empirically based models:

Empirical models are made by observation and experiments. The Majority of empirical models in friction modelling are based on the model by Daily, including the two models presented by Brunone and Vitkovsky.

2) Physically based models:

Physically models are based on mathematically described relationships of the system, where calibration constants are not needed. The majority of these models are developed form the model presented by Zielke (1968). He presented a model for laminar flow with frequency dependent friction. The unsteady term defined by Zielke, uses a weighting function $W(t)$ to account for the past velocity changes, and the pipe flow acceleration in a local point to foresee the transient behaviour [6]. Zielke`s model showed great result compered to experimental data, but was just considering low Re number. The model has later on been developed further by several other researchers to establish a more accurate model (Trikha 1975, kagawa et al 1983, Suzuki et al 1991) [7], also including turbulent flow (Bratland (1986), Zarzycki (2004), Vardy and Brown (1995,2004)) [6] and specified u-tube dampening model (Svingen (1996)) [8].

U-tube oscillations are propagating with low frequency, making the impact from elasticity of the system and water insignificant. The energy from the initial velocity in the headrace will in U-tube motion be converted to potential energy by the water increase in the surge shaft. By assuming inelastic conditions, the elasticity term can be neglected in the governing equation and the prorogation speed goes towards infinity. This applies that the change in flow parameters can be assumed to occur at the same time in every section of the pipe. This will naturally have consequences on the friction model that are used in simulations, since the convective acceleration term is effectively nulled in this type of transient.

Regardless of the model chosen in simulations, simulation results should be compared either to better simulation results or to experimental results. The validity of "better simulation results" should also be tested against experimental results, at some point. Experimental results of this type of transient flow for the frequencies and Re numbers resembling hydropower plant conditions have not been found, and for this reason a rig for testing the dynamics of such flows have been established at the Waterpower laboratory at NTNU. It is described in the following.

2. The dynamic test rig

A dynamic test rig is established in the Water laboratory at the Norwegian University of Science and Technology (NTNU). A simple sketch of the test rig is depicted in Figure 3.
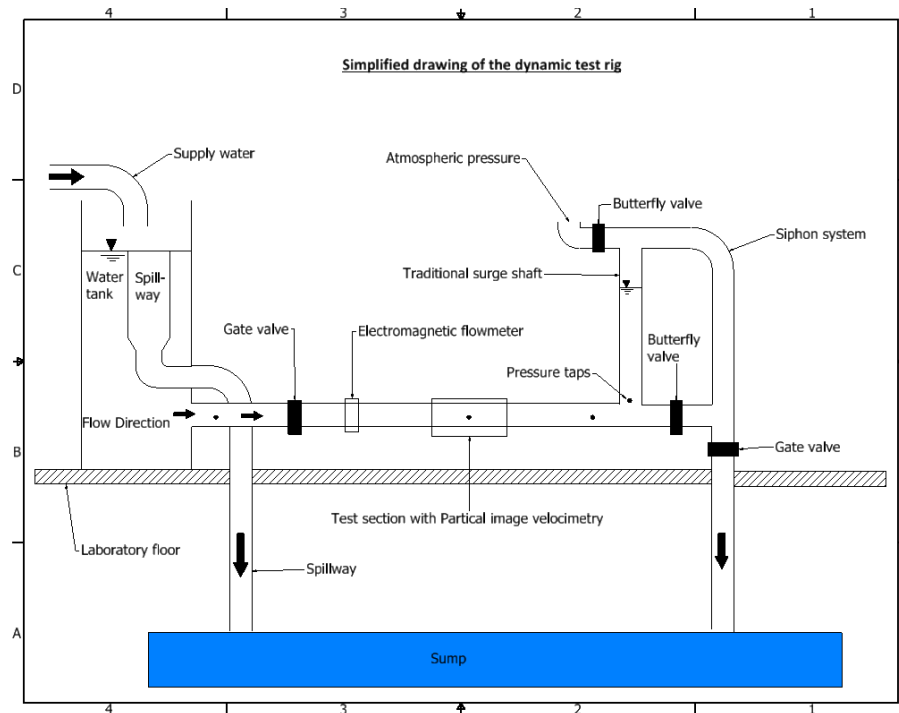
Figure 3. *Sketch of the dynamic test rig*

The rig is designed to generate harmonic oscillatory flow, and to measure water pressure, velocity and flow rate continuously. Dynamics are initiated by a rapid closure of the butterfly valve right downstream the traditional surge shaft. The surge shaft is designed to have the possibility to run as a traditional surge shaft or as a siphon system. Four valves are installed for the flow management, two butterfly valves and two gate valves. All valves are selected based on functionality and rate of flow disturbance. Four static pressure transducers are installed for pressure measurements. Three of them measuring the pressure in the penstock, one located at the penstock inlet, one in the middle of the pipe length and one right upstream the surge shaft. The last one is located in the bottom of the surge shaft, measuring the water level inside the surge shaft. The water level in the water tank is held constant by the functionality of the spillway, draining the excess water.

Flow rate and mean velocity is measured by an electromagnetic flowmeter, mounted approximately 5 m downstream the penstock inlet. Local velocity and flow field visualization, can be found by Particle Image Velocimetry (PIV) or other optical measurement techniques, installed in a transparent test section located approximately 8 m downstream the penstock inlet.

The size of the test rig and suggested experimental cases, are specified by the limitation of available space in the laboratory. The rig has the possibility to run with 11 m, 18 m or 29 m headrace tunnel. The flow rates are limited by the up-swing and down-swing, depicted in **Table 1.**

The reason for the structure resembling an inverted U is due to the desire of having the entire oscillating water column initially at the same condition. Considering normal surge shaft dynamic, where there is still water in the surge shaft while the water is flowing in steady state in the headrace tunnel. If the transient is initiated, the water in the headrace tunnel will decelerated, and the water in the surge shaft initially

accelerated. At some point in time, the entire water column is steady, but since the initial conditions were not the same, is it uncertain at what state the water in the two section are in. This is likely to be important for the dynamics involved in the harmonic oscillations after the initial upsurge, and this non-uniform distribution of the conditions is not ideal for producing measurement results used for validation of simple friction model. The inverted U, in principle a siphon, allows the entire water column to have the same initial velocity. By opening the top of the siphon to atmospheric pressure, the siphon flow will experience a water column separation. At the some point, the water will have a still water column rising up to the level of that siphon, where all the water has experienced the same accelerations and are in the same state, before the harmonic oscillation starts.

The valve management generating the U-tube oscillations are as follows,

i) Traditional surge shaft:
   All valves are open, using the gate valve furthest downstream to maintain the desired flow rate. To generate the U-tube oscillations, the butterfly valve located right downstream the traditional surge shat is rapidly closed.

ii) Siphon system:
   To make the siphon system run, is it necessary to fill the pipe system completely with water. This is made possible by closing all valves, except the butterfly valve at the top of the surge shaft, where water is guided into the system and filling the system with water. When the system is fully drained, the top butterfly valve is closed. To start the water to flow, the two gate valves are opened. Now the column separation, hence the U-tube oscillations can be generated by opening the top butterfly valve again.

3. Suggested experimental campaign

A suggestion for the test campaign is purposed in **Table 1.** Six different cases are purposed, where three test lengths, for both the traditional surge shaft and the siphon system are considered. The flow suggestions for each case are given by the system limitation on up-swing and down-swing, where the highest possible flow rate considering the limitations are purposed. Roughness, dynamic viscosity and loss coefficient is found from common literature. Frequency is calculated by Eq. (3).

Table 1. The six purposed test cases for the experimental campaign

Fixed/design parameters	Case 1	Case 2	Case 3	Case 4	Case 5	Case 6
Surge shaft function	Traditional oscillations	Column separation	Traditional oscillations	Column separation	Traditional oscillations	Column separation
Surge shaft	Traditional	Siphon	Traditional	Siphon	Traditional	Siphon
Headrace length, L	11 m	13.5 m *	18 m	20.5 m *	29 m	31.5 m *
Roughness, ϵ	0.002 mm	0.002 mm	0.002 mm	0.002 mm	0.002 mm	0.002 mm
Diameter, D	150 mm	150 mm	150 mm	150 mm	150 mm	150 mm
Flow, Q	0.016 m³/s	0.0377 m³/s	0.006 m³/s	0.0306 m³/s	0.005 m³/s	0.0247 m³/s
Pressure height, H	1	1	2	2	2	2

Dynamic viscosity at 10°C	1.31×10^{-3} Ns/m²	1.31×10^{-3} Ns/m²	1.31×10^{-3} Ns/m²	1.31×10^{-3} Ns/m²	1.31×10^{-3} Ns/m²	1.31×10^{-3} Ns/m²
k – loss coefficient	0.77	2.27	0.77	2.27	0.77	2.27
f – frequency	0.85 Hz	1.21 Hz	0.69 Hz	0.98 Hz	0.56 Hz	0.79 Hz

*Total length from the upper reservoir to the point of column separation (The top of the siphon)

4. Earlier experiences from friction models

In order to develop a new improved and simplified one-term friction model, it is desired to identify advantages and disadvantage from present friction models. The experience and results can be used to optimize the new model. Models just considering the local velocity has shown undesirably low damping after some time, thus an acceleration term has been introduced in the unsteady frictions models, such as the model by Brunone [5]. Source of deviation between real behaviour and simulation can be several reasons. The impact from a longer turning time of the oscillatory movement could be one of the main sources, due to constant time period and an decreasing amplitude. Increase in turning time, increases the time in low velocity area close to zero velocity. Zero velocity makes the Re number equal to zero as well, resulting in an estimation of zero friction for the steady state models. This contradicts with findings indicating that the actual friction in transitional flow is larger than at stationary flow [9].

A study done by Pingju Li in 2004 showed that the velocity profile during transient events were causing revers flows with increasing velocity gradients at the pipe wall, and a positive velocity in the centre of the pipe. In addition, showed Li that the front of the velocity profile was flat, similar to the turbulent velocity profile [10]. The finding by Li is illustrated in Figure 4.
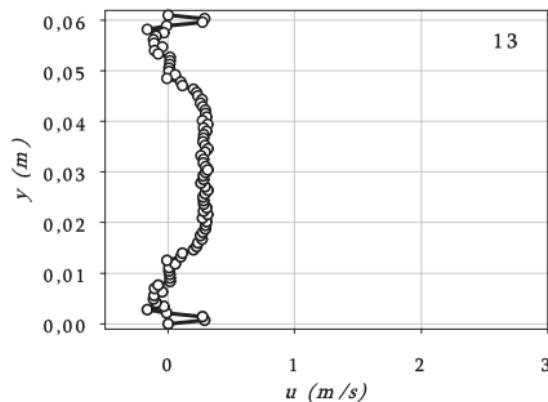
Figure 4. Velocity profile at transitional flow [10]

Hermod Brekke presented in 1984 an investigation showing that the frictional force was increasing as the length of the water column increased [11]. A similar study is of interest to utilize, pursuing experience and results that can help deriving an equation that can correct the differences and yield for all column lengths.

5. Simulation

Three different approaches on determine the U-tube oscillations are simulated. The methods are described below.

1) <u>Original steady state model and the quasi-steady state model</u>

Both the steady state and quasi-steady state model are using the basic Darcy-Weisbach head loss equation (Eq.(10)). Where the frictional losses are found by Eq.(11) at laminar flow and the Haaland approximation Eq.(13) at turbulent flow. As mention earlier, is the difference between these two models just that the quasi-steady state is updating the flow parameters for each time step [1].

2) <u>Ogawa et al. damping model [12]</u>

The model by Ogawa accounts for the flat velocity profile concluded by Li in his PhD. The approach by Ogawa et al, describes the U-tube oscillations by the equation of motion depict in Eq. (19).

$$\rho * A * L * \frac{dV}{dt} = -2 * \rho * g * A * Z - \pi * D * L * v * \frac{dV}{dy} \tag{19}$$

Where, Z is the water fluctuation from the equilibrium point in the surge shaft and v the kinematic viscosity.

To determine the velocity gradient $\frac{dV}{dy}$, giving y as the distance from the pipe wall to the center of the pipe. Ogawa introduced a velocity constant K_v.

$$\frac{dV}{dy} = K_v * \frac{V}{R} \tag{20}$$

Where R is the pipe radius. The velocity constant K_v, is given by the imaginer Re number Re_i, taking the imaginary maximum velocity V_{max}, of the liquid column in the vertical U-tube into consideration.

$$V_{max} = Z_0 * \sqrt{\frac{2 * g}{L}} \tag{21}$$

$$Re_i = \frac{V_{max} * D}{v} = Z_0 * \sqrt{\frac{2 * g}{L}} * \frac{D * Z_0}{v} \tag{22}$$

The relationship between the Re_i and the velocity constant were empirical estimated as

$$K_v = 25 * D * \left(1 + \frac{4.5 * 10^{-9}}{D^4}\right) * K_v' \tag{23}$$

$$K'_v = \frac{Re_i}{8.75 + 0.00233 * Re_i} \tag{24}$$

Given the equation of motion and the statements presented by Ogawa et al, the oscillating behaviour in a surge shaft can be written as [12],

$$\frac{d^2Z}{dt^2} + \frac{2 * v * K_v}{R^2} * \frac{dZ}{dt} + \frac{2 * g}{L} * Z = 0 \tag{25}$$

The implementation of the Ogawa et al. model is made through the calculation of the change in flow rate dQ, depicted by in Eq. (26), which is derived from Eq. (25).

$$dQ = dt \left(\frac{2 * g * Z * A}{L} - \frac{2 * V * K_v * Q_{new}}{R^2} \right) \tag{26}$$

3) <u>The unsteady friction model by Vitkovsky [5].</u>

Vitkovsky`s model is mainly developed for fast transients, such as the water hammer. However, if we look at the challenge on calculating the friction at the time of turning, the acceleration term presented in the model by Brunone can be used further to solve this zero velocity challenge. From the original governing equations can the convective term be neglected due to slow transients. As $a \rightarrow \infty$ and $\Delta x = \Delta L$, the Vitkovsky model can be expressed as Eq.(27), implementing the correction of direction to the change in time.

$$f = f_q + \frac{kD}{V|V|} \left(\frac{\partial V}{\partial t} \right) sign(V) \tag{27}$$

6. Results and discussion

Both steady state and unsteady state friction models are simulated. First, the steady state is considered, before looking further into the results for the unsteady state models.

6.1. Steady state and initial condition

Considering the system for all six cases, the flow characteristics can be estimated from the known initial values depict in **Table 1**. **Table 2.** shows the results of the system parameters, and Figure 5 and Figure 6 depicts the time simulation of the U-tube oscillations considering no frictional losses.

**Table 2.** Estimated parameters from initial conditions

Parameters	Unit	Case 1	Case 2	Case 3	Case 4	Case 5	Case 6
Reynolds number	-	103640	244210	38870	198220	32390	160000
Steady state friction factor	-	0.0177	0.0149	0.0219	0.0155	0.0229	0.0162
Total head loss	m	0.0776	0.4413	0.0188	0.4099	0.0203	0.3945
Time period of water hammer	s	0.03	0.037	0.049	0.056	0.079	0.086
Time period of mass oscillations	s	6.7	7.4	8.5	9.1	10.8	11.3
Frequency water hammer	Hz	33.3	27.2	20.4	17.9	12.6	11.6
Required sampling frequency on water hammer dynamics	Hz	66.7	54.3	40.8	35.8	25.3	23.3
Frequency mass oscillations	Hz	0.95	0.85	0.74	0.69	0.58	0.55
Required sampling frequency on mass oscillations	Hz	1.89	1.71	1.48	1.38	1.17	1.12
Hydrodynamic entry length	m	3.7	4.5	2.9	4.3	2.7	4
Mach number	-	0.0006	0.0015	0.0002	0.0012	0.002	0.0010
Pressure wave speed (speed of sound)	m/s	1467	1467	1467	1467	1467	1467
Highest upswing	m	0.93	2.36	0.45	2.37	0.48	2.37
Lowest downswing	m	-0.97	-2.55	-0.46	-2.55	-0.49	-2.55

It can be seen from **Table 2.** that all cases are turbulent. Head loss is dependent on the flow rate, resulting in a greater loss at higher velocity for the same cross section. The time period of the mass oscillations are larger than the time period of the water hammer. Thus, the two dynamics has to be studied separately. All cases have a Mach numbers lower than 0.3, hence the flow can be assumed incompressible [1]. The water deviation in the shaft is found satisfying for all cases, giving the limitation of not spilling water over the top or letting air into the headrace. Required sampling frequency is found from Nyquist sampling theorem [13]. Considering water hammer and mass oscillations the highest required sampling frequency is 66.7 Hz and 1.89 Hz respectively. All installed measurements devices are fulfilling this frequency requirement.

Figure 5 and Figure 6 shows the time simulations of the water fluctuations in the surge shaft, considering traditional surge shaft and siphon system respectively. The results confirms the findings in **Table 2**. The frequency will increase as the water string increases, and the flow rate determines the size of the water fluctuation.
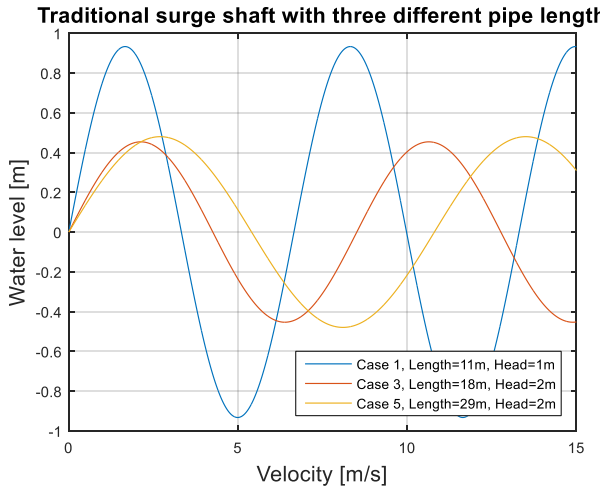
Figure 5. Time simulation of water fluctuation in the traditional surge shaft with three different pipe length
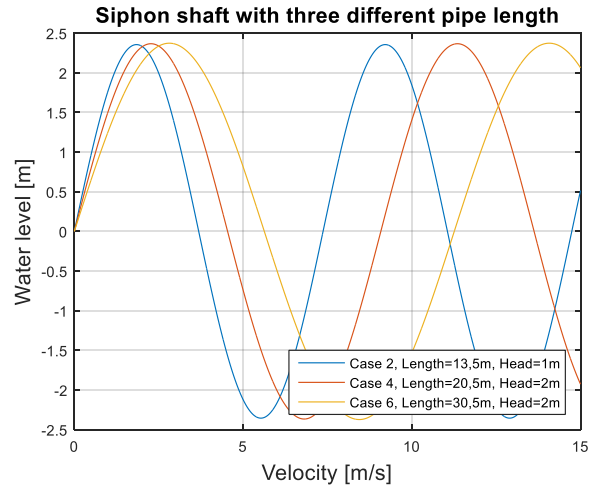
Figure 6. Time simulation of water fluctuation with siphon shaft with three different pipe length

## 6.2. Simulation models for unsteady flow

The quasi-steady state model, the model by Ogawa et al. and the model by Vitkovsky are simulated for traditional surge shaft with headrace lengths of 11m, 18m and 29m. Figure 7 to Figure 10 depicted the simulation results for case 1 with 11m pipe length.
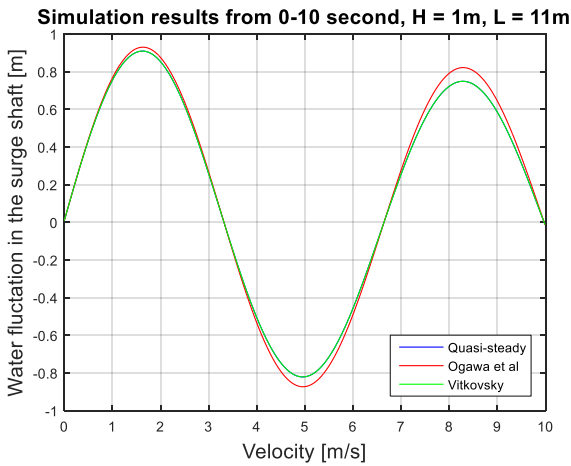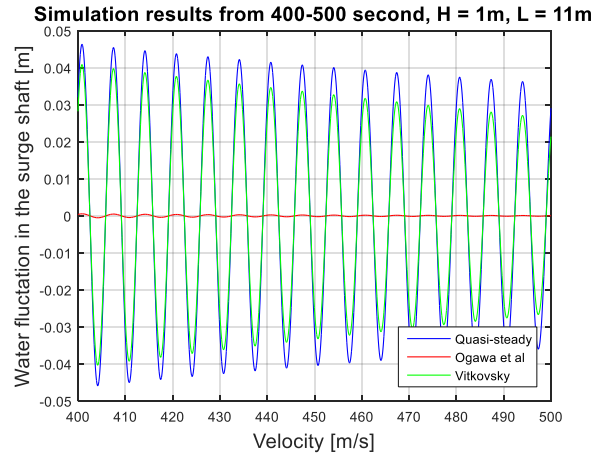

Figure 7. *Simulation results of the unsteady damping models from 0-10 second with 11 m pipeline*
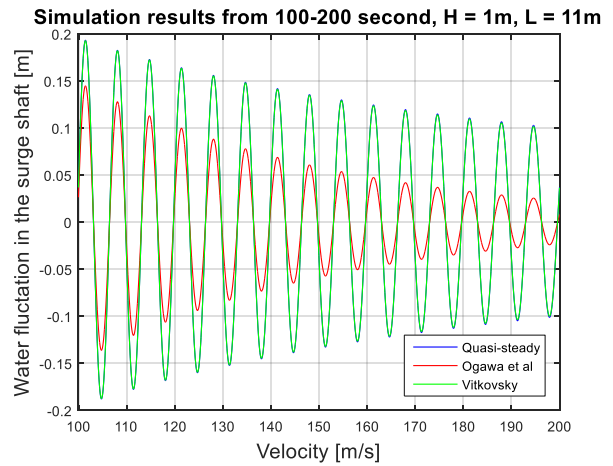
Figure 8. *Simulation results of the unsteady damping models from 100-200 second with 11 m pipeline*
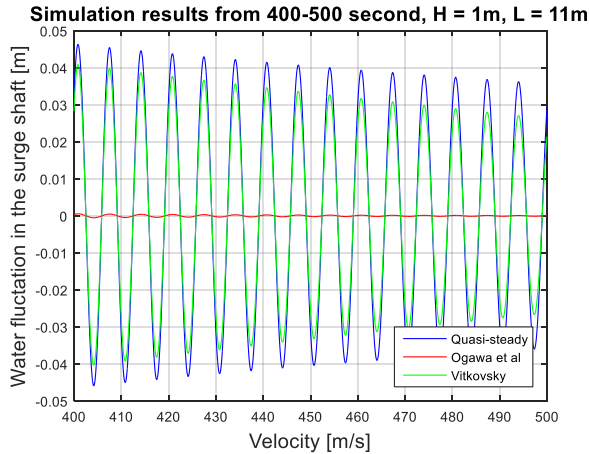
**Figure 9.** Simulation results of the unsteady damping models from 400-500 second with 11 m pipeline

Figure 10. Simulation results of the unsteady damping models from 1400-1500 second with 11 m pipeline

The simulation results above shows that all three models are quite similar in the initial oscillations. However, as time goes, the models are giving diverse results. The Ogawa et al. damps out the oscillations first, approximately after 500 second. The model by Vitkovsky follows the quasi-steady model longer, but after 1500 second, the oscillations are virtually damped out. The quasi-steady state is never fully damped out, giving a constant stationary oscillating result.

In order to get more knowledge on the performance of the different models, is it of interest to look closer on how the models are using and accounting for the different flow parameters. First, the Re number is evaluated, before looking closer at the velocity profile, acceleration and frequency.

The Re number is found from Eq. (12), and is specified by the velocity and density. Since the density is assumed to be constant at slow transients, the velocity will be the main deciding parameter. The velocity is depending on the movement of the oscillating dynamics, thus the time of the oscillating behaviour that is analysed is of importance. The Re number will always oscillate in phase with the velocity, being positive throughout the simulation, due to the absolute correction of the velocity. If the generated dynamics are large enough, is it possible to have an oscillating flow that fluctuate between all regimes. This is depicted in Figure 11, Showing the simulation result for the Re number in case 1.
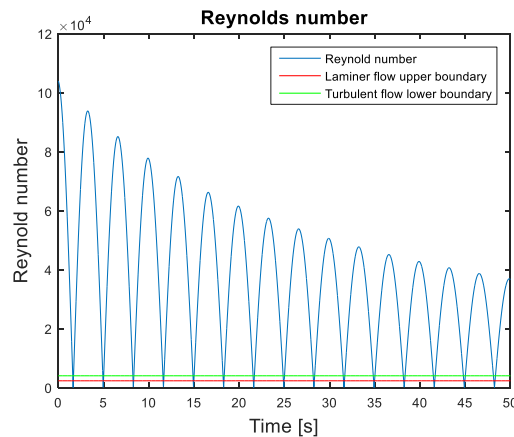
Figure 11. Simulation of the variating Reynolds number for case 1

As velocity moves toward zero (In the turn of the oscillations), the Re number will likewise decrease, making the Darcy-Weisbach friction factor to vanish. Figure 12 shows, if the velocity reaches a value

making the Re number equal to 2300, the friction factor gets a sudden drop before it gets heavily decreased as the velocity goes further to zero. Hence, the relation between the velocity and the steady state friction factor is changing as the velocity acts around zero. This implies the importance of finding a new method that is more suitable for predicting the frictional effect in the area of turning. Two issues are handled by accounting for the turning effect. The fact that the frictional force is larger in the turning area, and the deviation from the steady state frictional model.
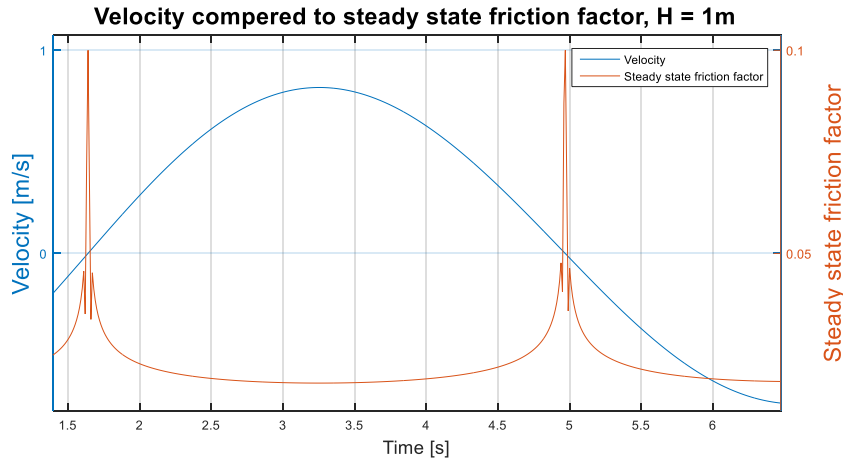

**Figure 12.** Relationship between Velocity and steady state friction factor

Using the Re number to estimate the friction needs thus a correction or replacement to achieve a suitable result for predicting the actual frictional force. Since the Re number is directly depending on the velocity in steady state models, is the zero velocity in the turnings neglecting the effect from the frictional force, by direct multiplication. If the velocity term could be included as an exponent, not as an individual term, the deviation in steady state models could maybe be solved. The model by Ogawa et al. shows a more realistic result in the final damping, making the oscillations to be fully damped out. The reason for this is that the velocity is implemented in the bottom of the fraction term, hence, the friction do not vanish if the velocity goes to zero.

The flow in harmonic oscillating behaviour will always accelerate or deaccelerate, depending on the time of the oscillations. Such velocity change makes it challenging to estimate friction with simple 1D-models, resulting in erroneous results [4]. Since U-tube oscillations acts nearly with the same oscillating period throughout the whole duration, is it of great curiosity to investigate the acceleration and deceleration impact further. Figure 10 shows how the quasi-steady state model underestimated the actual friction as time goes, giving a constant stationary oscillating behaviour. This shows that with decreasing amplitude, will the time of turning increase, making the velocity to stay closer to zero for a longer time interval. This will generate an erroneous result, since the steady state friction is depending on the Re number. The proposal to of include a term that accounts for the acceleration can thus be of great help.

How do frequency influence the damping? It is of interest to evaluate the flow parameters to see how the change in frequency effects the friction. The frequency is as mention decreasing as the pipe length increases, as shown in Figure 6. Figure 13 and Figure 14 depicts the simulation with 29 m headrace tunnel, giving study basics for friction respond in frequency change. **Table 3**. depicts readouts and calculations from simulation with 11 m and 29 m headrace.
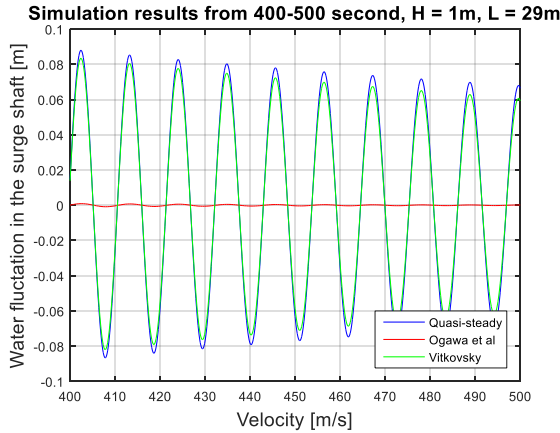
Figure 13. Simulation results of the unsteady damping models from 400-500 second with 29 m pipe length
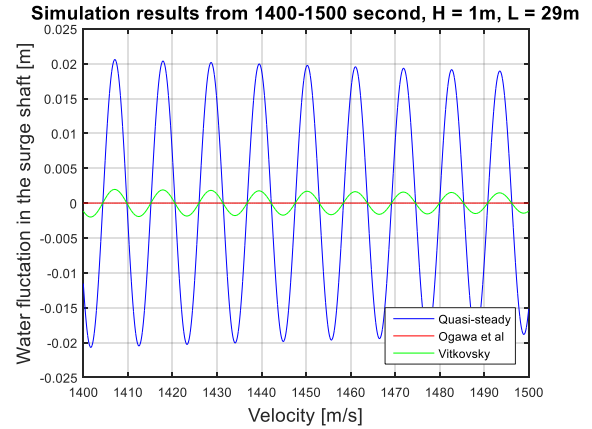
Figure 14. Simulation results of the unsteady damping models from 1400-1500 second with 29 m pipe length

Table 3. Readouts from simulation results for 11 m and 29 m headrace tunnel length

Traditional surge shaft	Readouts					
Headrace length	11m			29m		
Friction model of interest	Quasi-steady	Ogawa et al	Vitkovsky	Quasi-steady	Ogawa et al	Vitkovsky
First peak [m]	0.90	0.93	0.90	0.47	0.46	0.47
Tenth peak [m]	0.29	0.30	0.29	0.22	0.08	0.22
100 second	0.19	0.14	0.19	0.22	0.08	0.22
Deviation from first peak to tenth peak	68 %	67 %	68 %	53 %	83 %	53 %
Deviation from first peak to 100 seconds	79 %	84 %	79 %	53 %	83 %	53 %

The simulation results with 29 m headrace shows that the quasi-steady model and the model by Vitkovsky predicts less frictional loss with increasing length, which contradicts the findings by Brekke [11]. Ogawa et al. on the other hand, estimates a higher loss in the first periods, but as time goes, is the average friction quite similar for both lengths. Figure 13 shows that the Ogawa et al. damps the oscillations completely out at approximately 450 s for the 29 m case, slightly earlier than for the 11 m headrace length. On the other hand, has the model by Vitkovsky a longer dampening time for the 29 m headrace, where the oscillations is approximately zero after 2500 s, depicted in Figure 14. The quasi-steady model and the model by Vitkovsky has the largest maximum peak for the 29 m case, while the Ogawa et al. has the largest maximum peak for the 11 m case.

6.3. The new purposed one-term friction model

The idea of the ongoing work on developing a new friction model is to use the quasi-steady friction term and multiply this term with a self-designed constant B. In order to implement all necessary information, is it desired to make a constant that represents the behaviour from parameters describing the change in flow and system condition. The constant B can be optimized and derived by gaining experience from other model simulations in combination with measurements from the test campaign.

Eq. (29) depicts the idea of how the one-term friction model is thought to be presented. The method builds on the basic model by Vitkovsky.

$$f = f_q + \frac{kD}{V|V|}\left(\frac{\partial V}{\partial t}\right)sign(V) = B * f_q * sign(V) \tag{28}$$

$$f = \begin{cases} steady\ flow\text{:} & f = f_q & \frac{dV}{dt} = 0 \\ Unsteady\ flow\text{:} & f = B * f_q * sign(V) & \frac{dV}{dt} \neq 0 \end{cases} \tag{29}$$

1. Conclusion

At slow transients is it valid to assume that the water string acts as one large water string throughout the pipe system. The water will therefore have equal flow conditions in the whole string, hence the velocity change in the unsteady frictions models can be neglected in the new model. Ogawa et al. introduces a model that damps the oscillations to a complete stop, by implementing the velocity in the denominator, it can thus be beneficial to implement the velocity in such a way. Another possibility is to have the velocity parameter in exponent of the new correction term, making the term equal to one, considering zero velocity.

Simulation results indicates challenges to handle both the change in frequency and the calculations of the friction in the turning area. Giving a decrease in dampening at both frequency increase and turning, wish contradicts tests from real measurements.

2. Further work

In this paper, some selected friction models of interest have been compered and evaluated. To be able to validate the different models validity and performance, should the purposed experimental test be utilized. After accomplishing a closer study on the different models and compared theme up against the measurements, a new one-term friction model should be purposed.

In addition, would it also be of interest to look closer at other models, such as the model by Bjørnar Svingen, using the Rayleigh-dampening to establishing a specific model for U-tube oscillations considering the instantaneous mean flow velocity and diffusion $\frac{\partial^2 V}{\partial x^2}$ [8].

References

[1].   White, F.M., *Fluid Mechanics*, ed. Seven. 2011: McGraw-Hill Higher Education.

[2].   Tullis, J.P., *Hydraulics of pipelines : pumps, valves, cavitation, transients*. 1989, New York: Wiley.

[3].   Nielsen, T.K., *Dynamisk dimensjonering av vannkraftverk*. SINTEF rapport (SINTEF. Avdeling for strømningsteknikk : trykt utg.). Vol. STF67 A 90038. 1990, Trondheim: SINTEF, Strømningsmaskiner.

[4].   Sellevold, M.O.D., *Demping av U-røyrsvingingar i vasskraftverk.* 2013.

[5].   Bergant, A., A. Ross Simpson, and J. Vìtkovsk, *Developments in unsteady pipe flow friction modelling.* Journal of Hydraulic Research, 2001. **39**(3): p. 249-257.

[6].   Zarzycki, Z., *Improved method for simulating transients of turbulent pipe flow.* Journal of Theoretical and Applied Mechanics 49, 2011.

[7].   Vitkovsky, J.S., M. Bergant, A. Simpson, A. Lambert, M., *Numerical Error in Weighting Function-Based Unsteady Friction Models for Pipe Transients.* Journal of Hydraulic Engineering, 2006. **132**(7).

[8].   Svingen, B. and R. Vennatrø, *Transient og oscillerende hydraulisk demping i rør*. SINTEF rapport (SINTEF. Termisk energi og vannkraft). Vol. STF84 A96441. 1996, Trondheim: SINTEF, Energi, Termisk energi og vannkraft.

[9].   Bratland, O., *Single phase flow assurance.* 2009.

[10].   Li, P., *An Experimental Investigation of Velocity Distribution and Head Loss of Oscillatory Flow in a Rectangular Duct with Sand Roughness*. 2004, Fakultet for ingeniørvitenskap og teknologi.

[11].   Brekke, H., *[Doktoravhandling] : [141] 1 : A stability study on hydro power plant governing including the influence from a quasi nonlinear damping of oscillatory flow and from the turbine characteristics*. Vol. [141] 1. 1984, Oslo: H. Brekke.

[12].   Ogawa, A., et al., *Damped oscillation of liquid column in vertical U-tube for Newtonian and non-Newtonian liquids.* Journal of Thermal Science, 2007. **16**(4): p. 289-300.

[13].   Eldar, Y.C., *Sampling theory : beyond bandlimited systems*. 2014, Cambridge University Press.